Université de Nice–Sophia Antipolis – UFR Sciences

Ecole Doctorale STIC
Sciences et Technologies de l'Information et de la Communication

THESE

pour obtenir le titre de

DOCTEUR EN SCIENCES
de l'Université de Nice-Sophia Antipolis
Discipline: Automatique, Traitement du Signal et des Images

et le titre de

DOCTEUR EN GENIE TELEINFORMATIQUE
de l'Université Fédérale du Ceará
Discipline: Signaux et Systèmes

présentée et soutenue par

Raul LIBERATO DE LACERDA NETO

EXPLOITING THE WIRELESS CHANNEL FOR COMMUNICATION

Thèse dirigée par **Mérouane DEBBAH** et **João Cesar M. MOTA**
soutenue le 11 Décembre 2008 á EURECOM

Jury:

M. Pierre DUHAMEL	Directeur de Recherche au CNRS, LSS	Président
M. Claude OESTGES	Professeur à l'Université Catholique de Louvain	Rapporteur
M. Paulo S. R. DINIZ	Professeur à l'Université Fédérale du Rio de Janeiro	Rapporteur
M. David GESBERT	Professeur à l'EURECOM	Examinateur
M. Mérouane DEBBAH	Professeur au SUPELEC	Directeur de thèse
M. João Cesar M. MOTA	Professeur à l'Université Fédérale du Ceará	Directeur de thèse

To my family and my cherished wife,
for their love and support.

Abstract

The development of cellular communications during the 1980s made wireless networks one of the most important areas of technology. Fueled by the advances in wireless computer networks, high data rate connections have recently become the focus of research in the communication domain. The growth of the Internet and the introduction of a multitude of applications culminated in a new era of communications in which wireless networks play a very important role.

However, the wireless environment still offers some challenges that need to be addressed before reaching the prerequisites of future wireless networks. Due to imprecise channel characterization, much of the potential of the wireless environment is wasted. Furthermore, the requirements caused by multiple connections lead to the use of multiple access schemes that were not designed to cope with some of the wireless environment phenomenons. These two points are treated in this thesis.

The first part of this thesis is dedicated to the use of probability theory tools that enable the creation of models based only on partial knowledge of the environment. Using Jaynes' maximum entropy principle, we present a framework that allows us to infer on the channel characteristics by choosing probability distributions that maximize entropy under the constraints that represent our state of knowledge. This technique is considered as the most reliable method to perform inferences. Models for two different types of environment are derived: wideband channels and multiple-input multiple-output (MIMO) channels.

In the second part, the multiple access problem for ultra wideband (UWB) systems is assessed. Despite the large amount of work conducted during recent years on UWB technology, no scheme can cope with the high dispersion of UWB channels and still offer reasonable spectral efficiency. An innovative scheme that exploits the users' channels to guarantee multiple access is introduced, entitled Channel Division Multiple Access (ChDMA). This scheme provides a very simple solution and achieves high spectral efficiency.

Résumé

Le développement des communications mobiles pendant les années 1980s a fait des réseaux sans fil un des secteurs technologiques les plus importants. Stimulé par les avancements des réseaux d'ordinateurs, les raccordements élevés de débit sont récemment devenus le centre de la recherche dans le domaine de communication. La croissance de l'Internet et l'introduction d'une multitude d'applications ont abouti à une nouvelle ère des communications dans lesquelles les réseaux sans fil jouent un rôle très important.

Cependant, l'environnement sans fil offre toujours quelques défis qui doivent être adressés avant d'atteindre les pré-requis nécessaires pour des futurs réseaux sans fils. En raison de la caractérisation imprécise du canal, une grande partie du potentiel de l'environnement est gaspillé. En outre, le besoin des raccordements multiples mènent fréquemment à l'utilisation des arrangements qui n'ont pas été conus pour faire face à certains des phénomènes de l'environnement sans fil. Ces deux points sont traités dans cette thèse.

La première partie de cette thèse est consacrée à l'utilisation des outils de théorie des probabilités qui permettent la création des modèles basés seulement sur la connaissance partielle de l'environnement. A partir du principe de maximisation d'entropie, nous présentons un approche qui nous permet d'inférer sur les caractéristiques des canaux en choisissant les distributions de probabilité qui maximisent l'entropie sous des contraintes qui représentent notre état de la connaissance. Cette technique est considérée comme la plus fiable méthode d'inférence. Des modèles pour deux différents types d'environnement sont dérivés : canaux à large bande et canaux à sorties multiples à entrées multiples (MIMO).

Dans la deuxième partie, le problème d'accès multiple pour les systèmes ultra à large bande (UWB) est évalué. Malgré de la grande quantité de travail conduite pendant ces dernières années sur la technologie d'UWB, aucune technique d'accès multiple ne peut faire face à la dispersion élevée des canaux d'UWB ce qui engendre à une efficacité spectrale inefficace. Un arrangement innovateur qui exploite les canaux des utilisateurs pour garantir l'accès multiple est présenté, intitulé "Channel Division Multiple Access" (ChDMA). Cet arrangement fournit une solution très simple en obtenant une efficacité spectrale élevée.

Resumo

O desenvolvimento das comunicações móveis durante os anos 80 permitiu às redes sem fio de se tornarem um dos grandes marcos tecnológicos do século XX. Estimulado pelo avanço das redes de computadores, as conexões de alta velocidade se representam atualmente o centro da pesquisa no domínio da telecomunicação. O crescimento da internet e a introdução de uma grande gama de serviços culminaram em uma nova era nas quais as redes sem fio desempenham um papel muito importante.

Entretanto, o ambiente sem fio representa vários desafios que devem ser superados antes de alcançar os requisitos necessários das futuras redes sem fio. Em razão das características aleatórias do canal sem fio, uma grande parte de seu potencial deixa de ser aproveitado. Alem disso, necessidade de múltiplas conexões leva freqüentemente à utilização de arranjos que não foram concebidos para operar sobre o efeito de certos fenmenos do meio sem fio. Estes dois pontos são estudados nesta tese.

A primeira parte desta tese é dedicada à utilização de ferramentas da teoria das probabilidades. Estas ferramentas permitem a criação de modelos que descrevem o canal baseados apenas no conhecimento parcial do canal sem fio. A partir do principio da maximização da entropia, nós apresentamos uma técnica que nos permite de inferir sobre as características dos canais. Esta técnica é considerada como o método mais confiável de inferência. Modelos para dois tipos diferentes canais são estudados: canais de banda larga e canais de múltiplas entradas e múltiplas saídas (MIMO).

Na segunda parte, o problema de múltiplo acesso para sistemas de ultra larga banda (UWB) é tratado. Apesar da grande quantidade de trabalho conduzido durante estes últimos anos sobre a tecnologia UWB, nenhuma técnica de acesso múltiplo foi capaz de utilizar o canal de maneira eficiente. Uma solução inovadora que explora o ambiente disperviso é então proposto, intitulado “Channel Division Multiple Access” (CHDMA). Esta técnica fornece uma solução simples, obtendo uma elevada eficiência espectral.

Acknowledgments

I wish to express my gratitude to my supervisors, Professor Mérouane Debbah and Professor João César, for their friendly advices and encouragement words during these three years of Ph.D.. They were abundantly helpful and offered invaluable assistance, which were fundamental for the achievements presented herein.

I would like to thank the members of the supervisory committee. They were very supportive and provided me very good insights.

I would also like to thank all my friends and colleagues with whom I have had the pleasure of having various fruitfull discussions. These includes my co-authors, the members of the Mobile Communication Department at Eurecom, the members of the Radio Flexible Chair at Supelec and the members of the GTEL Laboratory at UFC. Special thanks to Dr. Maxime Guillaud for the discussions and collaborations on the domain of entropy maximization, Dr. Aawatif Menouni Hayar for all the discussions and collaboration on the proposal of ChDMA, Dr. Laura Cottatelucci for the discussions and collaborations on the asymptotic analysis of ChDMA, Prof. David Gesbert and Prof. Raymond Knopp from Eurecom for all the discussions and insights and M.Sc. Leonardo Cardoso and Dr. Sharon Betz that helped me on the corrections of my thesis.

On a practical note, I would like to convey thanks to Eurecom for providing the financial means and laboratory facilities during these three years. I also am indebted to the Region Provence Alpes Côte D'Azur (PACA) and the Fundação Cearense de Apoio ao Desenvolvimento Científico (FUNCAP), whom funded part of my work.

Finally, I would like to thank my family for their love and support. Special thanks to my wife Larissa for her understanding and endless love, helping me and giving me the motivation to finish this thesis.

Contents

List of Figures

List of Tables

Acronyms

Here we present the list of acronyms used in this document. The meaning of an acronym is indicated once, when it first occurs in the text.

A

AIC Akaike's Information Criterion

AMPS Advanced Mobile Phone System

AR Auto Regressive

AWGN Additive White Gaussian Noise

B

BPSK Binary Phase Shift Keying

BS Base Station

C

CDMA Code Division Multiple Access

ChDMA Channel Division Multiple Access

CIR Channel Impulse Response

CSI Channel State Information

D

dB decibels

DoF Degrees of Freedom

DS Direct Sequence

E

EMOS Eurecom MIMO Openair Sounder

F

FCC Federal Communications Commission

FDMA Frequency Division Multiple Access

FH Frequency Hopping

G

GSM Groupe Spécial Mobile or Global System for Mobile Communication

I

IR Impulse Radio

ISI Intersymbol Interference

ITU-R International Telecommunication Union - Radiocommunication Sector

L

LoS Line-of-Sight

LPD Low Probability of Detection

LPI Low Probability of Interception

M

MaxEnt Maximum Entropy

MC Multi-Carrier

MDL Minimum Description Length

ME Maximum Relative Entropy

MF Matched Filter

MIMO Multiple-Input Multiple-Output

MMSE Minimum Mean Squared Error

N

NLoS Non Line of Sight

O

OFDM Orthogonal Frequency Division Multiplexing

OFDMA Orthogonal Frequency Division Multiple Access

P

PDA Personal Digital Assistants

pdf Probability Density Function

pdp Power Delay Profile

Q

QPSK Quadrature Phase Shift Keying

R

RF Radio Frequency

RFID Radio Frequency Identification

RSIB Rhode & Schwarz Protocol

Rx Receiver

S

SDMA Space Division Multiple Access

SINR Signal-to-Interference-plus-Noise Ratio

SISO Single-Input Single-Output

SNR Signal Noise Ratio

SVD Singular Value Decomposition

T

TDD Time Division Duplex

TDMA Time Division Multiple Access

Tx Transmitter

U

UMTS Universal Mobile Telecommunications System

UWB Ultra-Wideband

V

VNA Vertical Network Analyzer

VSWR Voltage Standing Wave Radio

W

WBAN Wireless Body Area Network

WLAN Wireless Local Area Network

WMAN Wireless Metropolitan Area Network

WPAN Wireless Personal Area Network

WSN Wireless Sensor Network

Chapter 1

Introduction

"The beginning of knowledge is the discovery of something we do not understand."

(Frank Herbert)

Wireless communication has been a major research area since the ground-braking work of Maxwell, Hertz, Tesla and Marconi at the end of the 19th century. Even after a century of evolution and while it is considered one of the most successful engineering development, this domain is still experiencing great progress. Carried by the development of the internet and the portability and mobility of personal digital assistants (PDAs), the wireless communication is experiencing a new era, characterized by a large variety of services ubiquitously provided, requiring higher data rates and larger coverage.

This chapter briefly outlines the motivation and results of this thesis. First, the general aspects of the wireless communication are introduced with a description of their history and the actual trends. After that, the goals and results attained in this thesis are discussed. Finally, we provide an outline of the following chapters and present a list of all publications derived from this work.

1.1 Wireless Communication

The wireless technology is still experiencing great improvement even after one year of evolution. Today, the wireless environment is exploited not only for voice transmission (telephony service) but also for data communications. Spurred on by the advances of wireless computer networks (802.11abgn, 802.16, *etc.*), high data rate connections have recently become the focus of current and future wireless systems. Moreover, the growth of the Internet and the introduction of a multitude of applications have motivated a new era of communication, in which the wireless communication plays a very important role.

1.1.1 History in Brief

The story of wireless communication began after the works of Maxwell and Hertz at the end of the 19th century, when they introduced the concept of electromagnetic waves [20, 45, 48, 79]. A few years later, Tesla, Marconi and Landell were responsible for the first experiments and transmission demonstrations of these waves, which allowed them to obtain patents for the invention of the radio. Tesla was the first to describe and build wireless communication devices in 1893. However, Marconi was the one who popularized the technology after his unprecedent transmission across the English Channel, which gave him the title of "Inventor of radio communication" and a Nobel prize in 1909. After such experiments, and together with Thomas Edison, they developed the technology and during the 1900s the first commercial wireless system was created: a telegraph system that was able to send and receive messages across the Atlantic Ocean. Since then, wireless systems have emerged all over the world, especially in the entertainment domain (radio and television broadcast transmissions).

Two-way wireless communication only started to be developed when the military and police departments from the US adopted the technology for private communication. The first wireless system for closed user groups was deployed during the 1930s; police cars in Detroit were the first users to operate with bi-directional terminals. During the 1940s, the technology was introduced in the American market with the first civil bi-directional terminals.

Still during the 1940s, many researchers dedicated a lot of effort to consolidate wireless communication theory. In 1948, Claude Shannon made history with his landmark publication [63], entitled "*A Mathematical Theory of Communications*." In his work, Shannon introduced the concept of Information Theory as a discipline and established not only the theory of error-free communication, but also one of the most important

measure of performance in a wireless transmission: capacity. Capacity is a measure of the maximum achievable rate over the communication system and it represents one of the few measures able to compare performances of different systems.

During the 1950s and 1960s, attention for the development of the wireless communication turned to the commercial market. The technology spread all around the world and regulation agencies were created to control the development of wireless communication technology. In the following years, very important concepts were introduced [79], including the cellular principle and the multiple access techniques. The cellular principle is based on the geographical division of the area into cells and allows re-use of the wireless resources in different cells, enabling a great increase of the total system capacity, while multiple access techniques define how the wireless environment could be accessed by different users.

In 1976, the first mobile telephony system started operation in New York City, but it was in Japan that the first cellular mobile system was deployed in 1979 by NTT. During the 1980s, the technology obtained significative penetration into the international market with offers of reasonable portable devices, good speech quality and acceptable battery lifetimes. The US cellular standard, entitled "Advanced Mobile Phone System" (AMPS), marked the beginning of the cellular communication, when for the first time a wireless system was able to support 666 duplex channels.

Driven by the advantages of digital processing, few years later cellular networks evolved to use digital communication. This represented the beginning of the Digital Era, also known as second generation technology (2G). Europe introduced the first digital cellular standard labeled "Groupe Spécial Mobile" (GSM)[1]. Furthermore, motivated by the expansion of the Internet, the digital communication era was also characterized by the integration of mobile wireless networks to the Internet.

Since then, wireless communication has greatly improved in terms of data rates and coverage, with various wireless technologies introduced to fulfill the increasingly challenging requirements of the networks. Nonetheless, because of the increase in the number of services offered by wireless networks and the fusion of different networks, further improvements are necessary to enable higher data rates and more simultaneously user connections.

[1] In 1994, when the GSM was deployed in US, it was relabeled "Global System for Mobile Communications."

1.1.2 Threats of the Wireless Environment

The most important challenges for wireless communication come from the complexity of the wireless environment. Unlike the conventional wired environment, the wireless channel is characterized by a very strong random component that suffers from multi-path, fading and multi-access interference phenomena. Such effects introduce a new level of complexity that is really hard to predict. In more detail, these three phenomena are

Multi-path: Multi-path is particular to the wireless channel and is generated by the dispersion of the signal over the whole environment. Due to the various refractions, diffractions and reflections, the transmitted signal arrives at the receiver at different times, from different directions and with different attenuation levels.

Fading: The wireless environment experiences a very strong distortion, known as fading, as a result of the constructive and destructive combinations sum of various signals that arrive simultaneously at the receiver by different paths.

Multi-access interference: The wireless environment is not contained in a limited space as the conventional wireline or optical fiber communication. Consequently, the systems are susceptible to interference generated by adjacent systems or terminals. Thus, since the available spectrum is limited, wireless systems have to operate with a certain level of interference to guarantee multi-user access.

Moreover, further limitations are also imposed on the use of the wireless environment by international regulation agencies for health and economic reasons. Since biological studies may show that there are harmful effects from electromagnetic waves on living things, much attention has been dedicated to control wireless transmissions because these waves are irradiated everywhere around the antenna. As a result, international agencies impose strict policies and allow only limited transmit power levels. Furthermore, these agencies control and organize the wireless spectrum. The result is that civil transmissions are limited to specific bands within the wireless spectrum and it is usually very expensive to "own" spectrum.

At this point, I have to agree with Durgin when he affirmed [20] that:

> *"There are few things in nature more unwieldy than the power-limited, space-varying, time varying, frequency-varying wireless channel."*

A good understanding of the wireless environment properties allows engineers to deal with the channel impairments and approach optimal limits. This knowledge is fundamental and the development of new technologies is required not only to cope with the

channel particularities but also to exploit these particularities to increase communication performance. Future wireless communication systems will require a new level of communication efficiency. Although great improvements were observed during recent years, there is still room to improve system performance based on the complete optimization of system resources.

1.1.3 Degrees of Freedom (DoF)

One useful way to characterize wireless systems is to analyze a system's degrees of freedom (DoF). The DoF is a very general term that measures the number of parameters required to describe a variable or process. In the communication domain, this term is employed to quantify the number of independent parameters necessary to represent the wireless channel and the particularities of the wireless system. This concept allows one to concisely define the environment and provide a good understanding of its limitations.

DoF are classified in subcategories which depends on the characteristics of the wireless environment. They are usually based on the exploitable dimensions of the environment, which means that DoF have a multi-dimensional nature.

In the following, we present the most common DoF's domains:

Frequency: The wireless channel is often selective in frequency and spectrum-limited. This restricts the amount of information that can be transmitted through it. The frequency selectivity is directly related to the dispersion generated by the multipath phenomenon. The frequency DoF represent the number of independent or uncorrelated frequency channels that exist over the wireless channel spectrum. It is strongly related to the coherence frequency of the channel.

Time: Also due to the multipath phenomenon, wireless transmissions suffer from inter-symbol interference (ISI) and inter-system interference. Furthermore, the wireless environment is constantly changing because some objects are not static, making the channel also suffer from a time-varying component that is hard to predict. The temporal DoF represent the number of parameters necessary to predict the channel at a given moment. It is intimately dependent on the system bandwidth.

Space: Due to the fading and multipath phenomena, the wireless channel is location dependent, which means that different terminals suffer from different channel impairments due to their different locations. Consequently, mobility has a great impact on the system's performance. The spatial DoF represent the number of

independent channels that exist in the system due to the use of antenna arrays at the transmitter and/or at the receiver.

Polarization: Polarization in the electromagnetic field provides two DoF. Conventional wireless systems usually exploit this diversity to permit higher data rates.

Multi-user: The multi-user domain represents the number of users that a wireless system can support. The dimension is strongly related to the number of users available on the system. This domain is also treated as multi-user diversity.

Multi-system: As the number of wireless systems has increased over the two last decades, the idea of convergence of different system technologies has been introduced to enable mobile terminals to operate with different standards (see e.g. [49, 82]). Many mobile phones currently available on the market are multi-mode, which means that they can work with different standards. The multi-system diversity characterizes the amount of systems available in a wireless environment. This domain is commonly treated as system diversity.

1.1.4 Trends in Multi-User Communications

After many years of evolution, the wireless communication still has a lot of challenges to overcome. The expectation today is that the evolution of wireless communications will follow three directions to fulfill the prerequisites of the foreseen wireless systems (higher data-rates and ubiquitous communication):

Channel Modeling Characterization: Much of the wireless environment's potential is wasted due to imprecise channel characterization [68, 69]. On one hand, overly simplistic models lead to poor system rates because they cannot provide a good characterization of the channel distortions. On the other hand, overparameterized models may require the estimation of many parameters, which results in the allocation of system resources to the estimation process rather than communication, leading to inefficient resource allocations. Thus, channel modeling techniques are fundamental to the design of high data rate systems. Exploiting the DoF that characterizes the wireless environment, efficient modeling techniques could enable the representation of the major distortions based only on a small set of parameters that can be estimated.

Multiple Access Technology: Several multiple access techniques have been introduced [27, 32, 48, 56, 80]. However, due to the high data rate requirements, most

of them have been shown to be inefficient in certain systems and/or channel environments. Further research is necessary to allow multiple access in challenging scenarios.

Optimal Resources Allocation: Due to the limited resources available in wireless systems, appropriate resource allocation is required to enable high data rates [24, 86]. This domain represents the major topic of research in wireless communication.

1.2 About this Thesis

This thesis focuses on exploiting the wireless environment to improve communication capabilities. On one hand, we would like to study wireless channels and introduce new metrics that could provide a good characterization of the channel effects using only a limited number of parameters. On the other hand, we would also like to provide system solutions that could cope with the environment's distortions and exploits them to achieve better data rates. This approach lead us to the development of techniques based on two research axes: channel modeling characterization and multiple access technology. Consequently, this thesis is divided in two parts: modeling with entropy maximization and channel division multiple access.

The first part is dedicated to the use of advanced mathematical tools from the domains of probability theory and inductive inference that are employed to study the randomness of the wireless environment. We develop an information theoretic framework based on the principle of maximum entropy. The framework is designed to allow us to perform inferences about the channel when only partial knowledge is available. The main idea is to identify metrics that could characterize the environment when only a limited amount of data can be dedicated. We apply this framework to two different scenarios: wideband channels and multiple-input multiple-output (MIMO) channels. For both scenarios, we generate models that are later validated through real channel measurements.

The second part is dedicated to the study of multiple access techniques to low duty-cycle systems. Herein, we focus on the analysis of the ultra wideband (UWB) system, which is a candidate for future high data rate indoor networks. We show that none of the existing multiple access techniques were design to cope with the specifies of the low duty-cycle UWB technology. For this reason, we introduce a very simple idea that exploits the channel diversity to allow multiple access, which we call channel division multiple access (ChDMA). We verify the performance of the ChDMA when different

system configurations are employed.

1.2.1 Main Contributions

The main contributions of this thesis are:

- A unified framework for wireless channel modeling based on Maximum Entropy (MaxEnt) tools is presented.
- An analysis of how the entropy of the wideband channel scales with the bandwidth is provided. The model is evaluated with real measurements acquired in the Mobile Communication Laboratory at Eurecom.
- MIMO channel models are developed using the unified modeling framework when different prior assumptions are considered. These models are compared with measurement results acquired with the Eurecom MIMO open air sounder (EMOS)
- An original multiple access scheme for ultra wideband systems, called channel division multiple access (ChDMA), is introduced and analyzed [16, 17].

1.2.2 Thesis Outline

The outline of this thesis is as follows:

1.2.2.1 Chapter 2: Information Theoretic Approach for Modeling

This chapter provides theoretical grounds for modeling with partial information. In the light of probability theory and the principle of maximum entropy, we present a framework that allows the derivation of consistent models based on the information available.

1.2.2.2 Chapter 3: Modeling the Wideband Channel

Based on the framework presented in Chapter 2, we treat the modeling process of wideband channels. Two different types of knowledge are considered: the average channel power and the partial knowledge of the channel correlation vector. The results are presented based on indoor measurements carried in a typical office environment at Eurecom. We show in this chapter how the channel entropy scales with the bandwidth for different priors.

1.2.2.3 Chapter 4: Modeling the MIMO Channel

Employing the MaxEnt framework, we treat in this chapter the modeling process of a MIMO channel. Three different models are derived based on different states of knowledge: knowledge of the average channel power, knowledge of the full covariance matrix and the knowledge of the full covariance matrix rank. This last prior introduces a new method to characterize the environment. To evaluate how good the metric is, we carried out outdoor MIMO measurements around Eurecom to verify whether we could obtain better representations of the environment when the full covariance rank was known. We conclude that the full covariance rank could be good parameter to represent the MIMO channel environment.

1.2.2.4 Chapter 5: Channel Division Multiple Access (ChDMA)

We present in this chapter an original multiple access scheme called channel division multiple access that exploits the high temporal resolution of UWB systems to separate the users' signals. These signatures have interesting location-dependent properties that results in a decentralized flexible multiple access scheme, where the codes are naturally generated by the radio channel.

1.2.2.5 Chapter 6: Performance of ChDMA

This chapter presents some evaluation results of ChDMA systems. First, we analyze the impact of the system parameters on the ChDMA performance. We compare the performance of ChDMA with CDMA when the latter suffers only from flat fading channel impairment, and we observe that even under this ideal condition, ChDMA is able to outperform CDMA. After that, an asymptotic analysis as the number of users becomes larger is performed.

1.2.2.6 Chapter 7: Conclusions and Perspectives

This chapter contains concluding remarks. We also propose some future work to further extend and improve the results of this thesis.

1.3 List of Publications

In the following, we present the complete list of publications generated during the development of this thesis:

Journal papers:

- S. Lasaulce, A. Suarez, Raul de Lacerda and M. Debbah. "Using cross-system diversity in heterogeneous networks: Throughput optimization." *Elsevier J. of Performance Evaluation* (PEVA), 65, 11, 907-921, November 2008.

- Raul de Lacerda, M. Guillaud, M. Debbah and J. C. M. Mota. "Experimental validation of Maximum Entropy-based wireless channel models." To be submitted.

- Raul de Lacerda, A. M. Hayar, M. Debbah and J. C. M. Mota. "ChDMA: A simple multiple access scheme for UWB Systems." to be submitted.

Conference/Workshop papers:

- Raul de Lacerda, M. Debbah and A. Menouni. "Channel Division Multiple Access." *1st IEEE International Conference on Wireless Broadband and Ultra-Wideband Communications* (AusWireless'06), New SouthWales, Australia, March 13-16, 2006.

- Raul de Lacerda, A. Menouni, M. Debbah and B. H. Fleury. "A Maximum Entropy Approach to Ultra-Wideband Channel Modeling." 31st International Conference on Acoustics, Speech, and Signal Processing (ICASSP'06), Toulouse, France, May 14-19, 2006.

- Raul de Lacerda, A. L. F. de Almeda, G. Favier, J. C. M. Mota and M. Debbah. "Performance Evaluation of Supervised PARAFAC Receivers for CDMA Systems." *IEEE International Telecommunications Symposium 2006* (ITS'06), Fortaleza, Brazil, September 03-06, 2006.

- Raul de Lacerda, A. Menouni and M. Debbah. "Channel Division Multiple Access Based on High UWB Channel Temporal Resolution." *64th IEEE Vehicular Technology Conference 2006 Fall* (VTC Fall'06), Montreal, Canada, September 25-28, 2006.

- Raul de Lacerda and M. Debbah. "Some Results on the Asymptotic Downlink Capacity of MIMO Multi-user Networks." *40th Asilomar Conference on Signals, Systems and Computers*, Asilomar Conference Grounds, Pacific Grove, California, USA, October 29 - November 01, 2006.

- A. de Almeida, G. Favier, J. C. Mota and Raul de Lacerda. "Estimation of Frequency-Selective Block-Fading MIMO Channels Using PARAFAC Modeling and Alternating Least Squares." *40th Asilomar Conference on Signals, Systems and Computers, Asilomar Conference Grounds*, Pacific Grove, California, USA, October 29 - November 01, 2006.

- Alberto Suarez, Raul de Lacerda, M. Debbah and N. Linh-Trung. "Power allocation under quality of service constraints for uplink multi-user MIMO systems." *IEEE 10th Biennial Vietnam Conference on Radio and Electronics*, Hanoi, Vietnam, November 06-07, 2006.

- Raul de Lacerda, L. Sampaio, H. Hoffsteter, M. Debbah, D. Gesbert and R. Knopp. "Capacity of MIMO Systems: Impact of Polarization, Mobility and Environment, IRAMUS Workshop, Val Thorens, France, January 24 - 26, 2007.

- Raul de Lacerda and M. Debbah. "Channel Characterization and Modeling for MIMO and UWB Applications." *NEWCOM Dissemination Day*, Paris, France, February 15, 2007.

- Raul de Lacerda, A. Menouni, M. Debbah and C. le Martret. "Channel Division Multiple Access Technique" *NEWCOM Dissemination Day*, Paris, France, February 15, 2007.

- Raul de Lacerda, A. Menouni and M. Debbah. "Channel Division Multiple Access Technique: New multiple access approach for UWB Networks." *European Ultra Wide Band Radio Technology Workshop 2007*, Grenoble, France, May 10-11, 2007.

- Raul de Lacerda, L. Sampaio, R. Knopp, M. Debbah and D. Gesbert. "EMOS Platform: Real-Time Capacity Estimation of MIMO Channels in the UMTS-TDD Band." *International Symposium on Wireless Communication Systems 2007*, Trondheim, Norway, October 17-19, 2007.

- S. Lasaulce, A. Suarez, Raul de Lacerda and M. Debbah. "Cross-System Resources Allocation Based on Random Matrix Theory." *2nd International Conference on Performance Evaluation Methodologies and Tools*, Nantes, France, October 23-25, 2007.

- Raul de Lacerda, L. Cottatellucci and M. Debbah. "Asymptotic Analysis of Channel Division Multiple Access Schemes for Ultra-Wideband Systems." *9th IEEE In-*

ternational Workshop on Signal Processing Advances in Wireless Communications (SPAWC'08), Recife, Brazil, July 06 - 09, 2008.

Part I

Modeling with Entropy Maximization

Chapter 2

Information Theoretic Approach for Modeling

"The theory of probabilities is at bottom nothing but common sense reduced to calculus; it enables us to appreciate with exactness that which accurate minds feel with a sort of instinct for which ofttimes they are unable to account."

(Pierre-Simon Laplace)

In this chapter, we provide some theoretical grounds in which we can create models based on prior knowledge. In the light of probability theory and the principle of maximum entropy, we present a framework that enables the creation of models that are consistent with the available information.

First, a brief description of probability theory and inductive inference history is presented. After that, the principle of maximum entropy is introduced and we detail the mathematical background required for the modeling. Finally, some examples of the use of the modeling framework is presented, with a brief description of its limitations.

2.1 Probability Theory and the Inductive Inference

For centuries probability theory has been divided into two different schools: the frequentist school that sees probability as the long-run expected frequency of occurrence and believes only in data analysis, and the Bayesian school that is based on the plausibility concept and defines probability as the degree of believability. Until the 1970*s*, neither of these schools were able to present reliable solutions for many statistical inference problems [40], and some trials brought failures produced mathematical paradoxes, which threatened the credibility of very important results of the discipline. On one side, the frequentists were trying to solve problems based on experiments, which not only provided insights about very specific trials but also was based on assumptions that incorporated restrictions to the models and provided solutions that were not adapted to represent real life applications; on the other hand, the Bayesian approach required unambiguously desideratas[1] that were hard to define but very important to provide a deeper understanding of the relations between logic and randomness. However, during the 50*s*, with the seminal works of R. T. Cox, G. Pólya, H. Jeffreys, E. T. Jaynes and others, a larger and more precise rational thought was developed based on the so-called *Plausible Reasoning*.

Dating back to Bernoulli's and Laplace's works, the plausible reasoning presented by G. Pólya in 1954 via qualitative desiderata associated with consistency theorems derived by R. T. Cox in 1946 introduced the concept of incomplete information and eliminated the randomness present on the probability theory, unifying it to the statistical inference theory, as described by Jaynes in [40]:

"When one added Pólya's qualitative conditions to the consistency theorems of R. T. Cox, the result is a proof that, if degrees of plausibility are presented by real numbers, then there is an uniquely determined set of quantitative rules for conducting inference. That is, any other rule whose results conflict with them will necessarily violate an elementary – and nearly inescapable – desideratum of rationality or consistency."

From this point, a more general school, labeled *probability theory as extended logic*, was created. Their theory was able to re-derive the most important results of the old schools while also providing a very clear mathematical apparatus that could overcome the philosophical or ideological contradictions. Based on the same methods and

[1] Desiderata represents the axioms that govern the states of the desirable goals. As opposed to classical probability theory, such axioms are not restricted to binary quantities (true or false), but instead are generalizations that represent the degree of plausibility of each assumption.

mathematical rigor employed by the Bayesian school[2], extended logic theory was able to prove the major results of the frequentist school and the finitary algorithmic school[3] [62]. Nowadays, it is considered by many to be the most appropriate method to perform inferences to almost all scientific domains.

2.1.1 The Maximum Entropy Principle

The principle of maximum entropy, also known as the MaxEnt principle, is one of the fundamental pillars of extended logic theory. It postulates how statistics are affected by different forms of priors. The principle was the first theory that linked statistical mechanics and the information theory, providing with a single tool a clear methodology to perform statistical analysis. In 1957, Jaynes [38] showed that inferences could be performed by employing the entropy of thermodynamic particles. Defined as "a method for analyzing available qualitative information in order to determine a unique epistemic probability distribution," the generalization of his work resulted in one of a few techniques able to create models based on *a priori* knowledge. It provides a theoretical justification for conducting scientific inference in a consistent manner. Extensively used in a wide range of domains with success, the MaxEnt principle has become an important tool to perform inferences and it is stated as follows:

MaxEnt Principle: *When one makes inferences based on partial or incomplete information, he should draw them from that probability distribution that has the maximum entropy permitted by the information that he has.*

Later, Jaynes [39], Shore & Johnson [65] and Skilling [67] quantified the reliability of the MaxEnt prediction based on any prior information and studied the plausibility of the model. Jaynes introduced the concentration theorem and proved that MaxEnt inferences provide the most probable models. He exploited the combinatorial theory and showed that among all the possibilities, the models generated by the MaxEnt principle were the ones that have the highest likelihood to occur under the considered restrictions, *i.e.*, the prior knowledge. Meanwhile, Shore & Johnson [65] and Skilling [67] tackled the problem of the plausibility of the MaxEnt and tried to redefine the concept of entropy. Their work has focused on the justification of the MaxEnt principle as a consistent reasoning

[2]Many mathematicians still assume that the *probability theory as extended logic* represents only an evolution of the Bayesian school.

[3]The finitary algorithmic school is an evolution of the frequentist school of Kolgomorov, which eliminated the concept of randomness by introducing the algorithmic complexity concept.

that does not need any physical interpretation. They had shown that entropy relies on a plausible concept that is justified by itself and it does not need to represent any notion of measure as the previous works suggested.

Nevertheless, even with the large range of successful application of the principle, there remains controversy and debates about the MaxEnt theory. The principle was severely criticized by a large group of specialists that have shown some contradictions between the results derived by the MaxEnt principle and the ones derived by others well-developed statistical inference tools, in particular with the Bayesian conditionalization. These contradictory results disrespect the *consistency axiom*, which is a fundamental rule of the inference theory.

Consistency Axiom: *When the state of knowledge of two problems are the same, it should not matter what technique you use to perform inferences, the result must be the same.*

In 1996, Uffink [78] studied the contradictions presented between the MaxEnt method and the Bayesian conditionalization and pointed out that the problem relies on the conceptual nature of the information. This misunderstand was the main source of controversies. He showed that the MaxEnt principle was developed on the assumption that information is intended to characterize a state of belief whereas many were employing empirical data as the source of constraints for the inference. He shows that MaxEnt operated with constraints on probability distributions while Bayesian conditionalization use empirical data results. He also presented a deep analysis of the MaxEnt principle and questioned some of Jaynes' assumptions.

Recently, Caticha & Griffin [12, 13, 25] extended the MaxEnt principle and presented the proof that it could provide the same results of the Bayesian conditionalization by exploiting the concept of relative entropy. They titled the new approach as Maximum Relative Entropy (ME). Their work employs basically the same apparatus as the MaxEnt principle, but the analytical expression are modified by the relative entropy expressions. As a consequence, they unified both results and provided a unique tool able to simultaneously process data information and moments constraints on the inference without any loss of generality. However, questions related to the definition of the information are still an open issue.

2.1.2 The Priors

An important issue for inference theory is prior information. The reliability and consistency of the priors are fundamental to the precision of the inference tools. Confronted

with the difficulty to reason about the subjectivity of the priors, considerable effort has been spent to define methods to encode information in an objective manner. However, information is sometimes vague and difficult to introduce to a mathematical model. As a consequence, the priors have been a significant source of controversies since the first results of the inference theory appeared.

One alternative to seek objectivity when considering priors is to use reparametrization tools. Based on the projection of the information in a suitable parametric space, the process removes the subjectivity of the prior and transforms it into a mathematical entity that can be easily added to the MaxEnt expressions. Nevertheless, this method can also impose unwanted restrictions since the parametrization is performed inside a finite and well-defined space that does not necessarily represent the full characteristic of the prior. For this reason, Bernardo *et al.* [7] showed that non-informative priors might not exist.

Another type of data that can be fully exploited by the MaxEnt principle is constraints based on the data analysis. Caticha and Griffin [13] showed how moments and data could be simultaneously or sequentially employed in the modeling process by using the ME.

2.2 Entropy, Relative Entropy and Mutual Information

Before we start the modeling framework, let us introduce the basic expressions that we employ to create and compare the models. There are three important definitions that we need [14]: entropy, relative entropy and mutual information.

As presented by Jaynes [40], the entropy represents a measure of self information of a random variable and is defined as:

Definition: 2.1. *The entropy $\mathcal{H}(X)$ of a discrete random variable X with alphabet $\mathcal{X}$ and probability mass function $p[x]$ is given by*

$$\mathcal{H}(X) = -\sum_{x\in\mathcal{X}} p[x]\log p[x]. \tag{2.1}$$

We use the convention that terms with zero probability do not change the entropy, *i.e.*, given a term y with probability $p[y] = 0$, $p[y]\log(p[y]) = 0\log(0) \to 0$. The notion of entropy can also be extended to random variables defined inside a continuous space.

In this case, the entropy of a random variable X that lies inside a space $\mathbb{X}$ is given by:

$$\mathcal{H}(X) = -\int_{x\in\mathbb{X}} p(x)\log p(x)dx. \tag{2.2}$$

The relative entropy, also known as Kullback-Leibler divergence, is a measure of difference between two distributions. It is a nonnegative quantity that is employed to measure the distance between distributions and important for the generalization of the Maximum Entropy Principle [12].

Definition: 2.2. *The relative entropy $\mathcal{D}(p\|q)$ of two probability mass functions $p[x]$ and $q[x]$ is defined as*

$$\mathcal{D}(p\|q) = \sum_{x\in\mathcal{X}} p[x]\log\frac{p[x]}{q[x]}. \tag{2.3}$$

For the above definition, we also assume the convention that terms with zero probability do not change the entropy: $0\log\frac{0}{q} = 0$. Furthermore, we assume that both probability mass functions are defined on the same set $\mathcal{X}$ and that $q[x] > 0 \;\forall\; p[x] > 0$, otherwise $D(p\|q) = \infty$.

The mutual information is a measure of the amount of information that one random variable carries about another random variable.

Definition: 2.3. *The mutual information $\mathcal{I}(X;Y)$ of two random variables X and Y that have a joint probability mass function $p[x,y]$ and marginal probability mass functions $p[x]$ and $p[y]$, respectively, is given by*

$$\mathcal{I}(X;Y) = \sum_{x,y} p[x,y]\log\frac{p[x,y]}{p[x]p[y]}. \tag{2.4}$$

As with the entropy, the relative entropy and the mutual information can also be extended to the continuous case and are then defined in terms of probability density functions (pdf) instead of probability mass functions.

2.3 Modeling with Priors

MaxEnt modeling is based on the derivation of the pdf given a set of known parameters and the entropy maximization estimation of the other parameters in the way that imposes the least structure on the model. As a consequence, the models should be consistent with the priors and accurately describe the real environment.

Before we tackle more complicated problems based on the modeling of the wireless channel (Chapter 3 and Chapter 4), let us present some simple examples of the MaxEnt framework when some knowledge about the pdf is known. The idea is to show how to use the tool when only some partial information about the pdf is available.

2.3.1 No Knowledge Available

Assume that we want to identify the pdf $p(x)$ that maximizes the entropy under the constraints that:

$$p(x) \geq 0, \tag{2.5}$$

$$\int_{x\in\mathbb{X}} p(x)\mathrm{d}x = 1. \tag{2.6}$$

We can form the Lagrangian functional

$$\mathcal{L} = -\int_{x\in\mathbb{X}} p(x)\log(p(x))\mathrm{d}x + \mu_0\left(1 - \int_{x\in\mathbb{X}} p(x)\mathrm{d}x\right), \tag{2.7}$$

which allow us to apply the MaxEnt principle. For this, we differentiate the functional with respect to $p(x)$, the xth component of the pdf p, to obtain

$$\frac{\partial\mathcal{L}}{\partial p(x)} = -\log(p(x)) - 1 - \mu_0. \tag{2.8}$$

Setting this equal to zero will provide the maximum entropy distribution based on the knowledge available in hand, *i.e.*,

$$p(x) = e^{-1-\mu_0}, \tag{2.9}$$

which is constant for all value of x inside the support $\mathbb{X}$. This implies that the pdf that maximizes the entropy when no knowledge is available is the uniform distribution over the support $\mathbb{X}$.

This result seems to be trivial, but if we think about it, it is the best that we could infer on the pdf of x due our lack of knowledge. This absence of information obliges us to not have any preference to one subset of $\mathbb{X}$ over another, which means that inside the support $\mathbb{X}$, all possibilities are equiprobable.

2.3.2 Knowledge of Expectation of x

Assume that we know the expected value of x, which we denote as $\tilde{x}$. Our problem then has the following constraints:

$$\begin{aligned} p(x) &\geq 0, && (2.10)\\ \int_{x\in\mathbb{X}} p(x)\mathrm{d}x &= 1, && (2.11)\\ \int_{x\in\mathbb{X}} xp(x)\mathrm{d}x &= \tilde{x}. && (2.12) \end{aligned}$$

Employing the same approach as the previous case, we have that

$$\begin{aligned} \mathcal{L} &= -\int_{x\in\mathbb{X}} p(x)\log(p(x))\mathrm{d}x + \mu_0\left(1-\int_{x\in\mathbb{X}} p(x)\mathrm{d}x\right) && (2.13)\\ &\quad +\mu_1\left(\tilde{x}-\int_{x\in\mathbb{X}} xp(x)\mathrm{d}x\right) && (2.14)\\ \frac{\partial\mathcal{L}}{\partial p(x)} &= -\log(p(x)) - 1 - \mu_0 - \mu_1 x = 0 && (2.15)\\ &\rightarrow\ p(x) = e^{(-1-\mu_0-\mu_1 x)} && (2.16) \end{aligned}$$

We observe that this time, the distribution depends on the value x. To find the correct distribution, it is necessary to solve for the constants μ_0 and μ_1 that results in a pdf that agrees with the constraints.

2.3.3 Marginalization Property

The marginalization property is a very interesting characteristic of the MaxEnt approach. It allows the modeler to exploit the information available to infer on the pdf of a random variable, even when this information is not directly related to the random variable itself.

Assume that I want to estimate the pdf of a random variable X, but the only information that I have is about the random variable Y. If I know that X and Y are not independent, and I have some information about this dependence, I can marginalize the information that I have about Y to infer on the pdf of X, *i.e.*,

$$p(x) = \int_{\mathbb{X}} p(x|y)p(y)\mathrm{d}y. \quad (2.17)$$

2.3.4 Updating the Model

Recently, Griffin and Caticha [13, 25] have shown that there are two methods to incorporate information by using the MaxEnt approach. One is based on the methodology that we presented here that assumes some knowledge based on some priors about the moments of the random variable. However, it is also possible to use measurements to infer on the pdf of a random variable. The idea is to use the relative entropy expression to infer on the distribution $p(x)$ assuming that $q(x)$ was acquired through measurements. They also introduced an important principle, called principle of minimal updating, that claims that our state of belief should change if and only if the information available provides new arguments to change our opinion (for further details, please refer directly to [12]).

Principle of Minimum Updating: *Beliefs should be updated only to the extent required by the new information.*

2.4 Limitations

It is important to note that MaxEnt provides models that hide unnecessary details and respects the priors. However, inference is still only a guess based on the priors. Though MaxEnt models represent our best guest, they still greatly differ from the real state of what is being inferred. Nevertheless, when the priors define the complete characteristics of what is being modeled, the MaxEnt model result will be exactly correct.

The main limitation of the MaxEnt framework is how difficult it is to incorporate common information in the modeling process. MaxEnt was designed to cope with information that represents moments or characteristics of the random variable pdf. However, deterministic information is difficult to be incorporated into the model, *e.g.*, the number of chairs, tables or any reflector that could affect the link between the transmitter and the receiver.

2.5 Summary

In this chapter, we discussed probability theory and inductive inference. Particular, Bayesian probability theory has led to a profound theoretical understanding of various scientific areas and has shown the potential of entropy as a measure of our degree of knowledge. Based on the maximum entropy principle, we have presented a theoretical justification for conducting scientific inference.

The modeling framework is based on the analysis of the probability distributions that maximize the entropy under the constraints of the knowledge available. It was shown that such an approach avoids the introduction of arbitrary assumptions and provides the best representation of our state of knowledge.

However, the framework also suffers from some limitations. The information available cannot always be incorporated on the model because it is difficult to represent the state of knowledge. For this reason, only two types of information are allowed to be incorporated: moments or probability distributions.

In the following chapters, we employ the tools presented herein to model the wireless channel. In Chapter 3, we present some models that could represent the wideband channel, whereas in Chapter 4 we address the MIMO channel case.

Chapter 3

Modeling the Wideband Channel

"A scientist in his laboratory is not a mere technician: he is also a child confronting natural phenomena that impress him as though they were fairy tales."

(Marie Curie)

Recently, ultra wideband (UWB) technology has been considered for indoor short-range high data rate systems that could coexist with legacy systems without impairing their performance. Using a large bandwidth is often seen as a solution to enable very high data rates. However, channel uncertainty could limit the achievable rates, since it may be necessary to allocate a large fraction of the total rate to satisfactory estimate the channel.

This chapter aims to analyze how channel uncertainty scales with bandwidth in wireless channels. The idea is to assess the number of parameters necessary to provide a good model to represent the wideband channel. In this respect, a sound framework based on the MaxEnt principle, introduced in Chapter 2, is presented for wideband channel modeling [18]. The models are based on measurements performed by us at Eurecom. In this framework, the degree of channel uncertainty can be quantified through the notion of entropy which is analyzed with respect to the bandwidth.

3.1 Introduction

Ultra wideband systems are based on the radiation of waveforms that are formed by a sequence of very short pulses, each with a duration of a few hundred picoseconds. Such signals are usually free of sine-wave carriers and do not require radio frequency (RF) processing because they can operate at baseband. Due to the typical low power spectral density of UWB signals, which is usually below the thermal noise of the receivers, UWB transmissions are inherently difficult to detect and do not cause significant interference to narrowband systems that may operate within the same area. These basic properties make UWB systems an ideal candidate [31] for wireless local area networks (WLAN), wireless personal area network (WPAN), wireless sensor networks (WSN), wireless body area networks (WBAN) and radio frequency identification (RFID) tags (further comments about UWB systems are presented in Section 5.2).

Although appealing, the efficiency of UWB communication is still questionable. Indeed, for large bandwidths, channel uncertainty can limit the achievable rates of power constrained systems and therefore the capacity depends crucially on the channel model. In fact, recent results [55] have shown that capacity is a function of how the number of channel paths scales with the bandwidth (linear, sub-linear, *etc.*). This is because increasing the number of channel paths increases the number of parameters to be estimated, resulting in the need for more rate allocated to the estimation process. Consequently, the estimation of all channel paths can become a bottleneck for UWB communications.

Previous studies [33] have already analyzed channel uncertainty scaling through the number of significant paths. However, in many cases, additional criteria (such as the Akaike information criterion (AIC) [3] or minimum description length (MDL) [60]) have to be considered because, for noisy measurements, the notion of significant paths is subjective.

For this reason, we decided to evaluate how uncertainty scales when the MaxEnt modeling framework is employed to model the wideband channel. Two types of prior information are considered: channel power knowledge and knowledge of the partial autocorrelation sequence. This approach allows us to identify the number of parameters required to represent the channel.

Note finally that previous contributions have also focused on characterizing the wideband channel with a limited number of parameters (autoregressive models (AR) with few coefficients [77]). The benefit of such characterizations is that it is possible to reproduce the channel behavior using only a small number of parameters. This thesis

differs from those previous contributions by not assuming a priori knowledge of how many parameters are necessary. Rather, we consider a much more general model that identifies the optimal number of parameters. Furthermore, the analysis performed here is carried out in the frequency domain, whereas other works usually exploit the time domain correlation to characterize the environment.

3.2 Modeling UWB Channels with MaxEnt

The problem of modeling wideband channels is crucial for the efficient design of wireless systems. The wireless channel suffers from constructive/destructive interference and therefore yields a random frequency response for which one has to attribute a joint probability distribution.

Here, we provide some theoretical grounds to model the wideband channel based on a given state of knowledge. In other words, knowing only certain aspects related to the channel (power, measurements), the question that we try to answer is how to translate prior information into a model for the channel. This question can be answered using Bayesian probability theory [40] and the MaxEnt principle (see Chapter 2). MaxEnt tools are at present the clearest theoretical justification to conduct scientific inference based on the information available. It is a probability theoretic tool that singles out the distribution with the greatest entropy for the desired unknown quantities that fits the known information while avoiding the arbitrary introduction or assumption of information that is unknown. This approach has been successfully used in spectrum analysis [10] and signal interpolation problems [52, 58].

In the following, we model a discrete wireless channel whose gain is represented by a complex vector that characterizes the frequency response across the bandwidth W, ranging in frequency from W_0 to $W + W_0$. We assume that the frequency resolution[1] is represented by δ_f, so the channel gain can be represented by a complex channel vector $\mathbf{h}$ of length N, where N is equal to $\frac{W}{\delta_f}$, and the i^{th} element of $\mathbf{h}$ is the channel gain of frequency $W_0 + \frac{i}{N}W$. Furthermore, we assume that the maximum delay between two different paths is represented by $\tau_{\max}$, measured in seconds. Under these considerations, we derive models based only on the limited available knowledge and on the properties of the environment.

[1]The frequency resolution is the bandwidth of each frequency bin that is employed to represent the channel.

The goal of channel modeling is estimate the spectral autocorrelation function assuming that the channel is stationary during the modeling phase. The spectral autocorrelation function $R[k]$ of the channel entries is defined as

$$R[k] = \mathbb{E}\{h[i]h^*[i+k]\} \tag{3.1}$$

where $\mathbb{E}\{\cdot\}$ represents the expectation operator and $(\cdot)^*$ the complex conjugate operator. Furthermore, in this section, we analyze the entropy of the channel model, using it as a metric to determine the usefulness of additional information. Specifically, the value of additional information is measured by how much this information affects the entropy.

3.2.1 Channel Power Knowledge

Let us start by analyzing the simplest case: we model the UWB channel under the assumption that the sole information available is the knowledge that the finite channel has energy P. Based on the MaxEnt principle, we want to derive a consistent model that represents the power delay spectrum of the channel.

The power delay spectrum $S(\tau)$ is

$$S(\tau) = \frac{1}{N}\sum_{k=0}^{N} R[k]e^{j2\pi\tau k}, \tag{3.2}$$

where $\tau = \frac{\hat{\tau}}{T_s}$ is the normalized delay, the ratio of the delay in seconds $\hat{\tau}$ and the inverse of the frequency resolution $T_s = \delta_f^{-1}$.

The power carried by the channel is then

$$P = \int_{-\frac{\tau_{\max}}{2}}^{\frac{\tau_{\max}}{2}} S(\tau)d\tau. \tag{3.3}$$

Due to the fact that no information is given about the random process, we assume that $\mathbf{h}$ is a Gaussian random process, because this is the random process that has the highest entropy, resulting in a entropy of the channel response given by

$$\mathcal{H} = \log(\pi e) + \int_{-\frac{1}{2}}^{\frac{1}{2}} \log(S(\tau) + \epsilon)d\tau, \tag{3.4}$$

where ϵ is an arbitrarily small positive constant ($\epsilon > 0$) used to regularize the non-regular Gaussian process [14].

Applying the MaxEnt principle under the constraint that the power is known for a

given delay interval $\tau_{\max}$, we want to choose $R[k]$ (or equivalently, $S(\tau)$) to maximize (3.4) under the constraint of (3.3). Taking the Lagrangian results in the expression

$$\mathcal{L} = \mathcal{H} - \mu_0 \left(\int_{-\frac{\tau_{\max}}{2}}^{\frac{\tau_{\max}}{2}} S(\tau) d\tau - P \right), \tag{3.5}$$

where μ_0 is a Lagrange multiplier. Deriving the expression with respect to $R[k]$, we obtain

$$\begin{aligned}
\frac{\partial \mathcal{L}}{\partial R[k]} &= \int_{-\frac{1}{2}}^{\frac{1}{2}} \frac{1}{S(\tau)+\epsilon} \frac{\partial S(\tau)}{\partial R[k]} d\tau - \frac{\mu_0}{N} \int_{-\frac{\tau_{\max}}{2}}^{\frac{\tau_{\max}}{2}} e^{j2\pi\tau k} d\tau = 0 \\
&= \int_{-\frac{1}{2}}^{\frac{1}{2}} \frac{e^{j2\pi\tau k}}{S(\tau)+\epsilon} d\tau - \frac{\mu_0}{j2\pi k N} \left[e^{j2\pi k\tau} \right]_{-\frac{\tau_{\max}}{2}}^{\frac{\tau_{max}}{2}} = 0 \\
&= \int_{-\frac{1}{2}}^{\frac{1}{2}} \frac{e^{j2\pi\tau k}}{S(\tau)+\epsilon} d\tau - \frac{2\tau_{max}\mu_0}{N} \mathrm{sinc}(2\tau_{\max} k) = 0 \\
&\rightarrow \int_{-\frac{1}{2}}^{\frac{1}{2}} \frac{e^{j2\pi\tau k}}{S(\tau)+\epsilon} d\tau = \frac{2\tau_{\max}\mu_0}{N} \mathrm{sinc}(2\tau_{\max} k).
\end{aligned} \tag{3.6}$$

Define

$$Q(\tau) = \frac{1}{S(\tau)+\epsilon}, \tag{3.7}$$

and

$$q_k = \int_{-1/2}^{1/2} Q(\tau) e^{j2\pi k\tau} d\tau. \tag{3.8}$$

Applying (3.7) to (3.6), we have that

$$\int_{-\frac{1}{2}}^{\frac{1}{2}} Q(\tau) e^{j2\pi\tau k} d\tau = \frac{2\tau_{\max}\mu_0}{N} \mathrm{sinc}(2\tau_{\max} k) \tag{3.9}$$

$$q_k = \frac{2\tau_{\max}\mu_0}{N} \mathrm{sinc}(2\tau_{\max} k). \tag{3.10}$$

Thus,

$$Q(\tau) = \sum_{k=-\infty}^{\infty} \frac{2\tau_{\max}\mu_0}{N} \mathrm{sinc}(2\tau_{\max} k) e^{-j2\pi k\tau} = \frac{\mu_0}{N} \mathrm{rect} \frac{\tau}{2\tau_{\max}}, \tag{3.11}$$

where $\mathrm{rect}(\cdot)$ is the rectangular function.

Consequently, $S(\tau)+\epsilon$ results in a constant that does not depend on τ, but only on the interval $\{-\frac{\tau_{\max}}{2}, \frac{\tau_{\max}}{2}\}$. Applying the constraint (3.3), we obtain

$$S(\tau) = \begin{cases} \frac{P}{\tau_{\max}}; & \frac{-\tau_{\max}}{2} \leq \tau \leq \frac{\tau_{\max}}{2} \\ 0 \quad ; & \text{elsewhere.} \end{cases}$$

and

$$R[k] = \frac{P}{\tau_{\max}} \text{sinc}(k\pi\tau_{\max}), \quad \forall k. \tag{3.12}$$

In other words, if there is no knowledge except the maximum delay, the MaxEnt model is one with an infinite number of multipaths and with the power equally divided across the different paths. The methodology can be easily extended if the modeler knows the bandwidth (which determines the number of correlation coefficients $R[k]$).

3.2.2 Partial Autocorrelation Sequence Knowledge

Let us assume now that the available knowledge is captured through measurements and defined as a finite number of frequency autocorrelation coefficients. The number of coefficients is determined by the number of frequency samples N. Based on this knowledge, we want to derive a model to characterize this state of information without taking into account any other constraint, extrapolating the missing autocorrelation coefficients that may exist but are not known.

Using the same methodology as in the previous section, the following theorem due to Burg [14] is considered:

Theorem 3.1. *The maximum entropy rate stochastic process $\{h[i]\}_{i\in\mathbb{Z}}$ that satisfies the constraints*

$$\mathbb{E}\{h[i]h^*[i+k]\} = R[k], \quad \textit{for} \quad k = 0, 1, ..., N, \quad \forall\ i, \tag{3.13}$$

is the N-th order Gauss-Markov process of the form

$$h[i] = -\sum_{k=1}^{N} a_k h[i-k] + Z[i], \tag{3.14}$$

where Z is i.i.d. $\sim N(0,\sigma^2)$ and $a_1, a_2, ..., a_N, \sigma^2$ are chosen to satisfy Equation (3.13).

A process satisfying (3.14) is also called an (AR) process of order N. The coefficients

$(a_1, a_2, ..., a_N, \sigma^2)$ are obtained by solving the Yule-Walker equations:

$$R[0] = -\sum_{\ell=1}^{N} a_\ell R[-\ell] + \sigma^2, \tag{3.15}$$

$$R[k] = -\sum_{\ell=1}^{N} a_\ell R[k-\ell], \quad l = 1, 2, ..., N. \tag{3.16}$$

Fast algorithms such as the Levinson and Durbin algorithm [35] have been devised which exploit the special structure of these equations to efficiently calculate the coefficients a_ℓ from the autocorrelation coefficients $(R[0], ..., R[N])$. The power delay spectrum of the N-th order Gauss-Markov process (3.14) is

$$S_N(\tau) = \frac{\sigma^2}{\left|1 + \sum_{\ell=1}^{N} a_\ell e^{-i2\pi\ell\tau}\right|^2}. \tag{3.17}$$

As previous mentioned, we are interested in the channel model's entropy to analyze the utility of additional data. This entropy can be found as a function of the coefficients $(a_1, a_2, ...a_N)$.

In general, from a finite set of L measurements of the vector channel response $\{\mathbf{h}_1, ..., \mathbf{h}_L\}$, there are many ways to estimate the spectral autocorrelation coefficients. Herein, the estimated autocorrelation function is defined as

$$\hat{R}_N[k] = \frac{1}{L}\frac{1}{N-k}\sum_{l=1}^{L}\sum_{i=1}^{N-k} h_l[i]h_l^*[i+k], \quad k \geq 0. \tag{3.18}$$

Assuming that we want to estimate the AR coefficients $\hat{a}_k^{(N)}$ and the power delay spectrum $\hat{S}_N(\tau)$ based only on some elements of the autocorrelation function $\hat{R}_N[k]$, *i.e.*, M elements of the autocorrelation function $(\hat{R}_N[1], \hat{R}_N[2], ..., \hat{R}_N[M])$, which is only a fraction of the whole information carried by channel $(M < N)$. The entropy that should be maximized is given by:

$$\mathcal{H}_M = \log(\pi e) + \int_{-\frac{1}{2}}^{\frac{1}{2}} \log\left(\frac{\sigma^2}{\left|1 + \sum_{k=1}^{M} a_k^{(M)} e^{-i2\pi k\tau}\right|^2}\right) d\tau. \tag{3.19}$$

The non-zero roots of the power delay spectrum (3.17) determine the number of

distinguishable multipaths. Practically, although the roots may exist, some may not be significant and therefore may be unnecessary to model. In order to assess the number of significant modeling coefficients, we performed some measurements to analyze how the autocorrelation sequence affects the entropy $\mathcal{H}_N$, and to identify the number parameters M required to achieve a good description of the power delay spectrum $S(\tau)$.

3.3 Measurements

The measurements were carried out in the Mobile Communications Laboratory of Eurecom, which is a typical laboratory environment, rich in reflective and diffractive objects (radio frequency equipment, computers, tables, chairs, metallic cupboard, glass windows, *etc.*). The measurement device employed was a wideband vector network analyzer (VNA) which allows complex transfer function parameter measurements in the frequency domain, extending from 10MHz to 20GHz. This instrument has low inherent noise, less than -110dBm for a measurement bandwidth of 10Hz, and high measurement speed, less than 0.5ms per point. The maximum number of equally-spaced frequency samples (amplitudes and phase) per measurement was 2001. The measurement data were acquired and controlled remotely using the RSIB[2] interface permitting off-line signal processing and instrument control in MATLAB.

In order to perform true wideband measurements with sufficient resolution, we performed different measurements in several bands. The measurements were performed from 3GHz to 9GHz by concatenating three groups of 2001 frequency samples per 2GHz sub-bands ($3-5$GHz,$5-7$GHz,$7-9$GHz). This yielded a 1MHz spacing between the frequency samples. Systematic and frequent calibration (remotely controlled) was employed to compensate for the undesirable frequency-dependent attenuation factors that might affect the collected data. The wideband antennas employed were omnidirectional in the vertical plane and have an approximate bandwidth of 7.5GHz (varying from 3.1GHz to 10GHz). They were not perfectly matched across the entire band, with a voltage standing wave radio (VSWR) varying from 2 to 5.

[2]RSIB is a Rhode & Schwarz defined protocol that uses TCP/IP protocol for communicating with their instruments.

3.3.1 Measurement environment

The data was collected at spatially different locations with measurements performed for both line of sight (LoS) and non line of sight (NLoS) setting. The latter was achieved by inserting a large obstacle between the transmitter and receiver in order to attenuate the LoS path.

For each of the two measurement scenarios, we acquired 400 different complex frequency responses. The experiment was set by fixing the transmitting antenna on a mast, one meter above the ground, on a vertical linear grid of 20 centimeters, close to the VNA. The receiving antenna was placed over a table located six meters from the transmitting antenna and moving along a horizontal linear grid of 50 centimeters. Both antennas moved in steps of five centimeters.

We illustrate in Fig. 3.1 and Fig. 3.2 the average power delay spectrum of the measurements performed in the LoS and NLoS scenarios, respectively. As expected, the LoS scenario is less dispersive than the NLoS scenario. Note that the delay of 20 nanoseconds corresponds to the distance between the transmitter and the receiver.

3.3.2 Data Processing

We will first analyze the measurement results. For each scenario, we need to estimate the correlation vector using Eq. (3.18). The result is shown in Fig. 3.3, where we illustrate the energy of the estimated correlation elements $R[k]$. We observe that in the LoS scenario, the degree of correlation across the system bandwidth is quite high, whereas the NLoS scenario presents a correlation that decreases very quickly with the increase of the coefficient indices k. This result was expected: it is due to the very strong direct path that exists in the LoS scenario.

Based on the estimated correlation vector, we can verify how the entropy (3.19) scales with the number of coefficients a_k of our AR model (3.17). The variation of $\hat{H}^N$ versus N is plotted in Fig. 3.4. We observe that the entropy increases with the number of AR coefficients for both scenarios. Remarkably, the results show that, for a given channel representation complexity (here, the entropy), there is a point at which increasing the number of parameters does not significantly increase the entropy. In other words, AR modeling based on a limited number of parameters is adequate. The number of parameters is direct related to the coherence bandwidth of the environment, which means that any information out of the coherence bandwidth range is considered useless on the channel model. For our measurements, the entropy becomes almost constant when more than twenty coefficients are known, which implies that for both scenarios,

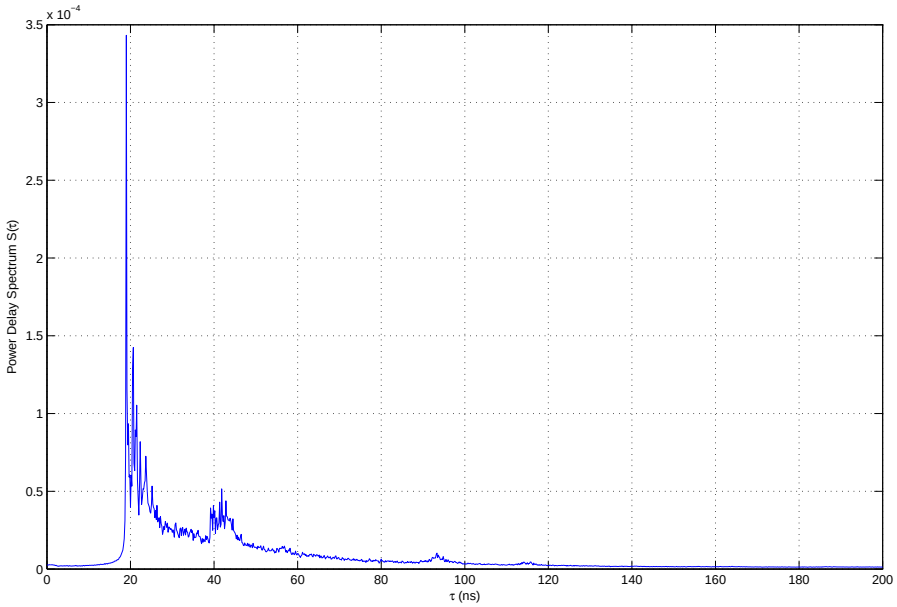

Figure 3.1: Estimated Power Delay Spectrum for the LoS scenario.

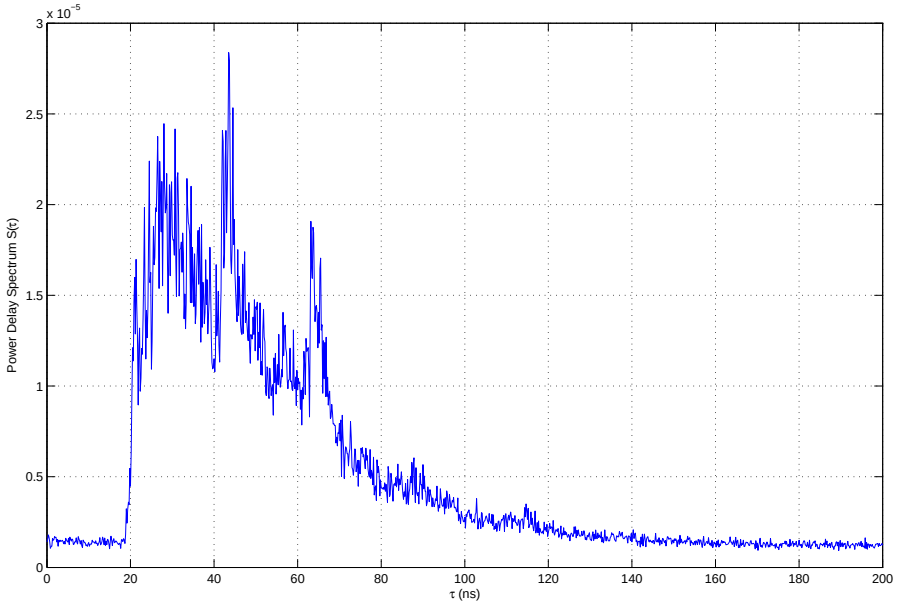

Figure 3.2: Estimated Power Delay Spectrum for the NLoS scenario.

the coherent bandwidth is around 20MHz.

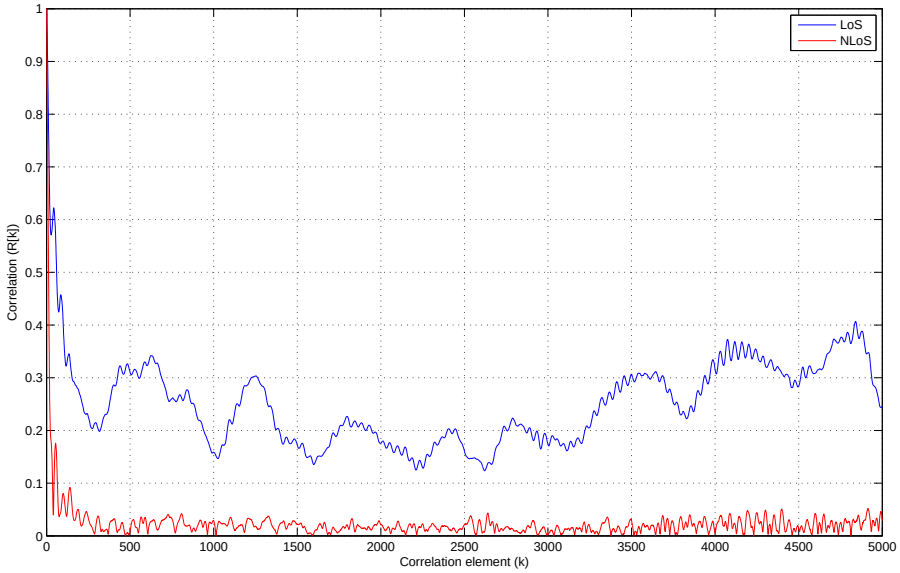

Figure 3.3: Estimated correlation coefficients.

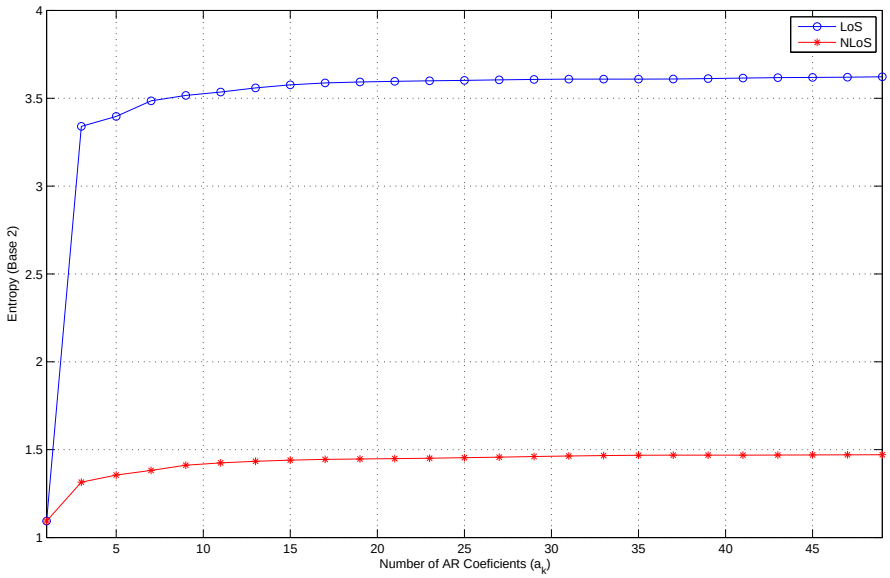

Figure 3.4: Entropy variation with respect to N.

3.4 Scaling of Channel Uncertainty

We observe that the coherence bandwidth of both scenarios is small relative to the whole UWB bandwidth. For this reason, our model could only represent our state of knowledge, and could easily identify the scaling law of the channel uncertainty, which defines the minimum number of variables required to describe the whole environment.

The scaling of channel uncertainty is directly related to the coherence bandwidth, due to the fact that any band that respects the coherence bandwidth can be modeled with our approach. Consequently, we could conclude that the channel uncertainty scales linearly with the bandwidth.

For example, if we would like to model the scenario previously presented, we would need to employ 50 parameters: 20 parameters to represent the correlation and 30 parameters to represent the random characteristic of the environment, which is due to the 30 independent frequency channels of bandwidth equal to the channel coherence bandwidth.

3.5 Summary

In this chapter, we modeled the ultra wideband channel based on the MaxEnt framework presented in Chapter 2. The idea is to provide a simple methodology to represent the UWB channel based on the available knowledge of the environment. The models are developed based on two types of prior knowledge: the channel power and the partial autocorrelation sequence.

When the channel power knowledge is the only information available, we observe that the best model (that is, the model that maximizes the entropy of the channel response estimation) is the model that spreads the power uniformly over the whole bandwidth. However, when a partial autocorrelation sequence is available, a more realistic model is derived based on Burg's theorem. By deriving the entropy of the channel model, we can analyze the performance as a function of the known data.

During the analysis, we evaluate the analytical expressions of the measurements carried out at Eurecom. We observed that each piece of information added will not have the same effect on the channel model and might complicate the model without bringing useful insights into the behavior of the propagation environment. In this respect, entropy is a useful measure and its slope characterizes how information scales with bandwidth. In particular, in wideband schemes, we have shown that it is possible to reproduce the channel frequency behavior with a limited number of coefficients since the channel uncertainty decreases due to the correlation. We have also provided a sound methodology

to model channels when additional constraints are given.

Chapter 4

Modeling the MIMO Channel

"Perfection is achieved, not when there is nothing more to add, but when there is nothing left to take away."

(Antoine de Saint-Exupéry)

In recent years, a large number of multiple-input multiple-output (MIMO) models for wireless communication have been proposed in the literature [4]. One of the most critical parameters identified by these models is the spatial correlation factor, which has been shown to have a very important influence on the channel capacity [64].

For this reason, we decided to study analytical models obtained through the MaxEnt principle introduced in Chapter 2. The principle enables the derivation of models when only limited information about the environment is available. MIMO models are obtained by assigning entropy-maximizing distributions to the unknown parameters – in particular, the spatial correlation – of the channel and marginalizing them out. The goal is to validate the models by comparing them with measured channels. Channel measurements were carried out with the Eurecom MIMO Openair Sounder (EMOS). The results presented in this chapter analyzes the corresponding probability density function of the channel matrix, which was shown to be described analytically by a function of the Frobenius norm.

4.1 Introduction

Recently, multiple-input multiple-output (MIMO) technology emerged as a promising option to provide high data rates without increasing the bandwidth or the transmit power [22, 72]. The results show that a significant increase in terms of data rates and link range are provided if multiple antennas are employed at the transmit and receive side [8, 23, 74]. The idea is to exploit the diversity inherent in the wireless channel to create orthogonal channels between the transmitter and receiver.

For this reason, a large number of models to represent the MIMO environment were proposed in the literature [4]. One of the most critical parameters identified by these models is the spatial correlation factor, which has been shown to have a very important influence on the MIMO performance [64].

In this chapter, we propose to analyze the MIMO channel from the MaxEnt perspective. Based on information about the statistics of the environment, we derive models that represent our state of knowledge. We start our approach by assuming that we know the average energy carried by the channel and we conclude that the model that represents our state of knowledge has channel gains chosen from Gaussian i.i.d. distribution. After that, we show that if we know the covariance matrix, the best model to represent our state of knowledge has channel gains chosen from a Gaussian distribution, but this time, the elements are correlated by the known covariance matrix. Finally, we introduce a new characterization of the environment, which is based on the rank of the covariance matrix. Then, we compare the results with some measurements, where we observe that knowledge of the rank can provide a better model to represent some characteristics of the environment.

4.2 Modeling MIMO Channels with MaxEnt

Considering a multiple antenna wireless system with n_t transmit antennas and n_r receive antennas, the MIMO received signal can be represented by

$$\mathbf{y} = \mathbf{H}\mathbf{x} + \mathbf{n}, \tag{4.1}$$

where $\mathbf{y}$, $\mathbf{x}$ and $\mathbf{n}$ denote respectively the received signal vector of size $(n_r \times 1)$, the transmitted signal vector of size $(n_t \times 1)$ and the additive white Gaussian noise (AWGN) vector of size $(n_r \times 1)$. $\mathbf{H}$ is a matrix of size $(n_r \times n_t)$ with complex entries that represents the MIMO channel in which each entry $h_{i,k}$ is the flat fading channel between

the transmit antenna k and the receive antenna i.

The entropy of the channel matrix can be expressed as

$$\mathcal{H} = \int_{\mathbb{C}^N} -p(\mathbf{H}) \log\left(p(\mathbf{H})\right) \mathrm{d}\mathbf{H} \tag{4.2}$$

where N is the total number of SISO channels, *i.e.*, $N = n_t n_r$, and

$$\mathrm{d}\mathbf{H} = \prod_{i=1}^{n_r} \prod_{k=1}^{n_t} \mathrm{d}h_{i,k}. \tag{4.3}$$

4.2.1 Average Channel Energy Knowledge

We start by analyzing the case where the sole knowledge available about the MIMO matrix is the finite average energy E carried by the channel [19]. Consequently, the constraints associated to the knowledge available are

$$\int_{\mathbb{C}^N} p(\mathbf{H})\mathrm{d}\mathbf{H} = 1, \tag{4.4}$$

$$\int_{\mathbb{C}^N} |\mathbf{H}|_F^2 \, p(\mathbf{H})\mathrm{d}\mathbf{H} = E, \tag{4.5}$$

where

$$|\mathbf{H}|_F^2 = \sum_{i=1}^{n_r} \sum_{k=1}^{n_t} |h_{i,k}|^2 . \tag{4.6}$$

Based on the constraints, we form the Lagrangian functional

$$\begin{aligned} \mathcal{L} = & -\int_{\mathbb{C}^N} p(\mathbf{H}) \log\left(p(\mathbf{H})\right) \mathrm{d}\mathbf{H} + \mu_0 \left[1 - \int_{\mathbb{C}^N} p(\mathbf{H})\mathrm{d}\mathbf{H}\right] \\ & + \mu_1 \left[E - \int_{\mathbb{C}^N} |\mathbf{H}|_F^2 \, p(\mathbf{H})\mathrm{d}\mathbf{H}\right], \end{aligned} \tag{4.7}$$

where μ_0 and μ_1 are Lagrange multipliers. Taking the Lagrangian functional derivative with respect to $p(\mathbf{H})$ and equaling to zero, results [21] in

$$\frac{\partial \mathcal{L}}{\partial p(\mathbf{H})} = -\log\left(p(\mathbf{H})\right) - 1 - \mu_0 - \mu_1 |\mathbf{H}|_F^2 = 0, \tag{4.8}$$

$$\rightarrow \quad p(\mathbf{H}) = \exp\left(-\mu_0 - 1 - \mu_1 |\mathbf{H}|_F^2\right). \tag{4.9}$$

The Lagrange multipliers must agree with the constraints, resulting in a final distri-

bution given by

$$p(\mathbf{H}|E) = \left(\frac{N}{\pi E}\right)^N \exp\left(-\frac{N\,|\mathbf{H}|_F^2}{E}\right) \tag{4.10}$$

$$\rightarrow \quad p(h_{i,k}|E) = \frac{N}{\pi E}\exp\left(-\frac{N\,|h_{i,k}|^2}{E}\right) = \mathcal{N}\left(0, \frac{E}{N}\right) \tag{4.11}$$

where $\mathcal{N}(0, \sigma^2)$ represents the pdf of a complex Gaussian variable with zero mean and variance σ^2.

Interestingly, the entropy maximization leads to a complex Gaussian distribution with zero mean and variance $\frac{E}{N}$, which is a very common assumption. Moreover, the result (4.10) implies that the entries are independent, which can be seen as a consequence due to the lack of information available during the modeling process. Any type of correlation between the entries represents a decrease on the entropy, which goes against the MaxEnt approach.

4.2.2 Full Covariance Matrix Knowledge

Suppose now that the knowledge available for the modeling is the full covariance matrix defined by

$$\mathbf{Q} = \int_{\mathbb{C}^N} \text{vec}(\mathbf{H})\text{vec}(\mathbf{H})^H p(\mathbf{H}) d\mathbf{H}, \tag{4.12}$$

where $\text{vec}(\cdot)$ is the vec operator that vectorizes a matrix by stacking its columns. For sake of simplicity, let us denote the vector $\text{vec}(\mathbf{H})$ as $\mathbf{h}$. Then, the covariance matrix elements can be defined as

$$q_{i,j} = \int_{\mathbb{C}^N} h_i h_j^* p(\mathbf{h}) d\mathbf{h}. \tag{4.13}$$

Based on the constraints, we form the Lagrangian functional

$$\begin{aligned}\mathcal{L} &= -\int_{\mathbb{C}^N} p(\mathbf{h}) \log\left(p(\mathbf{h})\right) \mathrm{d}\mathbf{h} + \mu_0 \left[1 - \int_{\mathbb{C}^N} p(\mathbf{h}) \mathrm{d}\mathbf{h}\right] \\ &\quad + \sum_{i=1}^{n_t}\sum_{j=1}^{n_t} \psi_{i,j}\left[q_{i,j} - \int_{\mathbb{C}^N} h_i h_j^* p(\mathbf{h}) d\mathbf{h}\right]\end{aligned} \tag{4.14}$$

which lead us to the introduction of $1 + N^2$ Lagrange multipliers.

Let us denote Ψ the matrix formed by the Lagrange multipliers $\psi_{i,j}$. Applying the

MaxEnt principle, the derivative of the Lagrangian functional is

$$\frac{\partial \mathcal{L}}{\partial p(\mathbf{h})} = -\log\left(p(\mathbf{h})\right) - 1 - \mu_0 - \mathbf{h}^H \Psi \mathbf{h} = 0, \tag{4.15}$$

$$\rightarrow \quad p(\mathbf{h}) = \exp\left(-1 - \mu_0 - \mathbf{h}^H \Psi \mathbf{h}\right), \tag{4.16}$$

which, after the proper normalization of the Lagrange multipliers according to the constraints, results in a pdf given by

$$p(\mathbf{h}|\mathbf{Q}) = \frac{1}{\det(\pi \mathbf{Q})} \exp(-(\mathbf{h}^H \mathbf{Q}^{-1} \mathbf{h})). \tag{4.17}$$

Similar to the previous case, entropy maximization results in a complex Gaussian distribution. Note that the energy constraint is redundant since

$$\int_{\mathbb{C}^N} |\mathbf{H}|_F^2 \, p(\mathbf{H}) \mathrm{d}\mathbf{H} = \mathrm{tr}(\mathbf{Q}) \tag{4.18}$$

where $\mathrm{tr}(\cdot)$ is the trace operator. Furthermore, if the entries of the full channel vector are independent, only the diagonal elements of the covariance matrix are nonzero, which leads to the same result obtained when only the energy constraint was imposed (4.10).

4.2.3 Covariance Matrix Rank Knowledge

Let us now assume that the only knowledge available is the rank L of the covariance matrix. Based on the marginalization property of the maximum entropy approach, the joint probability function of the channel vector entries can be expressed as

$$p(\mathbf{h}) = \int_{\mathbb{C}} p(\mathbf{h}|\mathbf{Q}) p(\mathbf{Q}) \mathrm{d}\mathbf{Q}. \tag{4.19}$$

This approach allows us to infer on the joint pdf of the channel entries based on some knowledge about the covariance matrix $\mathbf{Q}$. However, we need to estimate $p(\mathbf{Q})$. For this, we employ the maximum entropy approach over the constraint that the energy of $\mathbf{Q}$ is known and equal to E, which results in

$$\begin{aligned} \mathcal{L} = & -\int_{\mathbb{C}^{N^2}} p(\mathbf{Q}) \log\left(p(\mathbf{Q})\right) \mathrm{d}\mathbf{Q} + \mu_0 \left[1 - \int_{\mathbb{C}^{N^2}} p(\mathbf{Q}) \mathrm{d}\mathbf{Q}\right] \\ & + \mu_1 \left[E - \int_{\mathbb{C}^{N^2}} \mathrm{tr}(\mathbf{Q}) p(\mathbf{Q}) \mathrm{d}\mathbf{Q}\right]. \end{aligned} \tag{4.20}$$

This Lagrangian functional is very similar to the one presented in (4.7), and leads

us to

$$p(\mathbf{Q}) = \exp\left(-\mu_0 - 1 - \mu_1 \int_{\mathbb{C}^{N^2}} \mathrm{tr}(\mathbf{Q})\mathrm{d}\mathbf{Q}\right) \quad (4.21)$$

$$= \exp\left(-\mu_0 - 1 - \mu_1 \sum_{i=1}^{L} \mathbb{E}\{\lambda_i\}\right), \quad (4.22)$$

where λ_i represents the ith eigenvalue of the matrix $\mathbf{Q}$.

Note that matrix $\mathbf{Q}$, due to its structure, is a positive semi-definite complex matrix. Furthermore, it is a symmetric matrix which allows the Takagi factorization, *i.e.*, $\mathbf{Q} = \mathbf{V}\mathbf{D}\mathbf{V}^T$, where $\mathbf{D}$ is a diagonal matrix containing the eigenvalues λ_i of $\mathbf{Q}$ and $\mathbf{V}$ is a unitary matrix with the corresponding eigenvectors. This implies that $\mathbf{Q}$ follows a Wishart distribution [1] and can be expressed after normalization as $p(\mathbf{Q}|E) \sim \mathcal{W}(L, E\ \mathbf{I}_L)$, being $\mathbf{I}_L$ the identity matrix of size $(L \times L)$, *i.e.*,

$$p(\mathbf{Q}|E) = \frac{\det(\mathbf{Q})^{-\frac{1}{2}} \exp\left[\mathrm{tr}\left(-\frac{1}{2}\Upsilon^{-1}\mathbf{Q}\right)\right]}{2^{\frac{L^2}{2}}\Gamma_L\left(\frac{L}{2}\det(\Upsilon)^{\frac{L}{2}}\right)} \quad (4.23)$$

where $\Upsilon = E\ \mathbf{I}_L$ and the multivariate gamma function is expressed as a product of univariate gamma functions [76] as

$$\Gamma_N(a) = \pi^{\frac{n(N-1)}{4}} \prod_{k=1}^{N} \left[a - \frac{k-1}{2}\right]. \quad (4.24)$$

Substituting (4.23) into (4.19), we obtain the pdf of the channel vector $\mathbf{h}$ under the assumption that the covariance matrix $\mathbf{Q}$ has rank L. It is shown in [30] that under these constraints, $p(\mathbf{h})$ can be described in terms of the Frobenius norm of $\mathbf{h}$. Then, the result is

$$p(\mathbf{h}) = \frac{p_L(|\mathbf{h}|_F^2)}{s_L(|\mathbf{h}|_F^2)} \quad (4.25)$$

where

$$s_L(x) = \frac{\pi^L x^{L-1}}{(N-1)!}, \quad (4.26)$$

$$p_L(x) = \frac{2}{x}\sum_{i=1}^{L}\left(-L\sqrt{\frac{x}{E}}\right)^{L+1} \frac{K_{i+L-2}\left(2L\sqrt{\frac{x}{E}}\right)}{[(i-1)!]^2(L-1)!}, \quad (4.27)$$

where K denotes the Bessel K-function [28] and ! is the factorial function.

Unlike the two previous cases, the pdf of the entries of the channel matrix here does not follow a complex Gaussian distribution. For this reason, we provide a methodology to generate channel matrices that come from the distribution described in (4.25):

- Generate a random $L \times L$ Gaussian i.i.d. circularly symmetric matrix $\mathbf{B}$.
- Create the covariance matrix $\mathbf{Q}$ based on the generated matrix $\mathbf{B}$, where $\mathbf{Q} = \frac{1}{L}\mathbf{B}\mathbf{B}^H$
- Generate a random $L \times 1$ Gaussian vector $\mathbf{k}$ (according to the Maximum Entropy principle), conditioned on covariance $\mathbf{Q}$, living in an L-dimensional vector space.
- Create the vector $\mathbf{h}$ by mapping the vector $\mathbf{k}$ into the original N-dimensional subspace. This is done by applying a random unitary transformation $\mathbf{U} \in \mathcal{U}(\mathbf{N})$ to $\tilde{\mathbf{k}} = [\mathbf{k}\ 0 \dots 0]^T$, *i.e.*, $\mathbf{h} = \mathbf{U}\tilde{\mathbf{k}}$.

For validation purposes, we show in Fig. 4.1 the pdf generated by the analytical expression (4.25), labeled "Anlt.", and the pdf of the matrices created by the method described above, labeled "Simul.". We can see that for the three simulated cases (L = {1,4,8}), both pdf are the same.

4.3 Evaluating the Models

We have shown in the preceding section how we can create models of the pdf of the channel matrix entries when some information about the channel is available. Using the MaxEnt framework, analytical expressions were derived to represent three different states of knowledge: average channel energy, full covariance matrix and rank of the full covariance matrix. The two first cases (4.10) and (4.17) results in complex Gaussian distributions and justify the conventional assumption that MIMO channels could be represented by complex Gaussian matrices. However, when the knowledge available is the rank of the full covariance matrix, the pdf is expressed in a more complicated expression (4.25-4.25). For this reason, we propose in this section to evaluate if the full covariance matrix rank can be used to characterize the MIMO channel environment.

The evaluation is carried based on (4×2) MIMO measurements. The analysis is performed based on the probability distribution of the singular values of the MIMO matrix. The singular values have been shown to be direct related to the performance of the MIMO system [72]. To identify them, we employ the singular value decomposition

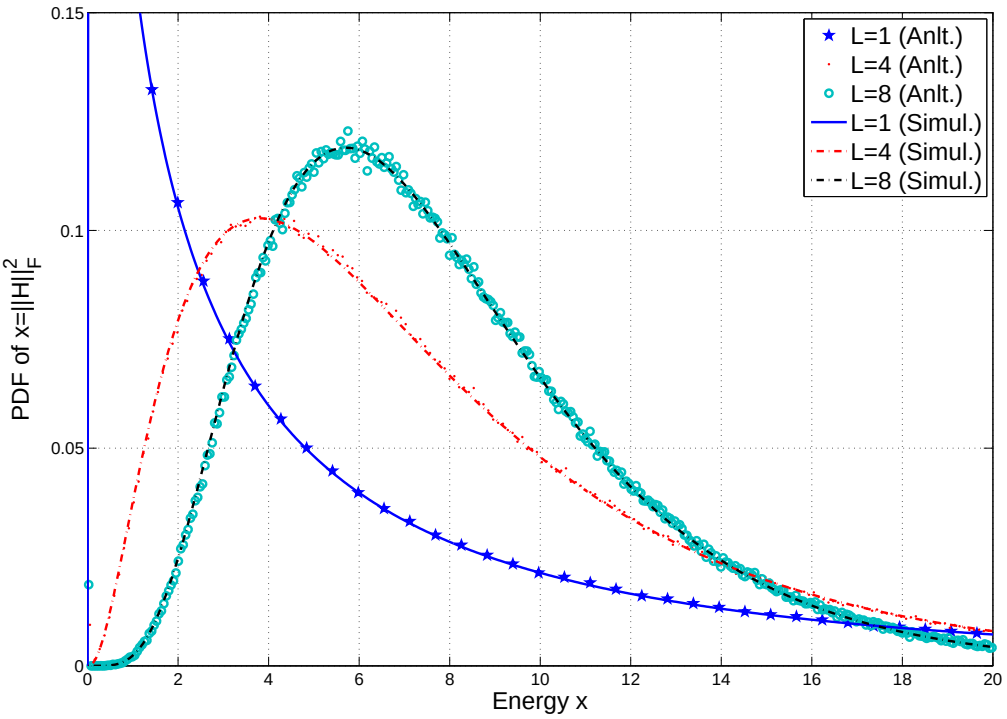

Figure 4.1: The pdf of the limited-rank covariance distribution for $n_t = 4$ and $n_r = 2$ with $E = 8$).

(SVD). SVD is a factorization that holds for any rectangular real or complex matrix and is presented in Theorem 4.1.

Theorem 4.1 (SVD Decomposition)**.** *Consider a* $(N \times K)$ *matrix* $\mathbf{H}$ *whose entries are either the field of real number of the field of complex number. Then, there exists a factorization of the form*

$$\mathbf{H} = \mathbf{U}\mathbf{D}\mathbf{V}^H$$

where $\mathbf{U}$ *is a* $(N \times N)$ *unitary matrix,* $\mathbf{D}$ *is a* $(N \times K)$ *diagonal matrix with nonnegative elements on the diagonal, and* $\mathbf{V}$ *is a* $(K \times K)$ *unitary matrix. Such a factorization is called singular value decomposition, being the nonnegative elements of matrix* $\mathbf{D}$ *the singular values of matrix* $\mathbf{H}$*.*

The idea is to analyze the singular value distribution and sees if it better characterized by the Gaussian i.i.d. model or by the model generated assuming a limited full covariance matrix rank. For such approach, we generate matrices based on the Gaussian i.i.d. model

Table 4.1: Measurement Characteristics

Parameter	Value
Center frequency	1907.6 MHz
Bandwidth	5 MHz
Base-Station Tx Power	34 dB
Number of Tx Antennas	4
Number of Rx Antennas	2

or by different values of the full covariance matrix rank and estimate the singular value distribution of these matrix when a power constraint is imposed. Once we estimate these distributions, we verify the best representation based on the relative entropy presented in Section 2.2.

4.3.1 Measurements

In order to analyze a real MIMO channel, we employed the Eurecom OpenAir platform [53]. Developed by the Mobile Department of Eurecom, the platform is composed of terminals that can operate with up to four transmit antennas and two receive antennas, allowing real-time radio signal processing, agile RF acquisition and channel sounder campaigns. For this last part, we developed together with the rest of the team a channel sounder called Eurecom MIMO Openair Sounder (EMOS) [15]. The main idea behind EMOS is to carry out real MIMO channel measurements on a real-time basis, without requiring the user to save large amounts of data to estimate the channel impulse responses (CSI), unlike [47]. For more details, we present in Appendix A the processing stages implemented in the EMOS.

The measurements were carried out on an outdoor scenario in the neighborhood of the Eurecom's building. The scenario is characterized by a semi-urban hilly environment, composed of short buildings and vegetation. The base-station antenna was situated in one of the highest buildings in the area that has a direct view of the surroundings. The main radio characteristics adopted for the measurement are listed in Table 4.1.

For the analysis, four different campaigns were performed, all of them in different places around the Eurecom building without any direct LoS. Due to the interest in the MIMO characterization of the environment and the requirement of a large amount of channel estimations, we assume that the environment properties were the same for the whole transmitted bandwidth during a large interval of time. This is the only method that we found which would allow us to have enough channel estimations to derive a pdf that represents the environment.

4.3.2 Comparing the pdf of the Singular Values

The first part of the analysis was to estimate the pdf of the singular values for the Gaussian i.i.d. case and the case where the covariance matrix rank is known. We assume that the MIMO channel matrices were normalized, providing average power equal to $E = \sqrt{n_t}$. Furthermore, the pdf of the singular values were jointly analyzed, meaning that the pdf is a two dimension function that depends on the values of the two singular values (s_1, s_2).

In Fig. 4.2, we plot the joint pdf distributions based on the channel matrix that satisfy the constraints presented in Section 4.2.1 and Section 4.2.3. We can observe that although the matrices carry exactly the same expected energy, the pdfs of of the models created with low covariance matrix rank are highly concentrated in small values of (s_1, s_2).This implies that decreasing the rank of the covariance matrix has the effect of increasing the correlation between the singular values. On the other hand, when the rank of the full covariance matrix increases, the pdf of the singular values becomes more similar to the Gaussian i.i.d. case. However, even when the covariance matrix is full-rank, there still is a difference between it and the pdf of the Gaussian i.i.d. case.

Considering the measurements, we decided to analyze the four scenarios separately and also when we consider all scenarios as one single scenario. Then, we employ the relative entropy to identify the best singular value pdf to represent each campaign. We present in Table 4.2 the relative entropy results of each measurement with respect of the pdf presented by the different models derived in this chapter. Based on the results, we observe that none of the measurements are well represented by the Gaussian i.i.d. case. Actually, even when we considered the data from all scenarios, the best model to represent the environment is for the case where the rank of the full covariance matrix is assumed to be 6.

Table 4.2: Relative Entropy Result

	All data	Campaign 1	Campaign 2	Campaign 3	Campaign 4
$L = 1$	1.8218	2.1269	0.6270	1.4901	2.1269
$L = 2$	1.3698	1.7169	0.3280	1.0626	1.7169
$L = 3$	1.3329	1.6343	0.2346	0.9794	1.6343
$L = 4$	1.1251	1.4697	**0.2241**	**0.8778**	1.4697
$L = 5$	1.2487	1.5555	0.2704	0.9382	1.5555
$L = 6$	**1.0927**	1.3875	0.3915	0.8782	1.3875
$L = 7$	1.1566	**1.3672**	0.6082	0.8859	**1.3672**
$L = 8$	1.2059	1.4709	0.8018	0.9483	1.4709
Gaussian i.i.d.	2.6638	2.4502	5.6192	1.8646	2.4502

4.4 Summary

In this chapter, we modeled the MIMO channel based on the MaxEnt framework introduced in Chapter 2. The idea is to provide models that could represent our state of knowledge of the MIMO environment. Consequently, three models were developed based on three different states of knowledge: average energy of the channel, full covariance of the channel matrix and the rank of the covariance matrix.

We have shown that when the average channel power is known, the MaxEnt framework lead us to Gaussian i.i.d. distributions of the channel entries. The second case, when we assumed that the full covariance matrix is known, we also obtained a Gaussian distribution, but this time the entries of the channel matrix are not independent, and the distribution depends on the parameters of the covariance matrix. However, the covariance matrix requires a lot of knowledge about the environment, and even in the same scenario, different positions will usually result in different covariance matrix. For this reason, we decided to generalize the covariance knowledge, and we assumed that only the information about the rank of the covariance matrix is known. By using the marginalization property of the MaxEnt approach, we derived a new distribution that depends only on the rank of the covariance matrix. This idea results in a new metric to characterize the MIMO environment and represents our state of knowledge based only in few parameters.

For comparison purposes, we decided to evaluate the distribution of the singular values of the channel matrix. We concluded that the rank of the covariance matrix completely changes the behavior of the singular value distribution. Finally, we showed some results based on measurements performed at Eurecom. We verified what is the best model to characterize the measurements and we concluded that all the measurements could be better characterized by assuming the knowledge of the covariance matrix rank.

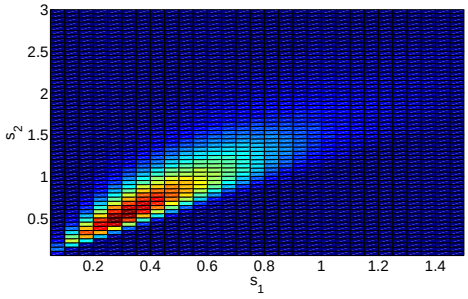

(a) MaxEnt channel when L is 2.

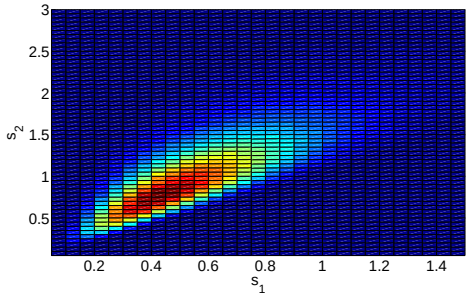

(b) MaxEnt channel when L is 3.

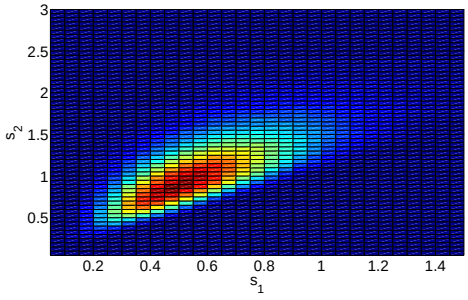

(c) MaxEnt channel when L is 4.

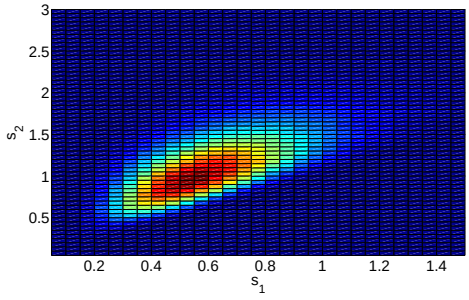

(d) MaxEnt channel when L is 5.

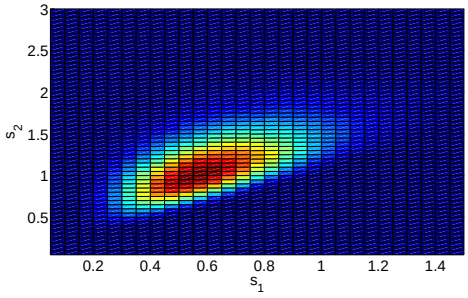

(e) MaxEnt channel when L is 6.

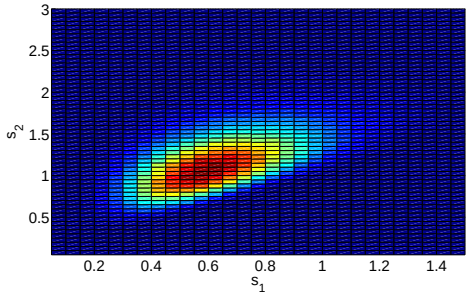

(f) MaxEnt channel when L is 7.

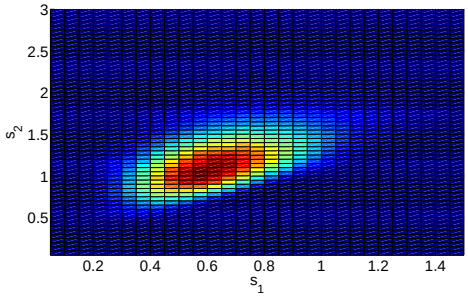

(g) MaxEnt channel when L is 8.

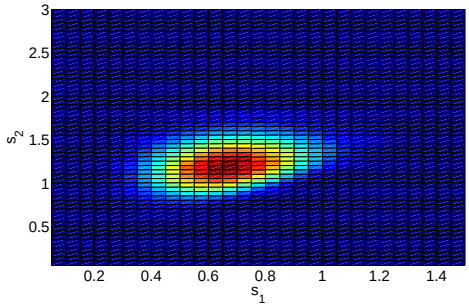

(h) Gaussian i.i.d. channel.

Figure 4.2: Joint pdf of (s_1, s_2) for a 4 x 2 MIMO channel.

Part II

Channel Division Multiple Access

Chapter 5

Channel Division Multiple Access (ChDMA)

"No problem can be solved from the same level of consciousness that created it."

(Albert Einstein)

Recent advances in wireless communications required not only a better understanding of the wireless environment but also a great improvement of the transceiver mechanisms. These mechanisms are extremely important to cope with the random characteristics of the channel to guarantee multi-user communication.

In this chapter we present an overview of the methods used to access the channel and we introduce a very simple multiple access scheme to UWB systems. First, we discuss the fundamental concepts behind multiple access and present the classical schemes. Then, we briefly describe the UWB system, which may be used in future for indoor short-range high data-rate networks. We observe that none of the multiple access schemes were designed to be employed in a low duty cycle regime and so we introduce channel division multiple access (ChDMA) as an option. We conclude that ChDMA is a promising multiple access scheme that simplifies the transmitter complexity when multi-user UWB is employed and exploits the natural diversity of the wireless environment to provide multi-user communication.

5.1 Fundaments of Multiple Access Techniques

Multiple access is a fundamental requirement of many wireless systems. It allows different terminals to share system resources. Basically, the schemes define the terminals' policies to allocate common resources and transmit without interfering too much with the whole system.

There are several different ways to allow multiple users to communicate on the same channel [34, 56, 80], however only schemes from a selected group of multiple access techniques, called circuit switched methods, provide a solution to allow "simultaneous" communications[1]. These methods define how the system resources should be shared to guarantee the communication of several users over the same wireless channel. The name circuit switched comes from the fact that system resources are allocated in such a way that all terminals seem to be physically connected by electrical circuits.

In the following, we present an overview of the four classical multiple access schemes: frequency division multiple access (FDMA), time division multiple access (TDMA), spatial division multiple access (SDMA) and code division multiple access (CDMA). More information can be found in [34, 56, 80, 27].

5.1.1 Frequency Division Multiple Access (FDMA)

FDMA was designed to exploit the frequency domain for multiple access. The available system bandwidth is subdivided into several non-overlapping frequency channels to allow simultaneous communications. The FDMA principle is similar to the basic principle that is currently used to allocate the radio spectrum by assigning different frequency bands to different systems. To mitigate interference that may appear from imperfect filtering, guard bands are employed between adjacent channels. The FDMA scheme is illustrated in Fig. 5.1(a).

This scheme was the most common multiple access technique for analog communication systems [27] and today it is still used in a large variety of systems. However, FDMA suffers from a hard constraint on the number of users. The scheme only offers a fixed number of orthogonal channels and the number of transmitting users in the system cannot exceed the number of channels. Furthermore, guard bands are required to protect transmitted signals from adjacent channel interference, implying in a significant loss of

[1]The term simultaneous communication is employed hereafter both for systems when the users transmit at exactly the same time or if they share a fixed window of time to perform their transmission.

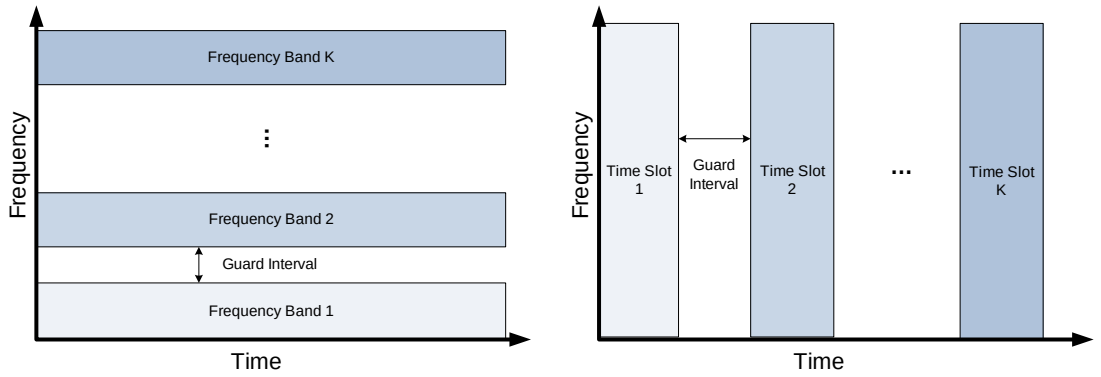

(a) FDMA Scheme. (b) TDMA Scheme.

Figure 5.1: Multiple access schemes.

precious bandwidth. For this reason, this technique is usually combined with a second multiple access scheme to allow more simultaneous connections.

5.1.2 Time Division Multiple Access (TDMA)

Where FDMA divides the channel into small frequency bands, TDMA divides it into small time slots to create non-overlapping access channels. The users take turns accessing the channel in different time slots, in a round-robin fashion. Only one user uses the channel at any given moment, but each user has a slot to transmit. TDMA also requires guard intervals to mitigate system imperfections, synchronism problems and interference between adjacent channels. Fig. 5.1(b) illustrates the TDMA scheme.

This scheme is employed in many wireless systems due to its flexibility to allow a large number of simultaneous communications by increasing dynamically the number of time slots. Nevertheless, increasing the number of users decreases the user's symbol rate. Furthermore, TDMA also suffers from reduced efficiency due to guard interval requirements, even if very complex receiver equalizers are employed.

5.1.3 Space Division Multiple Access (SDMA)

SDMA is a more recent scheme that exploits the ability of multi-antenna architectures to format beams in specific spatial directions. This allows multiple communications to be simultaneously held over the same frequency band and during the same time slot as illustrated in Fig. 5.2.

This scheme is an option when multi-antenna arrays are employed in one or both

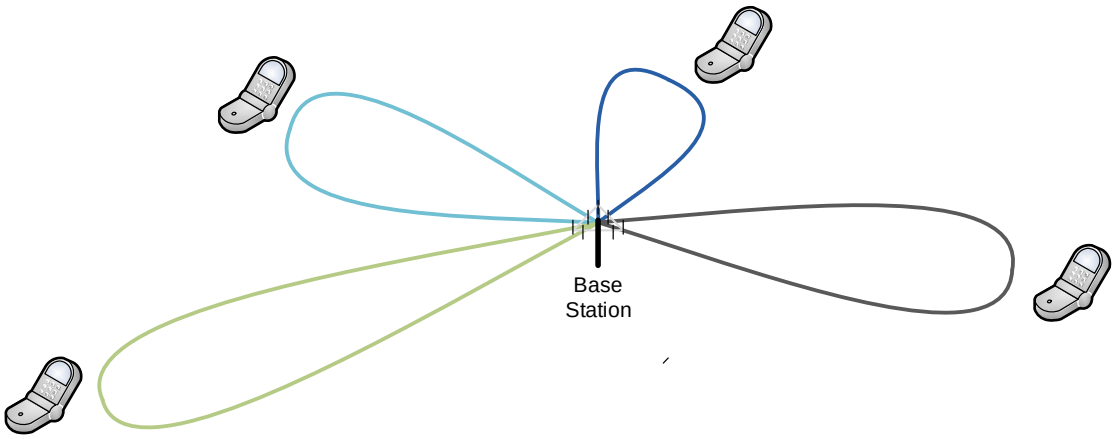

Figure 5.2: Space division multiple access scheme.

sides of the wireless communication systems. As transceivers have evolved and with the introduction of multibeam antennas and MIMO systems, SDMA has become an efficient multiple access scheme that provides diversity and multiplexing gains.

However, SDMA suffers from several restrictions. The number of beams simultaneously created is directly related to the number of antennas employed at the array, which means that implementing such scheme is expensive. Additionally, the beams created by such an approach are not perfect and the efficiency of the scheme depends on the relative positions of the terminals or the correlations between their channels.

5.1.4 Code Division Multiple Access (CDMA)

CDMA is a technique that relies on the use of codes to guarantee separability between simultaneous communications over the same frequency band. The codes are designed to provide an acceptable degree of separability between simultaneously transmitted signals while all terminals share exactly the same system resources. Additionally, CDMA can provide secure communication and robustness against natural interference and jamming.

It is a very flexible multiple access scheme whose properties are related to the code set employed by the system. The framework is general enough to enable the use of codes that explore simultaneously all domains of the communication systems (frequency, time and space). For this reason, CDMA can be designed so that codes could mimic the characteristics of all previously presented schemes.

CDMA was originally developed for military and police communications because the transmissions are hard to detect (low probability of detection (LPD) and low probability

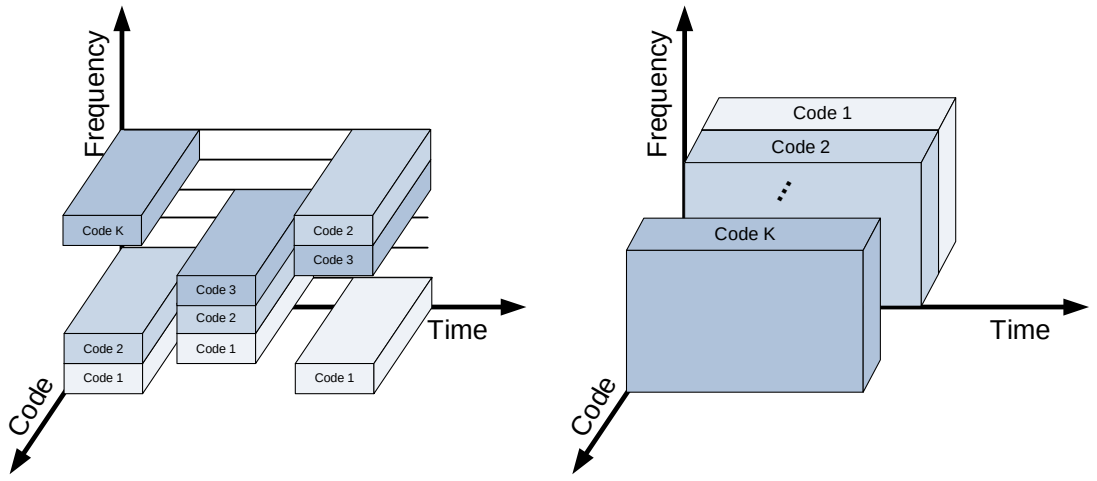

(a) FH-CDMA Scheme. (b) DS-CDMA Scheme.

Figure 5.3: Code division multiple access scheme.

of interception (LPI)). Even if the signal is detected, it is still very hard to decode without knowing the codes. Below, we present a brief list of some special types of CDMA:

Frequency Hopping (FH): FH-CDMA is scheme where users encode their information by switching among different frequency channels. The users simultaneously transmit their signals but each terminal employs a different frequency jumping sequence known only by the transmitter and the receiver. This technique can be seen as a hybrid multiple access scheme that simultaneously exploits the advantages of FDMA and TDMA, while also providing secure communication. It is mainly used by the army.

Direct Sequence (DS): DS-CDMA is a scheme where terminals employ redundancy codes to create diversity at the receiver, allowing it to detect and separate simultaneously transmitted signals over the same channel. This scheme is also known as direct sequence spread spectrum (DSSS) due to the fact that the code spreads the signal across a wider bandwidth. Codebooks can be designed to ensure the separability of different transmitted signals at the receiver.

Multi Carrier (MC): MC-CDMA is an orthogonal frequency division multiplexing[2]

[2]OFDM [32] is a multiplexing technique that allows the transmitter to simultaneously send different signals over the same channel.

(OFDM) system where each user transmits its symbol over all the subcarriers, phase shifted, according to the users' code. It was designed to provide multiple access in OFDM-based systems. The advantage of this technique is that information sent by all users are spread over all bandwidth by employing the OFDM process providing a robust scheme even under high frequency selectivity.

Although CDMA can be seen as the ultimate multiple access scheme, it also presents limitations. To have a low degree of correlation between the user codes, the system must limit the number of possible simultaneously connected terminals. Code sets with good correlation properties are often highly sensitive to synchronization problems, resulting in the need of complex techniques like code waveform design, power control, forward error correction, automatic repeated request systems and multi-user detection to guarantee a good performance.

5.2 Ultra WideBand Systems

Recently, UWB communication has received a lot of attention because it could coexist with legacy systems while delivering very high data rates [2, 31, 54]. Foreseen as applicable for indoor short-range high data rate links (WLAN, WPAN, WSN, WBAN, RFID, *etc.*), UWB systems could have large capacity and be very flexible, making them attractive for applications such as localization, security, emerging automotive and home-based "location awareness."

The idea of UWB technology is to transmit signals across a much wider frequency band than conventional systems. A traditional UWB transmitter works by sending pulses across a very wide spectrum of frequencies, generally by employing pulses of few nanoseconds. By spreading its power across a broad spectrum, an UWB system improves rate speed and reduces interference with other wireless systems.

Standardized by the American Federal Communications Commission (FCC) and the International Telecommunication Union Radiocommunication Sector (ITU-R) as a system whose bandwidth exceeds the lesser of 500MHz or at least 20% of fractal bandwidth [2, 31, 54], in the United States, the FCC has mandated that UWB radio transmissions can legally operate in the range from 3.1 GHz up to 10.6 GHz, at a limited transmit power of -41dBm/MHz. Operating over a very wide bandwidth has many benefits, including the significant reduction of the fading effect, since the short-impulse nature of the UWB waveform prevents a significant overlap of the signals. Furthermore, the short duration of UWB pulses makes the system less sensitive to multi-path effects than narrow-band

systems because shorter pulses have much less opportunity to collide with their reflections, which is the usual cause of signal degradation [31]. For this reason, UWB is more advantageous in high dense indoor channels, even if it still suffers from some degradation due to the limited bandwidth. Some studies have demonstrated that UWB systems offer their greatest promise for very high data rates when the range is less than approximately 10m, due to the FCC's current power limitation on UWB transmissions.

It is common knowledge that increasing the bandwidth enables higher data rates. However, for limited power transmissions, the increase on the bandwidth represents higher noise power, which degrades the system performance. In 1949, Golay [26] showed that employing on-off keying (pulse position modulation) with very low duty cycles [3] mitigates the noise effect. In 1969, Kennedy [42] proved that over an infinite bandwidth Rayleigh fading multipath channel with perfect channel knowledge at the receiver, the use of frequency shift keying signals together with low duty cycle transmissions achieves maximum rate, the same as the infinite bandwidth non-fading additive white Gaussian channel with Gaussian signaling. In [73], Telatar and Tse extended the proof for multipath channels with any number of paths. Assuming no inter-symbol interference (ISI), they show that the achievable rate is

$$\gamma = \left(1 - 2\frac{T_d}{T_c}\right)\rho \tag{5.1}$$

where ρ is the signal to noise ratio (SNR) and T_d and T_c are, respectively, the delay spread and the coherence time interval. In particular, by transmitting at very low duty cycles, the capacity of the infinite-bandwidth AWGN channel can be achieved in a fading multipath channel with any number of paths. Consequently, low duty cycle signals are fundamental to cope with the wireless environment [55].

There are two methods to explore the UWB channel [2]: the single-band and the multiband. In the single band, all users employ the same pulse to transmit signals. Also known as impulse radio UWB (IR-UWB), the transmitted signal is spread over the whole UWB spectrum. In the multiband case , however, the spectrum is divides in channels of at least 500MHz. Then, users have to employ different pulses to access different wideband channels [5, 41], requiring more complex receivers. For this reason, we focus here on the IR-UWB method, which is still the most popular signaling scheme employed in UWB systems.

[3] Duty cycle represents the proportion of time during which the system is in an "active" state.

5.2.1 The Impulse Radio Signaling

The IR-UWB is one of the solutions to allow UWB communication [84]. In an IR-UWB system, the transmitters radiate low duty cycle waveforms formed from very short baseband electrical pulses with the duration of few hundred picoseconds. Such signals are free of sine-wave carriers and do not require the use of local oscillators or mixers, so IR-UWB transceivers are simpler and cheaper than conventional narrow-band transceivers. The system bandwidth is determined by the shape and duration of the pulse employed. Typically, Gaussian monocycle and Hermitian pulses [6] are employed.

Due to the high channel resolution of UWB systems, the multi-paths can be resolved, improving the signal's immunity to interference effects and robustness to multi-path fading. Moreover, for the same SNR, the coverage of UWB is larger than conventional narrow-band systems because its low frequency components have good penetration properties. This is one of the reasons that UWB technology is also largely used in radar applications [70, 71].

5.2.2 Multiple Access in IR-UWB

Despite the many aforementioned advantages, the issue of multiple access in IR-UWB systems has proved to be a challenge. There have not been any proposal to provide a multiple access scheme in the multi-user setting that benefit from low duty cycle transmissions. All techniques thus presented were developed to provide orthogonal communication channels to enable simultaneously connected terminals. However, all of those approaches were designed under almost ideal wireless environments, ignoring the multipath effect, which always exist in UWB systems.

Since wireless environments usually have many scatterers (reflectors and deflectors), the transmitted signal arrives at the receiver by different paths and with different delays. This makes wireless channels, in general, frequency selective, a property which, particularly for UWB systems, eliminates the advantages of the classical multiple access schemes:

FDMA: Since conventional systems IR-UWB have no carriers, they cannot employ FDMA. This multiple access scheme is considered only when multi-band UWB is employed, offering the possibility to have different users employing different pulses (shapes and length) [5, 41] to transmit.

TDMA: At a first glance, TDMA could be seen as a good option to solve IR-UWB's problem of multiple access. However, TDMA is highly sensitive to asynchronism,

which is inherent to IR-UWB communication. Furthermore, the high dispersion of the UWB channel requires large guard intervals between different user access, which cause low spectral efficiency.

SDMA: SDMA requires the use of antenna arrays, which means the use of multiple antennas on at least one side of the communication. This implies that the terminals must be bigger and more expensive, which goes against the goal of UWB communications.

CDMA: Although both, UWB and spread spectrum techniques, benefit from using a large bandwidth, they differ in how they achieve large bandwidth communication. In conventional spread spectrum techniques, information bits are broken into chips and the chips are modulated with either a fixed carrier frequency (DS-CDMA) or in a set of carrier frequencies (FH-CDMA). In IR-UWB communication, there is no carrier frequency and the short duration of the pulses directly generates the extremely wide bandwidth. Spread spectrum techniques can offer few MHz of bandwidth, while UWB pulses provide several GHz of bandwidth. This is due to the fact that transmissions without the use of low duty cycles, the data rate goes to zero for very high bandwidths [46]. Consequently, CDMA provides a very inefficient technique for UWB channels. Under low duty cycle regime, no code set has been proposed.

As stressed above, none of the classical multiple access schemes work with the carrier-free low duty cycle properties of IR-UWB. So we developed a novel scheme for multiple access for IR-UWB systems. In the following, we present a scheme that exploits the benefits of low duty cycle transmissions without adding guard intervals while still offering a low interference level between simultaneous communications. We achieve this by using the channels as user signatures.

5.3 Channel Division Multiple Access (ChDMA)

Channel division multiple access (ChDMA) is a scheme that provides a solution to multi-user access in low duty cycle systems [16, 17]. In this scheme, each user uses its channel to modulate the transmitted signal. As a result, the channels work as codes that can be exploited at the receiver to separate the signals transmitted by different users.

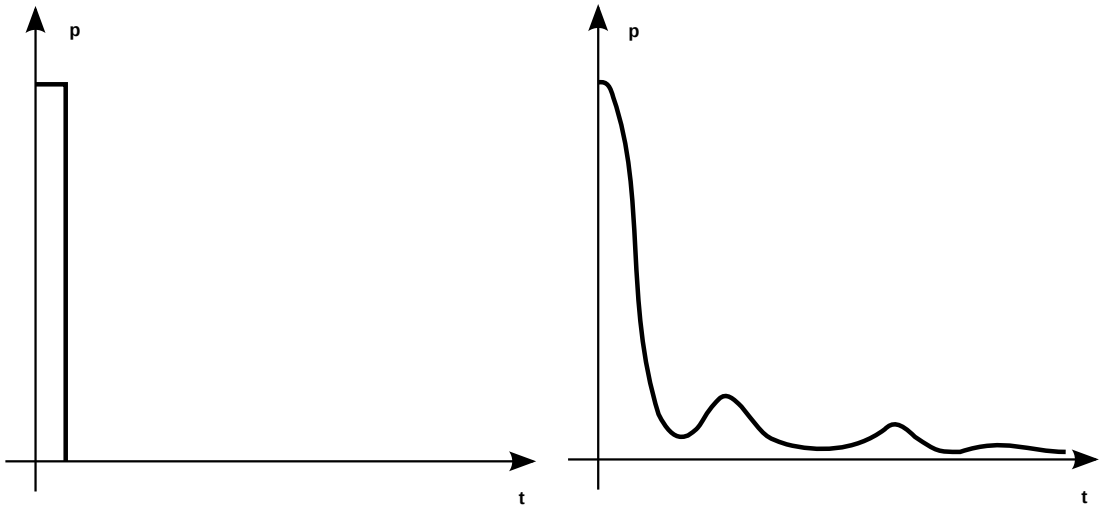

(a) Transmitted signal. (b) Received signal.

Figure 5.4: Channel division multiple access scheme.

5.3.1 The ChDMA Principle

The ChDMA scheme works because UWB channels have a large coherence time (typically about 100 μs) relative to their delay spread (typically around 15-40 ns, depending on the user environment). In the scheme, each user sends a modulated peaky signal following the duty-cycle scheme of IR-UWB system, as illustrated in Fig. 5.4(a). At the receiver, the signal arrives affected by the channel, as represented in Fig. 5.4(b). Assuming that the receiver knows the channels, it can use this information to identify different transmitted signals.

Equivalent to DS-CDMA, but with the wireless channel employed as signaling codes, ChDMA benefits from the intrinsic properties of the wireless environment, that are often considered as obstacles. The codes are naturally generated by the environment, simplifying the transmitter side. Due to the wireless channel effects (path loss, shadowing, multipath, *etc.*), the channels are position-dependent and have a very strong random component. Combined with the wideband nature of UWB channels and the highly dispersive nature of indoor environments, this results in very long and uncorrelated channels that guarantee good separation capabilities and efficient codes as we show in Chapter 6. In the end, the system bandwidth and the duty cycle are the parameters that define the degrees of freedom (see Section 1.1.3) that can be exploited to separate the various transmitted signals.

5.3.2 The Wireless Channel

Let us first model the wireless channel between user k and the BS. This channel can be represented by L_k paths spread over a temporal window of length T_d, where T_d represents the delay spread of the environment[4]. The infinite bandwidth, time invariant channel representation can be expressed as

$$c_k(\tau) = \sum_{l=1}^{L_k} \lambda_{l,k}\delta(\tau - \tau_{l,k}), \qquad \text{with } 0 \leq \tau_{l,k} \leq T_d, \tag{5.2}$$

where $\lambda_{l,k}$ and $\tau_{l,k}$ represent, respectively, the complex gains and the delays of the l-th path of user k. The band-limited channel models is then generated by employing a bandpass filter g at both sides (transmitter and receiver), which results in a channel $h_k(\tau)$ given by

$$h_k(\tau) = \sum_{l=1}^{L_k} \lambda_{l,k} g(\tau - \tau_{l,k}). \tag{5.3}$$

The channel vector $\mathbf{h}_k$ is obtained by sampling $h_k(\tau)$ at intervals T_i, *i.e.*,

$$\mathbf{h}_k[n] = \int_{nT_i}^{(n+1)T_i} h_k(\tau)d\tau = \int_{nT_i}^{(n+1)T_i} \sum_{l=1}^{L_k} \lambda_{l,k} g(\tau - \tau_{l,k})d\tau. \tag{5.4}$$

where the channel vector length N is given by the ratio between the symbol period T_s and the temporal resolution T_i,

$$N = \frac{T_s}{T_i}. \tag{5.5}$$

Then, we can build the channel matrix based on the concatenation of all channel vectors,

$$\mathbf{H} = [\mathbf{h}_1 \ \mathbf{h}_2 \ \ldots \ \mathbf{h}_K]. \tag{5.6}$$

In the frequency domain, the wireless channel presented in Eq. (5.3) can be written

[4]The delay spread T_d is defined as the $\max_{\forall t,l}(\tau_{l,k})$

as

$$H_k(f) = \sum_{l=1}^{L_k} \lambda_{l,k} |G(f)|^2 e^{-j2\pi f \tau_{l,k}}. \tag{5.7}$$

where $G(f)$ represents the Fourier transform of the bandpass filter g.

In the discrete case, assuming that we have N samples to represent the frequency channel vector $\bar{\mathbf{h}}_k$, the filter $G(f)$ can be represented as a vector

$$\bar{\mathbf{g}}[n] = |G(f_r n)|^2 \tag{5.8}$$

where f_r is the frequency resolution defined by

$$f_r = \frac{W}{N} \tag{5.9}$$

Then, the frequency channel elements vector is

$$\bar{\mathbf{h}}_k[n] = \sum_{l=1}^{L_k} \lambda_{l,k} |G(f_r n)|^2 e^{-j2\pi f_r n \tau_{l,k}}, \qquad 0 \le n \le N-1. \tag{5.10}$$

which allows the following decomposition

$$\bar{\mathbf{h}}_k = \mathbf{D}(\bar{\mathbf{g}}) \cdot \mathbf{A}_k \cdot \mathbf{b}_k, \tag{5.11}$$

where

$$\mathbf{D}(\bar{\mathbf{g}}) = \begin{pmatrix} |\bar{\mathbf{g}}[0]|^2 & 0 & \dots & 0 \\ 0 & |\bar{\mathbf{g}}[1]|^2 & \ddots & 0 \\ \vdots & \ddots & \ddots & \vdots \\ 0 & 0 & \dots & |\bar{\mathbf{g}}[N-1]|^2 \end{pmatrix}, \tag{5.12}$$

$$\mathbf{A}_k = \begin{pmatrix} 1 & \dots & 1 \\ w^{\tau_{1,k}} & \ddots & w^{\tau_{L,k}} \\ \vdots & \ddots & \vdots \\ w^{(N-1)\tau_{1,k}} & \ddots & w^{(N-1)\tau_{L,k}} \end{pmatrix}, \tag{5.13}$$

$$\mathbf{b}_k = \begin{pmatrix} \lambda_{1,k} \\ \vdots \\ \lambda_{L,k} \end{pmatrix}, \tag{5.14}$$

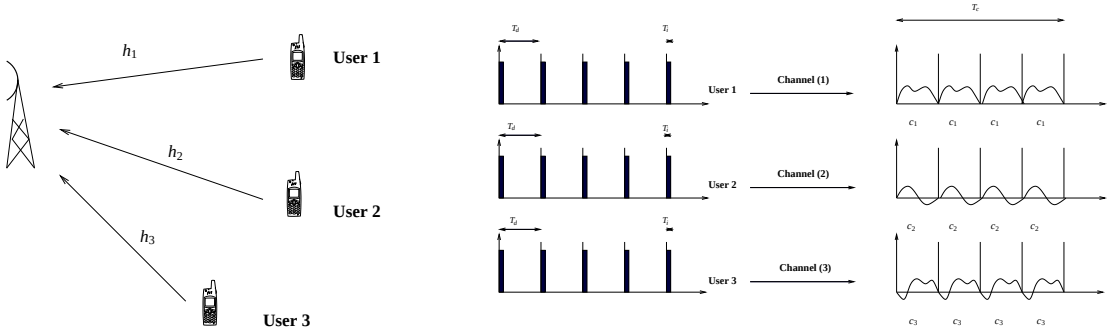

(a) Multiple access of 3 users.

(b) Transmitted and received signals

Figure 5.5: Channel division multiple access scheme.

being w equal to $e^{-j2\pi f_r}$.

Without loss of generality, the number of paths is assumed to be exactly the same for all users ($L^{(k)} = L$). The general case can be easily treated.

5.3.3 The ChDMA System Model

Let us consider a multi-user single-band IR-UWB system with K single antenna users. Each uplink channel between user k and the base station (BS) is considered to be frequency selective and suffers from additive white Gaussian noise. The transmissions are carried by very short electric pulses of length T_i. These pulses define the system bandwidth ($W = T_i^{-1}$) and the sampling rate. The interval between consecutive transmissions is denoted as T_s, and it provides the symbol rate ($f_s = T_s^{-1}$). It is important to note that, since the duty cycle is low, the pulse length T_i employed by the pulse signaling is only a small fraction of T_s ($T_i \ll T_s$).

The basic system scheme is presented in Fig. 5.5(a). In the example, three mobiles are transmitting to the same destination across the same wireless medium. Each mobile sends a modulated pulse, *i.e.*, a pulse modulated by a symbol. Transmitted through the channel, the signal is distorted by the wireless environment, as illustrated in Fig. 5.5(b). This distortion can be regarded as a modulation scheme. At the receiver, under the assumption that the BS knows the channels of different users, it is able to detect and demodulate the received signals by using the channel as a code. Since the users have different locations, each transmitted signal is affected by a different channel, and the signaling scheme provides enough diversity to separate the information sent by different users.

For the sake of simplicity, the system is considered to be symbol-synchronous[5], which means that the maximum delay between all user paths is bounded by T_s and the ISI is avoided. Since the model does not change whether one is in frequency or time (since the Fourier transform is unitary), we will keep the same notation. Then, in the BS, the received signal can be represented as being

$$\mathbf{y} = \mathbf{H}\mathbf{s} + \mathbf{n}, \tag{5.15}$$

where $\mathbf{y}$ is a N-dimensional complex vector that represents the received signal; $\mathbf{H}$ is a $N \times K$ complex matrix that represents the wireless channel; $\mathbf{s}$ is a K-dimensional complex vector that contains the transmitted symbols of various users, typically binary phase-shift keying (BPSK) symbols (taken from $\{+1, -1\}$) due to the low spectral efficiency of low duty cycle systems; and $\mathbf{n}$ is a N-dimensional complex additive white Gaussian noise vector of variance σ^2.

Note that ChDMA is a system where the channel is fundamental on its performance. For this reason, we provide in the following a model that represents the UWB channel and allow us to further analyze the ChDMA scheme.

5.3.4 Spectral Efficiency and Capacity

The spectral efficiency of a system is a measure of the amount of information that can be transmitted between the transmitters and the receivers of a system over a given bandwidth. It represents the efficiency of the system and it is largely used to compare the performance of different systems.

In the field of information theory, Claude E. Shannon introduced the capacity notion in his seminal work of 1948 [63]. Shannon's capacity represents a theoretical bound of the maximum achievable error-free rate that can be transmitted over a channel. In his work, he provided a mathematical model (Fig. 5.6) by which it is possible to compute the maximum amount of bits that could be transmitted per channel access [14] based on the mutual information (see Section 2.2) between input and output. The spectral efficiency is then calculated by dividing shannon's capacity by the access time and system bandwidth, being measured in $bits/s/hz$.

[5] Symbol synchronization means that all users transmit their symbols during a fixed interval. Under typical low-duty cycle UWB communication, ($T_d \ll T_s$), so the symbol-synchronous assumption does not restrict our model.

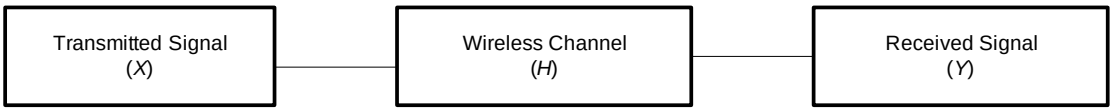

Figure 5.6: Representation of a communication system.

For the ChDMA, the mutual information (see Section 2.2) between input and output of our model (see Eq. 5.15) is

$$\begin{aligned}
\mathcal{I}(\mathbf{s};(\mathbf{y},\mathbf{H})) &= \mathcal{I}(\mathbf{s};\mathbf{H}) + \mathcal{I}(\mathbf{s};\mathbf{y} \mid \mathbf{H}) && (5.16)\\
&= \mathcal{I}(\mathbf{s};\mathbf{y} \mid \mathbf{H}) && (5.17)\\
&= \mathcal{H}(\mathbf{y} \mid \mathbf{H}) - \mathcal{H}(\mathbf{y} \mid \mathbf{s},\mathbf{H}) && (5.18)\\
&= \mathcal{H}(\mathbf{y} \mid \mathbf{H}) - \mathcal{H}(\mathbf{n} \mid \mathbf{H}) && (5.19)
\end{aligned}$$

In the case of Gaussian signaling, the entropy can be written in terms of the covariance matrix, *i.e.*,

$$\mathcal{H}(\mathbf{x}) = \log_2 \det(\pi e \mathbf{Q}), \tag{5.20}$$

for

$$\mathbf{Q} = \mathbb{E}\{\mathbf{x}\mathbf{x}^H\}. \tag{5.21}$$

Since

$$\begin{aligned}
\mathbb{E}(\mathbf{n}\mathbf{n}^H) &= \sigma^2 \mathbf{I}_N, && (5.22)\\
\mathbb{E}(\mathbf{y}\mathbf{y}^H) &= \sigma^2 \mathbf{I}_N + \mathbf{H}\mathbf{H}^H && (5.23)
\end{aligned}$$

the spectral efficiency is then

$$\begin{aligned}
\gamma_{Gauss} &= \frac{1}{T_s W}\left[\mathcal{H}(\mathbf{y} \mid \mathbf{H}) - \mathcal{H}(\mathbf{n} \mid \mathbf{H})\right]\\
&= \frac{T_i}{T_s}\left[\log_2 \det\left(\pi e(\sigma^2 \mathbf{I}_N + \mathbf{H}\mathbf{H}^H)\right) - \log_2 \det\left(\pi e(\sigma^2 \mathbf{I}_N)\right)\right]\\
&= \frac{1}{N}\log_2 \det\left(\mathbf{I}_N + \frac{1}{\sigma^2}\mathbf{H}\mathbf{H}^H\right) && (5.24)
\end{aligned}$$

For $K \to \infty$, γ_{Gauss} can be decomposed as

$$\gamma_{Gauss} = \frac{1}{N}\sum_{i=1}^{K}\log_2\left(1+\mathrm{SINR}_i\right). \tag{5.25}$$

The signal to noise ratio $\frac{1}{\sigma^2}$ is related to the spectral efficiency γ by $\frac{1}{\sigma^2} = \frac{N}{K}\gamma\frac{E_b}{N_0}$ [81].

For BPSK and QPSK (quadrature phase-shift keying) signaling, Ralf Müller, Wenyan He and Costas N. Georgiades [36, 51] provided expressions for the mutual information,

$$I(\mathbf{s};(\mathbf{y},\mathbf{H})) = -\int f(H)dH\int f(\mathbf{y}|H)\log_2 f(\mathbf{y}|H)d\mathbf{y} - N\log_2(\pi e\sigma^2) \tag{5.26}$$

with

$$f(\mathbf{y}|H) = \sum_{\mathbf{s}\in S} p(\mathbf{s})\left(\frac{1}{\pi\sigma^2}\right)^N \exp\left(-\frac{\|\mathbf{y}-H\mathbf{s}\|^2}{\sigma^2}\right). \tag{5.27}$$

Then, the spectral efficiency for the BPSK signaling case is given by

$$\gamma = \frac{1}{N}\left\{\log_2 2 - K\log_2 e - \mathbb{E}_H\left[\mathbb{E}_{\hat{\mathbf{n}}}\left(\log_2\sum_{\mathbf{s}\in S}\exp\left(-\frac{\|\hat{\mathbf{n}}+H(\bar{\mathbf{x}}-\mathbf{x})\|^2}{\sigma^2}\right)\right)\right]\right\}. \tag{5.28}$$

However, this expression is very hard solve. For this reason, we derived the spectral efficiency expressions for the MF and MMSE receivers (see Appendix B). The spectral efficiency of these receivers are

$$\gamma_{\mathrm{BPSK}} = \frac{1}{N}\sum_{i=1}^{K}\left[1-\int_{-\infty}^{+\infty}\frac{e^{-\frac{v^2}{2}}}{\sqrt{2\pi}}\log_2\left(1+e^{-2\ \mathrm{SINR}_i-2\sqrt{\mathrm{SINR}_i}v}\right)dv\right], \tag{5.29}$$

for the BPSK and

$$\gamma_{\mathrm{QPSK}} = 2\gamma_{\mathrm{BPSK}}. \tag{5.30}$$

for the QPSK.

5.3.5 Comparing ChDMA with DS-CDMA

ChDMA scheme is very similar to the DS-CDMA scheme. However, the system models have minor differences, resulting in different system performances.

The DS-CDMA system model with white Gaussian channels and K users can be written as follows, where we assume that each user k transmits over a flat-fading channel h_k and employs a codeword $\mathbf{c_k}$ of length N:

$$\mathbf{y} = \mathbf{Cs} + \mathbf{n} = [h_1\mathbf{c}_1 \; h_2\mathbf{c}_2 \; \ldots \; h_K\mathbf{c}_K] \begin{bmatrix} s_1 \\ s_2 \\ \vdots \\ s_K \end{bmatrix} + \begin{bmatrix} n_1 \\ n_2 \\ \vdots \\ n_K \end{bmatrix} \tag{5.31}$$

note that this is the same as Eq. (5.15) with the substitution of $\mathbf{C}$ for $\mathbf{H}$.

Wideband ChDMA is strictly equivalently to narrow-band DS-CDMA in terms of system representation. Since both systems have the same model, they share the same spectral efficiency expressions [81]. Nevertheless, the DS-CDMA model does not consider the multipath effect. Under high dispersive conditions, CDMA was shown to suffer a dramatic loss in terms of spectral efficiency[46], unless the channel is quasi-static, varying very slowly. This loss occurs because as the bandwidth increases, the power available to estimate each path is too small for accurate channel detection techniques to work well, significantly degrading the SNR.

ChDMA does not suffer from the same limitations and the model (5.15) already represents the most important effects observed on wireless environments. Actually, the dispersive channel is fundamental in providing enough diversity to allow the receivers to separate the signals sent by different users. The low power limitation of UWB systems is overcome by concentrating each user's energy in a very short pulse.

In Chapter 6, some results comparing ChDMA with DS-CDMA is presented. For the ChDMA case, we employ realistic fading effects, whereas the DS-CDMA is employed over flat-fading channels.

5.4 Summary

UWB radio is an emerging technology bringing major advances in wireless communications, networking, radar, imaging, and positioning systems. The large bandwidths enable very high achievable capacities.

The FCC and the ITU-R have already standardized UWB and restricted the technology to very low output energy levels for short-range communications. None of the conventional multiple access techniques are adapted to the highly dispersive nature of UWB environments. For this reason, we proposed a new concept that provides a mul-

tiple access scheme that explores the low duty cycle characteristic of IR-UWB systems to guarantee simultaneous communications. This scheme is the channel division multiple access.

The ChDMA proposal is, in many ways, similar to the CDMA scheme. They share the same concept but the signatures of ChDMA are designed naturally by the wireless environment. This simplifies the transmitter architecture and provide a natural multiple access scheme for IR-UWB systems to cope with the highly dispersive nature of the UWB channel. Nevertheless, the system cannot control the degree of separability between different users' "codes," which can be a problem if two users have very correlated channels. However, in very dense environments, even if the users are very close, the channel resolution of UWB systems is high and we expect a low degree of correlation between different channels.

Although wideband systems typically have poor spectral efficiency, we present some results in Chapter 6 that show that IR-UWB systems can achieve very high spectral efficiencies, being a real option for high data rate networks.

Chapter 6

Performance of ChDMA

"The possession of knowledge does not kill the sense of wonder and mystery. There is always more mystery."

(Anais Nin)

ChDMA is a promising multiple access scheme foreseen to be employed in low duty cycle IR-UWB systems for uplink communication. The idea is detailed in Chapter 5 and depends on the fact that any signal transmitted in a dispersive channel suffers from an distortion that can be exploited as a modulation scheme. When this distortion is known at the receiver, the channels distortions are treated as signature waveforms very similar to the DS-CDMA spreading codes.

In this chapter we present some initial analysis of the spectral efficiency performance of ChDMA systems. First, we present three receiver structures that we will study in different system configurations: the optimal receiver, the matched filter (MF) and linear minimum mean square error (MMSE) receiver. Using these different receivers, we compare the performance of ChDMA with the ideal DS-CDMA system. It is shown that under certain conditions ChDMA can even outperform ideal CDMA, providing a real option for future communication systems. Then, an asymptotic analysis in terms of number of users and frequency resolution is carried on to give some insights about the behavior of the ChDMA scheme.

6.1 Numerical Performance

Consider the system model presented in Section 5.3.3 to evaluate the spectral efficiency of using three different receivers. We assume in the sequel that users are symbol-synchronous and that the receiver has full knowledge of the environment. Consequently, the receiver treats the channel impulse responses (CIRs) as signature waveforms. In this chapter we compare the ChDMA scheme with flat-fading synchronous DS-CDMA schemes employing two different codes: orthogonal Hadamard codes and random binary codes. The analysis is performed through Monte Carlo simulations where different configurations are evaluated to identify the relationship between the spectral efficiency and various system parameters.

For the following, some assumptions are made:

Assumption 1: The channels are complex random matrices whose entries come from a zero-mean Gaussian distribution such that

$$\mathbb{E}(\mid \mathbf{h}_i \mid^2) = 1. \tag{6.1}$$

We assume that the entries are i.i.d. with variance $\frac{1}{\sqrt{N}}$, which means that the energy is uniformly distributed over the channel taps. In Section 6.1.4, this assumption is relaxed and a power delay profile model is introduced to distribute the energy in a non-uniform way.

Assumption 2: DS-CDMA system is simulated to be compared with the performance of ChDMA. To create a fair comparison between both systems, the spreading code length N for DS-CDMA is $N = \frac{T_s}{T_i}$. Each spreading code word is equally likely and chosen independently by each user; equivalently each chip is independently picked from the finite set $\{-\frac{1}{\sqrt{N}}, \frac{1}{\sqrt{N}}\}$. The performance of DS-CDMA is evaluated in a flat-fading white Gaussian channel, which is the scenario that offers an upper bound of the DS-CDMA's performance.

Assumption 3: For sake of objectivity, the results presented in this section are limited to the analysis of Gaussian signaling spectral efficiency expressions. The conclusions are also valid to the BPSK and QPSK signaling, respecting the performance differences of each signaling scheme.

Assumption 4: The asynchronism considered in Section 6.1.4 is generated by the introduction of delays d_i on the channel impulse responses. Due to the symbol syn-

chronism, these delays are bounded,

$$d_i \leq T_s - T_d \quad \forall i, \tag{6.2}$$

and randomly generated, following a uniform distribution on $[0, T_s - T_d]$.

Each data point in the plots is generated by averaging 2000 Monte Carlo simulations for different system configurations. Furthermore, each data point is generated independently of the other.

To simplify notations, we express the time interval between consecutive transmissions T_s and the delay spread of the channel T_d in terms of sampling frequency f_i. This allows us to generalize the results for any case where the relations between T_s, T_d and T_i are satisfied.

6.1.1 Receiver Structures

As we have shown in Chapter 3, UWB channels are highly dispersive; this fundamental characteristic motivated us to develop ChDMA. This scheme simplifies the transmitter technology and allows the use of CDMA tools at the receiver to identify and to separate the signals of different users.

In this section, we analyze the performance of ChDMA using three different receiver structures:

- the optimal receiver,
- the matched filter, and
- the minimum mean square error receiver.

6.1.1.1 Optimal Receiver

The optimal receiver is the receiver that minimizes the probability of symbol error among all receiver structures. It is based on the analysis of the posterior probabilities of the transmitted signal [56], *i.e.*, given the received signal and the channel matrix, the optimal receiver estimates the transmit signal $\hat{\mathbf{s}}$ such that:

$$\hat{\mathbf{s}} = \underset{\hat{\mathbf{s}}}{\operatorname{argmin}}(|\mathbf{y} - \mathbf{H}\hat{\mathbf{s}}|). \tag{6.3}$$

where $\mathbf{y}$ and $\mathbf{H}$ are defined in (5.15) and represent respectively the received signal and the channel matrix.

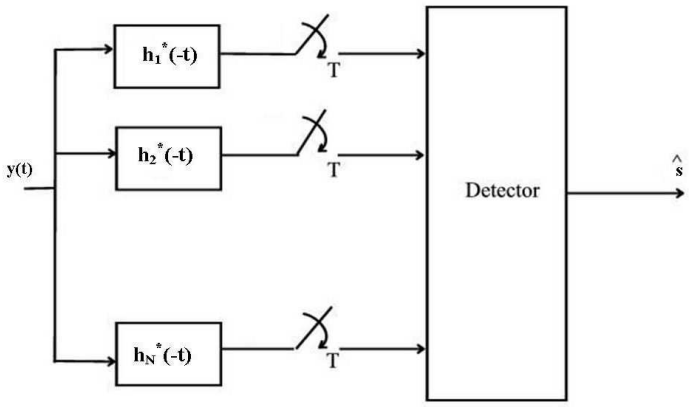

Figure 6.1: Matched Filter Scheme.

This receiver rule is to find the signal $\hat{\mathbf{s}}$ such that $\mathbf{H}\hat{\mathbf{s}}$ minimizes the distance to the received signal $\mathbf{y}$. For equiprobable symbols, the optimal receiver is the maximum likelihood receiver. However, this receiver has to check all possible values of $\hat{\mathbf{s}}$. This minimizes the error but it has very high computational processing requirements and the complexity of the analysis increases exponentially with the number of users.

Although implementing the optimal receiver is generally not feasible in practice, it provides an upper bound of ChDMA's achievable performance. The analytical expression for the spectral efficiency of the optimal receiver is known and presented in Section 5.3.4, Eq. (5.24).

6.1.1.2 Matched Filter (MF)

The MF is the simplest receiver structure considered in this work. It is the best linear receiver for estimating the transmitted signal in the presence of additive Gaussian noise. In this case, it maximizes the SNR, and hence, minimizes the probability of error. The processing correlates the signal with a time-reversed version of the estimated channel, as illustrated in Fig. 6.1.

As shown in [35, 80], when employing the MF, the signal-to-interference plus noise ratio (SINR) of each user is then given by

$$\mathrm{SINR}_{\mathrm{MF}_i} = \mathbb{E}\left\{ \frac{|\ \mathbf{h}_i^H \mathbf{h}_i\ |^2}{\sigma^2(\mathbf{h}_i^H \mathbf{h}_i) + \sum_{j=1, j\neq i}^{K} |\ \mathbf{h}_i^H \mathbf{h}_j\ |^2} \right\}. \tag{6.4}$$

where $\mathbf{h}_i^H$ represents the linear filter employed in the MF.

Then, the spectral efficiency of the MF is calculated by substituting Eq. (6.4) in Eq. (5.25).

6.1.1.3 Linear Minimum Mean Square Error (MMSE) Receiver

The linear MMSE receiver [37, 43, 57, 59, 85] is also a linear filter that differs from the MF due to the fact that it minimizes the mean square error:

$$\underset{\mathbf{f}}{\operatorname{argmin}}\ \mathbb{E}\{(\mathbf{s}-\mathbf{f}\mathbf{y})^2\} \tag{6.5}$$

The MMSE maximizes the SINR over all linear receivers [50], but at a price of higher complexity, due to the fact that the filter considers the interference level, which requires the knowledge of all channels.

The linear MMSE filter is given by [43],

$$\mathbf{f}_i = \left(\tilde{\mathbf{H}}_i\tilde{\mathbf{H}}_i^H + \sigma^2\mathbf{I}\right)^{-1}\mathbf{h}_i, \tag{6.6}$$

where $\tilde{\mathbf{H}}_i$ is $(N \times (K-1))$ matrix which contains all time response vectors $\mathbf{h}_j$ for all $j \neq i$ and $\mathbf{I}$ represents the identity matrix.

The SINR for liner filtering is given by

$$\text{SINR}_i = \quad \mathbb{E}\left\{\frac{|\ \mathbf{f}_i^H\mathbf{h}_i\ |^2}{\sigma^2(\mathbf{f}_i^H\mathbf{h}_i) + \sum_{j=1,j\neq i}^{K}|\ \mathbf{f}_i^H\mathbf{h}_j\ |^2}\right\}. \tag{6.7}$$

Hence, the SINR_{MMSE_i} is obtained by substituting Eq. (6.6) into Eq. (6.8). Tse and Hanly [75] simplified the expression and proved that we can represent the linear MMSE SINR as

$$\text{SINR}_{\text{MMSE}_i} = \mathbf{h}_i^H(\tilde{\mathbf{H}}_i\tilde{\mathbf{H}}_i^H + \sigma^2\mathbf{I})^{-1}\mathbf{h}_i. \tag{6.8}$$

As in the MF case, the spectral efficiency of the linear MMSE receiver is calculated by substituting Eq. (6.6) in Eq. (5.25).

6.1.2 Number of Users to Spreading Factor Ratio (K/N)

We first analyze the impact of the number of users K and the spreading factor N on the ChDMA performance. We focus our analysis on the region where the K/N ratio is smaller than one ($K/N \leq 1$), due to the fact that UWB systems are short range

networks, which implies that there are few users compared to the large spreading factor current employed in IR-UWB technique.

In the CDMA case, Verdu and Shamai [81] have shown that when the number of users and the spreading factor both go to infinity, but at a constant ratio, the spectral efficiency depends only on the K/N ratio. The results from this asymptotic regime provided good approximations for finite values of K and N. Consider here similar condition for the ChDMA.

Considering a delay spread equal to the interval between consecutive transmissions ($T_s = T_d$), we analyze the spectral efficiency of the ChDMA for two different spreading factor values $N = 32$ and $N = 256$. In Fig. 6.2, the performance of the optimal receiver is evaluated for an energy per bit to noise spectral density ratio (E_b/N_o) of $5dB$. The figure shows the performance of the ChDMA, the DS-CDMA with random codes and the DS-CDMA with orthogonal codes for the two values of N. The spectral efficiency does not change when different spreading factor values are employed. For a very high ratio K/N, DS-CDMA considerably outperforms ChDMA because it does not suffer from interference, whereas ChDMA does. However, ChDMA could outperform DS-CDMA for a small number of users, because DS-CDMA codes are generally built to explore only the real domain whereas the ChDMA "codes" are based on the channel responses, which means that each "chip" is represented by a complex number. If the receiver were an energy detector, the performance of ChDMA would be similar to that offered by DS-CDMA with random spreading codes; this performance is also shown in Fig. 6.2.

Fig. 6.3 and Fig. 6.4 present respectively the performance of the MF and the linear MMSE receiver under the same conditions as for the optimal receiver in Fig. 6.2. The MF is more sensitive to the spreading factor, but both receivers depend only slightly on the spreading factor. For a spreading factor higher than one hundred ($N \geq 100$), the spectral efficiency variation with N is negligible. Using a MF receiver, DS-CDMA with orthogonal codes always outperforms ChDMA even for very small number of users. This is because the MF is not designed to cope with the interference. On the other hand, the linear MMSE receiver performs nicely as well as the optimal receiver. Actually, for DS-CDMA with orthogonal codes, the linear MMSE presents the same results of the optimum receiver. For ChDMA, the linear MMSE receiver does not achieve the same performance as the optimal receiver, but it still outperforms DS-CDMA when only few users are connected.

The results in this section can provide insights for system design. Even though DS-CDMA with orthogonal codes could present better spectral efficiency than ChDMA, as has been seen so far in this section, when effects like time-offset and channel multipath

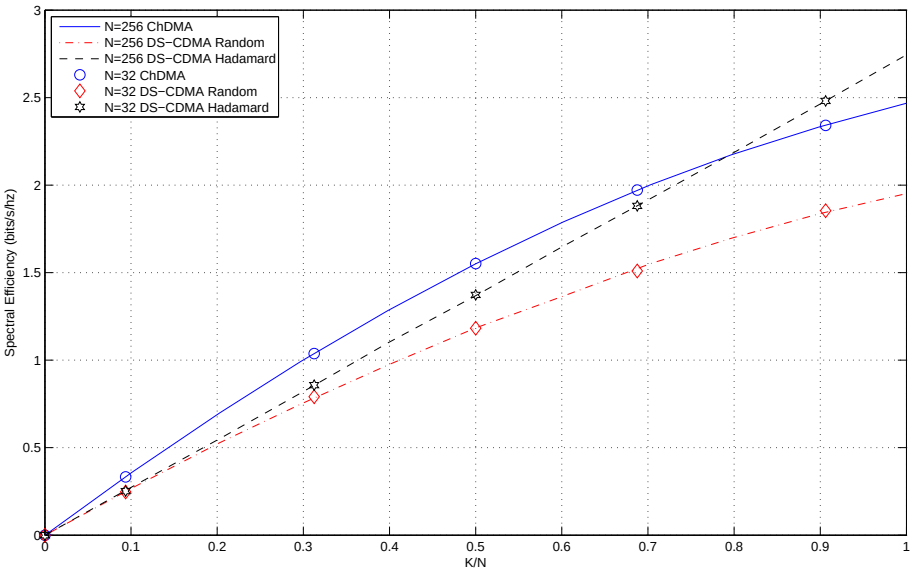

Figure 6.2: Performance of optimal receiver ($E_b/N_o = 5$dB and $T_d = T_s$).

are considered, ChDMA does better relatively.

6.1.3 Energy per Bit to Noise Ratio (E_b/N_o)

As shown in the previous section, for $N > 100$, the spectral efficiency depends almost exclusively on the ratio K/N. For this section, we will assume that $N = 128$ and we will consider two values of the ratio: $K/N = 0.2$ and $K/N = 0.5$).

Fig. 6.5 shows the performance of the optimal receiver for different values of E_b/N_o. The spectral efficiency of all systems increase almost linearly with the increase of E_b/N_o. The gap between the spectral efficiency of ChDMA and DS-CDMA is preserved. For both K/N values that we considered in the figure, as well as other values we investigated of ratios lower than 0.7, ChDMA outperforms the DS-CDMA even if orthogonal codes are employed.

In Fig. 6.6 and Fig. 6.7, we present the performance of the MF and the linear MMSE receiver, respectively. Different from the optimal receiver case, the spectral efficiency of ChDMA using the MF is almost constant with the increase of E_b/N_o, whereas the performance of DS-CDMA grows more than linearly. The reason for this is that the MF does not counteract interference, so the ChDMA performance is limited by the interference level; increasing E_b/N_o will not ameliorate it. However, the linear MMSE

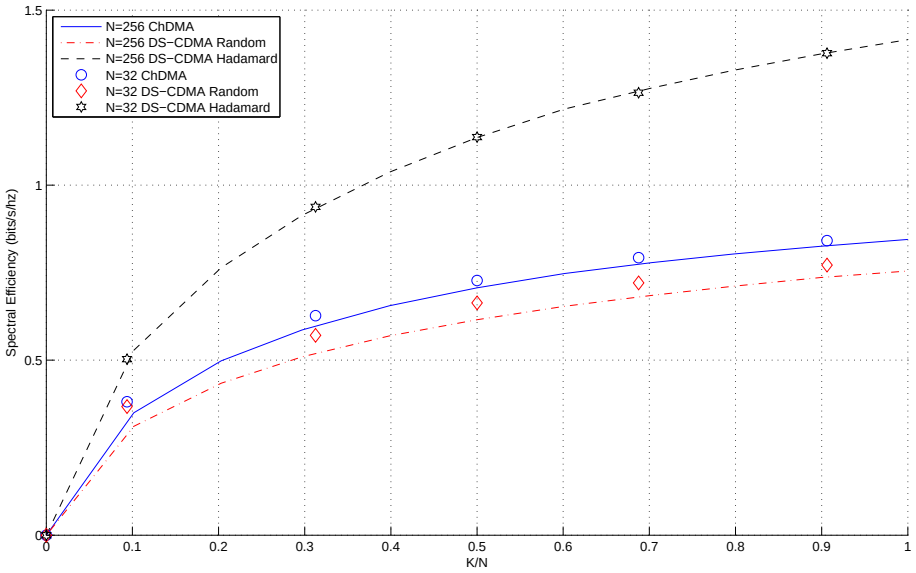

Figure 6.3: Performance of MF ($E_b/N_o = 5$dB and $T_d = T_s$).

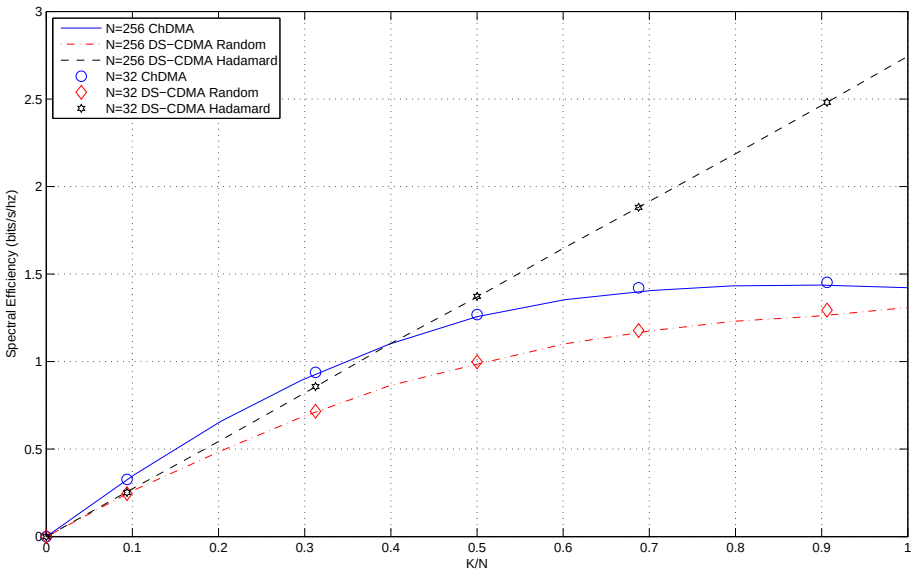

Figure 6.4: Performance of linear MMSE ($E_b/N_o = 5$dB and $T_d = T_s$).

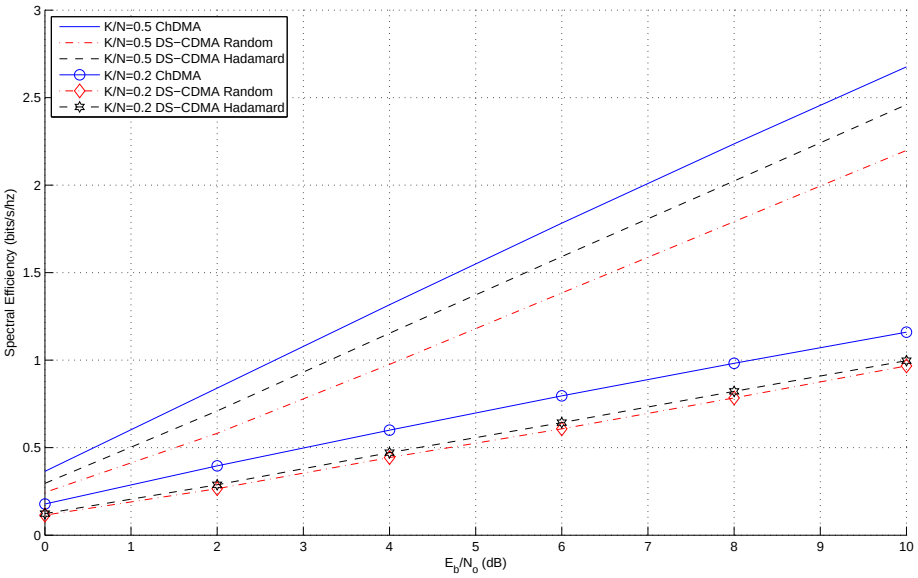

Figure 6.5: Performance of Optimum Receiver ($T_d = T_s$).

receiver performs much better than the MF, similar to the optimal receiver, presenting an almost linear gain for the spectrum efficiency with the increase of E_b/N_o.

6.1.4 Channel Delay Spread and User's Asynchronism

In the previous sections of this chapter, the delay spread T_d was equal to the interval between consecutive symbols T_s. This is because we would like to compare the ChDMA and the DS-CDMA under the same system configuration. However, in a realistic environment, the delay spread should be shorter than the interval between consecutive symbols. Here, we would like to show some of the real improvements that ChDMA has to offer to IR-UWB systems.

Usually, IR-UWB systems are designed to operate over different channel conditions. Even if the channel delay spread of the users is the same, it is difficult to perfectly synchronize all transmit signals at the receiver. For this reason, we evaluate the performance of ChDMA when users are symbol-synchronous and the delay spread is only a fraction of the interval between consecutive transmissions. If the users are perfectly synchronized, by decreasing T_d, the spectral efficiency will decrease because the channel energy will be concentrated in few channel taps, resulting in smaller signatures and a higher interference level. However, if the messages of different users arrive at different

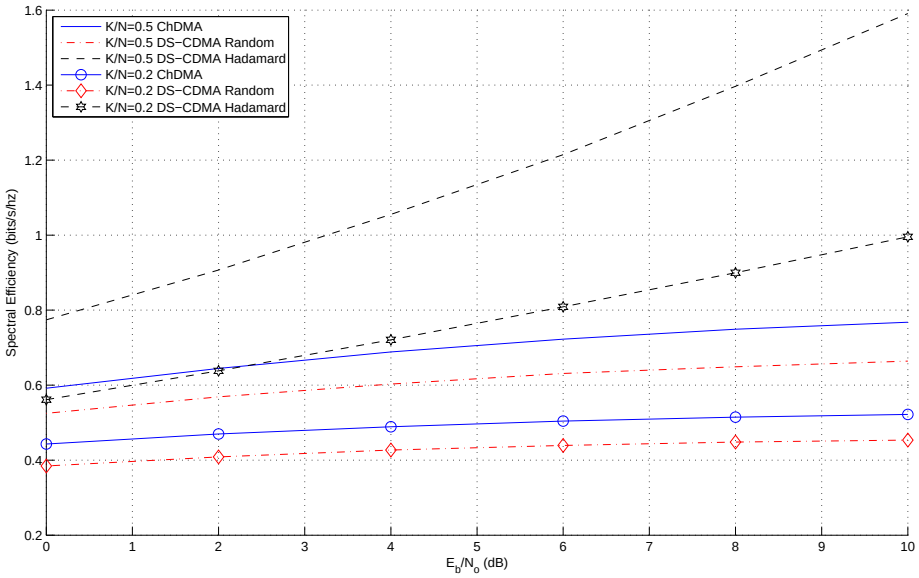

Figure 6.6: Performance of MF ($T_d = T_s$).

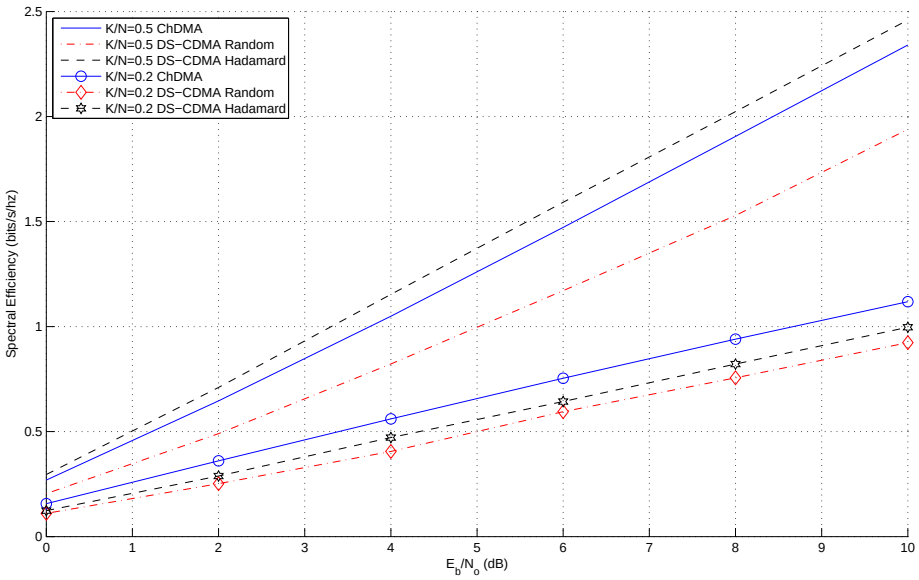

Figure 6.7: Performance of linear MMSE Receiver ($T_d = T_s$).

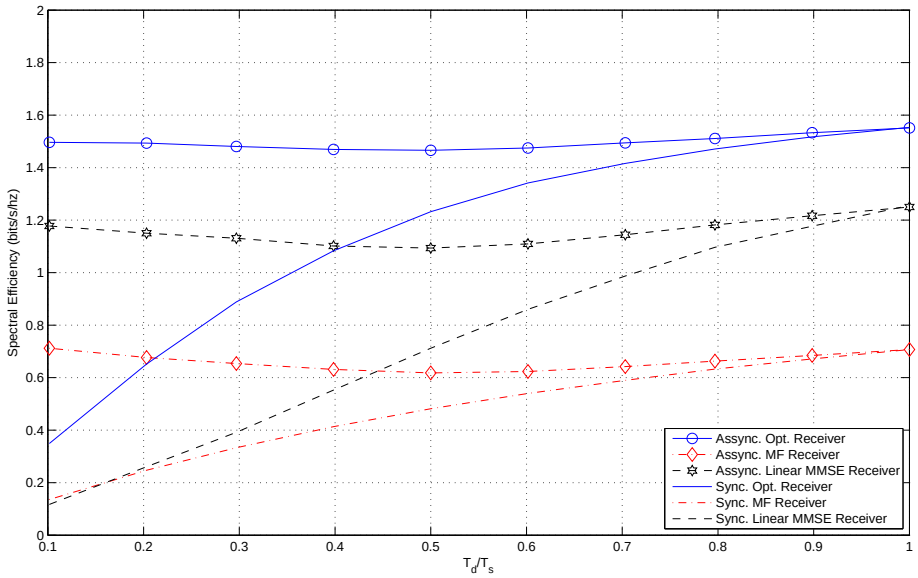

Figure 6.8: Impact of asynchronism ($K/N = 0.5$ and $E_b/N_o = 5dB$).

times asynchronously, the receiver will be able to exploit this feature to increase the degree of interference cancelation.

In Fig. 6.8, we present the spectral efficiency as a function of the delay spread. For perfectly synchronized ChDMA, decreasing the spread spectrum length (or increasing the symbol interval) results in a loss of performance when the system uses any of the three receivers. However, if the system is asynchronous, the performance is nearly independent of the ratio T_d/T_s. The same effect was also observed for different values of K/N and E_b/N_o.

Asynchronism is beneficial to ChDMA and provides robustness against low dispersive environments, allowing increased inter-symbol intervals without a corresponding spectral efficiency loss. The results presented here assume symbol synchronism, which is often employed in wireless networks through the use of beacon signals. The assumption of symbol-synchronization can be relaxed when there are many transmitters and a large interval between consecutive transmissions. Due to the different location of the transmitters, resulting in different signal delays and channel delay spreads, synchronism at the receiver is an unrealistic assumption.

6.2 Asymptotic Performance

In this section, we will analyze how the spectral efficiency behaves in the asymptotic regime. This asymptotic analysis allows us to find tractable expressions that provide a good understanding of the ChDMA limiting behavior. To this aim, we derive analytical expressions of the spectral efficiency under the assumption that the number of users and the size of the bandwidth increase at a constant ratio. Moreover, the UWB channel is modeled as linear combinations of continuous pulses of finite duration, following one of two different power delay profiles: uniform or exponential. We study the impact of these regimes on the spectral efficiency of ChDMA.

6.2.1 Further Assumptions

Considering the same system model presented in Section 5.3.3, where the channel has L_k distinguishable paths (see Eq. (5.3)), and $\lambda_{k,\ell}$ and $\tau_{k,\ell}$ represent respectively the amplitude and the delay of the ℓ-th path of user k. The amplitudes $\lambda_{k,\ell}$ are complex random variables that follow a normal distribution with zero mean and variances $\sigma^2_{k,\ell}$ such that $\sum_{k=1}^{L_k} \sigma^2_{k,\ell} = P_k$. Without loss of generality, we assume that $P_k = 1$.

To keep the notation simple, we assume that all the users have the same number of distinguishable paths ($L_k = L$) and the analysis is performed in the frequency domain (see Eq. (5.7)). Furthermore, the bandpass filter $g(t)$ is considered ideal and is represented by a dirac delta impulse function[1], *i.e.*, $g(t) = \delta(t)$. The channel bandwidth is represented by W and is the inverse of sample interval ($W = T_i^{-1}$). The frequency resolution[2] W_c is the inverse of the symbol interval ($W_c = T_s^{-1}$). This implies that the baseband representation of the system is within the frequency interval $\left[-\frac{N}{2}W_c, \frac{N}{2}W_c\right]$.

6.2.2 Cases of Study

Throughout this section we analyze the capacity of the above proposed multiple access scheme in the following two cases:

Case 1: The complex amplitudes $\lambda_{k,\ell}$ and the path delays $\tau_{k,\ell}$ are random variables that are mutually independent and statistically independent over all the K users

[1]This can be obtained through the use of a bandpass filter at the transmitter and receiver.

[2]In order to respect the coherence bandwidth of the system, the frequency resolution has to satisfy the following inequality: $W_c \leq \frac{1}{T_d}$.

and all the L paths. The delays $\tau_{k,\ell}$ are random variables uniformly distributed in the interval $[0, T_d]$. The amplitudes $\lambda_{k,\ell}$ are complex random variables with zero mean and variances $\frac{1}{L}$. Furthermore, if $T_d \neq W_c^{-1}$, the number of paths L is assumed to be large enough that the random function $H_k(f)$ is Gaussian with zero mean.

Case 2: The complex amplitudes $\lambda_{k,\ell}$ and the path delays $\tau_{k,\ell}$ of user k are jointly random variables with joint probability density function $f_{\Lambda_1 \ldots \lambda_L, T_1 \ldots T_L}(\lambda_1, \ldots \lambda_L, \tau_1 \ldots \tau_L)$. We assume that elements of one set $(\lambda_{k,j}, \tau_{k,j})$ are statistically dependent of each other but statistically independent of any element of any other set $(\lambda_{k',j'}, \tau_{k',j'})$ $\forall$ $k' \neq k$ and $j' \neq j$, *i.e.*,

$$f(\lambda_{k,1}, \ldots, \lambda_{k,L}, \tau_{k,1}, \ldots, \tau_{k,L}) = \prod_{\ell=1}^{L} f_\ell(\lambda_{k,\ell}, \ldots, \tau_{k,\ell}). \tag{6.9}$$

Furthermore, consistent with the general assumptions in Section 5.3.3 , we assume that

$$\int_{\mathbb{C}} p_\ell(\lambda_{k,\ell}, \tau_{k,\ell}) \mathrm{d}\lambda_{k,\ell} = \begin{cases} \frac{L}{T_d} & \text{for } \frac{T_d(\ell-1)}{L} \leq \tau_{k,\ell} \leq \frac{T_d \ell}{L} \\ 0 & \text{otherwise,} \end{cases} \tag{6.10}$$

where $\ell = 1, \ldots L$. The joint distribution $f_{\Lambda_1 \ldots \lambda_L, T_1 \ldots T_L}(\lambda_1, \ldots \lambda_L, \tau_1 \ldots \tau_L)$ allows us to take into account the power delay profile under the assumption that random variables $\lambda_{k\ell}$ are dependent of the delays $\tau_{k\ell}$. The marginal distributions of $\lambda_{k,\ell}$ are Gaussian with zero mean and variances $\sigma^2_{\Lambda_\ell}$ and the number of paths L is large enough that the random function $H_k(f)$ is Gaussian with zero mean.

6.2.2.1 Case 1

Thanks to the independence of $\lambda_{k,\ell}$ and $\tau_{k,\ell}$ over all users, the columns of the channel matrix $\mathbf{H}$ are statistically independent. In order to characterize the matrix $\mathbf{H}$ completely, it is sufficient to determine the covariance matrix of one of the Gaussian vector $\mathbf{h}_k$, for $k = 1, \ldots K$. The m^{th} component of the vector $\mathbf{h}_k$ is

$$h_{m,k} = \sum_{\ell=1}^{L} \lambda_{k,\ell} G\left(W_c(m-1) - \frac{W_c N}{2}\right) \mathrm{e}^{j2\pi W_c(m-1)\tau_\ell}, \tag{6.11}$$

for $m = 1, \ldots, N$. Then, the (m, n) element of the covariance matrix $\mathbf{C}^{(1)} = \mathbb{E}\{\mathbf{h}_k \mathbf{h}_k^H\}$ is

$$\begin{aligned} C_{m,n}^{(1)} &= \sum_{u=1}^{L}\sum_{v=1}^{L} \mathbb{E}\{\lambda_{k,u} G\left(W_c(m-1) - \tfrac{W_c N}{2}\right) \cdot \mathrm{e}^{j2\pi W_c(m-1)\tau_u} \lambda_{k,v}^* \\ &\quad \cdot G^*\left(W_c(n-1) - \tfrac{W_c N}{2}\right) \mathrm{e}^{-j2\pi W_c(n-1)\tau_v}\} \\ &= G\left(W_c(m-1) - \tfrac{W_c N}{2}\right) G^*\left(W_c(n-1) - \tfrac{W_c N}{2}\right) \\ &\quad \cdot \sum_{u=1}^{L} \mathbb{E}\{\lambda_{k,u}\lambda_{k,u}^* \mathrm{e}^{j2\pi W_c(m-n)\tau_u}\} \qquad (6.12) \\ &= G\left(W_c(m-1) - \tfrac{W_c N}{2}\right) G^*\left(W_c(n-1) - \tfrac{W_c N}{2}\right) \\ &\quad \cdot \left(\frac{1}{T_d}\int_0^{T_d} \mathrm{e}^{j2\pi W_c(m-n)\tau} d\tau\right) \sum_{u=1}^{L} \sigma_{\Lambda_u}^2 \qquad (6.13) \\ &= G\left(W_c(m-1) - \tfrac{W_c N}{2}\right) G^*\left(W_c(n-1) - \tfrac{W_c N}{2}\right) \\ &\quad \cdot \mathrm{e}^{j\pi W_c(m-n)T_d} \mathrm{sinc}\left(W_c(m-n)T_d\right). \qquad (6.14) \end{aligned}$$

where $\mathrm{sinc}(x) = \frac{sin(\pi x)}{\pi x}$.

Considering that $g(t)$ is Dirac delta impulse function, we have that

$$C_{m,n}^{(1)} = \mathrm{e}^{j\pi W_c(m-n)T_d} \mathrm{sinc}\left(W_c(m-n)T_d\right). \qquad (6.15)$$

Therefore, the matrix $\mathbf{C}$ for case 1 can be written as

$$\mathbf{C}^{(1)} = \mathbf{S}(W_c T_d, W_c T_d), \qquad (6.16)$$

where $\mathbf{S}(x, y)$ is a $N \times N$ matrix with elements given by

$$s_{i,j}(x, y) = \mathrm{sinc}\left(x(i-j)\right) \mathrm{e}^{j\pi y(i-j)}. \qquad (6.17)$$

Then, thanks to the Toeplitz structure of the matrix $\mathbf{C}^{(1)}$, the following eigendecomposition holds when $N \to \infty$ [29],

$$\mathbf{C}_{\infty}^{(1)} = \lim_{N\to\infty} \mathbf{F}_N^H \mathbf{D}^{(1)} \mathbf{F}_N \qquad (6.18)$$

where

$$\mathbf{F}_N = \frac{1}{\sqrt{N}} \begin{pmatrix} 1 & 1 & 1 & \cdots & 1 \\ 1 & \omega^1 & \omega^2 & \cdots & \omega^{N-1} \\ \vdots & \vdots & \vdots & \ddots & \vdots \\ 1 & \omega^{(N-1)} & \omega^{2(N-1)} & \cdots & \omega^{(N-1)(N-1)} \end{pmatrix}$$

with $\omega = \mathrm{e}^{\frac{j2\pi}{N}}$ and $\mathbf{D}^{(1)}$ is a diagonal matrix with elements

$$d_{n,n} = \begin{cases} \frac{1}{W_c T_d}, & \text{for } 0 \leq n-1 \leq N W_c T_d \\ 0, & \text{otherwise.} \end{cases} \tag{6.19}$$

Note that $\mathbf{D}^{(1)}$ does not depend on L, but only on the delay spread T_d and the frequency resolution W_c.

6.2.2.2 Case 2

Based on the assumption that elements that characterize each path is mutually dependent but statistically independent of elements of any other path, and that (6.10) implies that the marginal distribution of $\tau_{k,\ell}$ is uniformly distributed in the interval $\left[\frac{T_d(\ell-1)}{L}, \frac{T_d \ell}{L}\right]$, $\mathbb{E}\{\lambda_{k,\ell}\} = 0$, and $\mathbb{E}\{|\lambda_{k,\ell}|^2\} = \sigma^2_{\Lambda_\ell}$ with $\sum_{k=1}^{L_k} \sigma^2_{\Lambda_\ell} = 1$. The $(m,n)-$th element of the covariance matrix $\mathbf{C}^{(2)} = \mathbb{E}\{\mathbf{h}_k \mathbf{h}_k^H\}$ is given by

$$\begin{aligned} C^{(2)}_{m,n} &= \sum_{\ell=1}^{L} \sigma^2_{\Lambda_\ell} G\left(W_c(m-1) - \frac{W_c N}{2}\right) G^*\left(W_c(n-1) - \frac{W_c N}{2}\right) \\ &\quad \cdot \mathbb{E}\{\mathrm{e}^{j2\pi W_c (m-n)\tau_\ell}\} \qquad (6.20) \\ &= \sum_{\ell=1}^{L} \sigma^2_{\Lambda_l} G\left(W_c(m-1) - \frac{W_c N}{2}\right) G^*\left(W_c(n-1) - \frac{W_c N}{2}\right) \\ &\quad \cdot \mathrm{e}^{j\pi W_c (m-n)\frac{T_d}{L}(2\ell-1)} \mathrm{sinc}\left(\frac{W_c T_d}{L}(m-n)\right). \qquad (6.21) \end{aligned}$$

Considering that $g(t)$ is a Dirac , (6.20) reduces to

$$C^{(2)}_{m,n} = \sum_{\ell=1}^{L} \sigma^2_{\Lambda_\ell} \cdot \mathrm{e}^{j\pi W_c (m-n)\frac{T_d}{L}(2\ell-1)} \mathrm{sinc}\left(\frac{W_c T_d}{L}(m-n)\right). \tag{6.22}$$

Therefore, the matrix $\mathbf{C}$ for case 2 can be written as

$$\mathbf{C}^{(2)} = \sum_{\ell=1}^{L} \sigma_{\Lambda_\ell}^2 \cdot \mathbf{S}\left(\frac{W_c T_d}{L}, \frac{W_c T_d}{L}(2\ell - 1)\right). \tag{6.23}$$

Asymptotically, for $N \to \infty$, the following eigen-decomposition holds

$$\mathbf{C}_\infty^{(2)} = \lim_{N\to\infty} \mathbf{F}_N^H \mathbf{D}^{(2)} \mathbf{F}_N \tag{6.24}$$

with

$$d_{n,n} = \begin{cases} \frac{\sigma_{\Lambda_\ell}^2 L}{W_c T_d} & \text{for } \frac{NW_cT_d}{L}(\ell-1) \le n-1 \le \frac{NW_cT_d}{L}\ell, \\ 0 & \text{otherwise.} \end{cases} \tag{6.25}$$

As one can observe, we have that $\mathbf{D}^{(2)} = \mathbf{D}^{(1)}$ when the $\lambda_{k,\ell}$ have identical distributions, *i.e.*, $\sigma_{\Lambda_\ell}^2 = \frac{1}{L}$, $\forall \ell = 1, \ldots, L$. This result shows that assumptions performed on case 2 does not introduce any modification/constraint on the asymptotic behavior of ChDMA for the case where no information about the delay profile is provided.

6.2.3 Spectral Efficiency Expressions

The spectral efficiency of ChDMA was presented in Section 5.3.4, Eq. (5.24). Let us decompose the $\mathbf{H}$ matrix in agreement of Section 6.2.2, we have that

$$\gamma = \frac{1}{N} \log\det\left(\mathbf{I}_N + \rho \mathbf{H}\mathbf{H}^H\right) \tag{6.26}$$

$$= \frac{1}{N} \log\det\left(\mathbf{I}_N + \rho \sqrt{\mathbf{D}^{(a)}} \mathbf{V}\mathbf{V}^H \sqrt{\mathbf{D}^{(a)}}^H\right) \tag{6.27}$$

where $\rho = \frac{\gamma}{\beta}\frac{E_b}{N_0}$, $a = 1, 2$ if the channel is modeled as in case 1 or in case 2 respectively, and $\mathbf{V}$ is an $N \times K$ matrix with random i.i.d. entries with zero mean and unitary variance.

The following theorem provides the spectral efficiency as $K, N \to \infty$ with constant ratio. In the asymptotic case, the spectral efficiency is deterministic and only depends on a few macroscopic system parameters.

Theorem 6.1. *Let* $\mathbf{H}$ *be an* $N \times K$ *matrix of random independent columns and let the elements of each column be correlated Gaussian random variables with zero mean and covariance matrix* $\frac{\mathbf{C}}{N}$. *Let us assume that asymptotically, as* $N, K \to \infty$, *while* K/N *remains constant, the empirical eigenvalue distributions of the matrices* $\mathbf{C}$ *converge to*

deterministic distribution density functions $f_{\mathbf{C}}(v)$*. Then, when* $K, N \to \infty$ *with* $\frac{K}{N} \to \beta$*, the spectral efficiency* γ *converges to a deterministic limit*

$$\gamma_\infty = \frac{1}{\ln 2} \int_0^\rho \frac{1}{x} \left[1 - \frac{1}{x} m\left(-\frac{1}{x} \right) \right] \mathrm{d}x, \tag{6.28}$$

with

$$m(z) = -\left(z - \frac{1}{\beta} \int \frac{v}{1 + v m(z)} \mathrm{d} f_{\mathbf{C}}(v) \right)^{-1} \tag{6.29}$$

where $m(z)$ *is the unique positive solution to (6.29).*

Proof The spectral efficiency (6.26) can be rewritten as

$$\begin{aligned} \gamma &= \frac{1}{N} \sum_i^N \log\left(1 + \rho \lambda_i(\mathbf{H}\mathbf{H}^H)\right) \\ &= \int \log(1 + \rho x) \left(\frac{1}{N} \sum_{i=1}^N \delta(x - \lambda_i) \right) \mathrm{d}x, \end{aligned} \tag{6.30}$$

where $\lambda_i(\mathbf{H}\mathbf{H}^H)$ is the eigenvalues of $\mathbf{H}\mathbf{H}^H$. Then, in the asymptotic regime, when $N \to +\infty$, the spectral efficiency can be described in terms of the eigenvalue distribution of $\mathbf{H}\mathbf{H}^H$ [66], *i.e.*,

$$\gamma_\infty = \int \log\left(1 + \rho\lambda\right) \mathrm{d} f_{\mathbf{H}\mathbf{H}^H}. \tag{6.31}$$

However, we can also represent the spectral efficiency as

$$\gamma_\infty = \int_0^\rho \frac{\mathrm{d}\,\gamma_\infty}{\mathrm{d}\,\rho} \mathrm{d}\,\rho. \tag{6.32}$$

Since

$$\begin{aligned} \frac{\mathrm{d}\,\gamma_\infty}{\mathrm{d}\,\rho} &= \frac{1}{\ln(2)} \int_0^\infty \frac{\lambda}{1 + \rho\lambda} \mathrm{d}\, f_{\mathbf{H}\mathbf{H}^H}(\lambda) \\ &= \frac{1}{\ln(2)\rho} \left(1 - \frac{1}{\rho} \int_0^\infty \frac{1}{\frac{1}{\rho} + \lambda} \mathrm{d}\, f_{\mathbf{H}\mathbf{H}^H}(\lambda) \right) \\ &= \frac{1}{\ln(2)\rho} \left(1 - \frac{1}{\rho} m\left(-\frac{1}{\rho} \right) \right), \end{aligned} \tag{6.33}$$

where $m(z)$ represents the Stieltjes transform [44]. Consequently, we can observe that Theorem 6.1 holds

$$\gamma_\infty = \frac{1}{\ln 2}\int_0^\rho \frac{1}{x}\left(1-\frac{1}{x}m\left(-\frac{1}{x}\right)\right)\mathrm{d}\,x. \tag{6.34}$$

For case 1 (see Eq. (6.19)) and case 2 (see Eq. (6.25)) the limiting eigenvalue probability density functions of the covariance matrix $\mathbf{C}$ are given by

$$f_{\mathbf{C}}^{(1)}(v) = (1-W_cT_d)\delta(v) + W_cT_d\delta\left(v-\frac{1}{W_cT_d}\right) \tag{6.35}$$

and

$$f_{\mathbf{C}}^{(2)}(v) = (1-W_cT_d)\delta(v) + \frac{W_cT_d}{L}\sum_{\ell=1}^{L}\delta\left(v-\frac{\sigma_{\Lambda_\ell}^2 L}{W_cT_d}\right) \tag{6.36}$$

respectively.

6.2.4 Performance Analysis

In this section, we present the results obtained by asymptotic analysis (Eq. 6.28) and compare them with the results obtained by the Monte Carlo simulations of ChDMA systems of finite dimensions (Eq. 6.26). For finite simulated systems, we consider two different methods to build the channel matrix: in Method 1, random paths are generated under the restrictions discussed in Section 6.2.2, while Method 2 randomly generates i.i.d. gaussian matrix $\mathbf{V}$ and multiplies it by the deterministic matrix $\mathbf{D}^{(a)}$ to obtain the channel matrix. We study four particular parameters: the number of multipaths (L), the ratio β, the number of frequency samples of the wireless channel (N) and the energy per bit to noise ratio (E_b/N_o).

The results are obtained by averaging over 500 Monte Carlo simulations. We considered an environment with a maximum delay spread of $25ns$. Furthermore, when β, the number of frequency samples N, the frequency resolution W_c, the ratio E_b/N_0 or the number of multipaths L are not given, we assume that they are respectively 0.8, 50, $40M$Hz, 5dB and 100.

6.2.4.1 Validation

As a first step, we validate numerically the assumptions made to derive the asymptotic results and we compare the resulting spectral efficiency with known results in the

literature.

In Fig. 6.9, the impact of the number of frequency dimensions on the spectral efficiency is presented. As the number of dimensions increase, the spectral efficiency of all the simulated channels converge to the asymptotic theoretical value. Convergence was also observed for different system configurations, but the speed of converge is strongly dependent on all the system parameters.

Fig. 6.10 shows how the spectral efficiency is affected when the number of channel paths changes. For small values of L, the averaged spectral efficiency of Method 1 is lower than the spectral efficiency of Method 2 whose the energy is equally spread over all the bandwidth. On the other hand, when the number of paths increases modestly, the assumption presented in (6.18) holds even for small values of N ($N = 50$).

It is possible to verify that the spectral efficiency γ_∞ reduces to the expression for the asymptotic spectral efficiency per chip of CDMA systems with random spreading codes studied by Verdú and Shamai in [81] when $T_d = W_c^{-1}$ and the power delay profile is uniform. Fig. 6.11 compares the spectral efficiency as a function of the system load β in case of finite simulated channels with the asymptotic theoretical spectral efficiency of CDMA as $\frac{E_b}{N_0} = 10dB$. Although the plots are obtained assuming a very low number of frequency dimensions in the finite case ($N = 50$), the two curves match completely for different values of β.

6.2.4.2 Power Delay Profile

In this section we investigate the impact of a nonuniform power delay profile (PDP) on the spectral efficiency of ChDMA systems. We consider an exponentially decaying PDP when the assumptions of case 2 are enforced. This type of profile is more realistic and it is largely used to characterize the UWB environment [11, 61]. Such profile is defined by assuming that the variance of the complex channel gains are $\sigma^2_{\Lambda_\ell} = \frac{\alpha_1}{L(1-e^{-\alpha T_d})} e^{-\alpha \tau_\ell}$, where α is the decay factor.

To analyze the impact of the PDP, we consider five different decay factor values in the exponential decaying profile. Fig. 6.12 shows the spectral efficiency of a ChDMA system with exponential PDP as a function of the load β for $\alpha = 0.01$, 1, 5, 10. Furthermore, the performance of the system with exponentially decaying PDP is compared to case of uniform PDP (solid line) with $\alpha = 0$. Increasing the parameter α increases the spectral efficiency when the system load β is sufficiently large, because the channel energy is concentrated in a small portion of the channel interval. This concentration creates an inefficient utilization of the available system dimensions and the receivers cannot separate

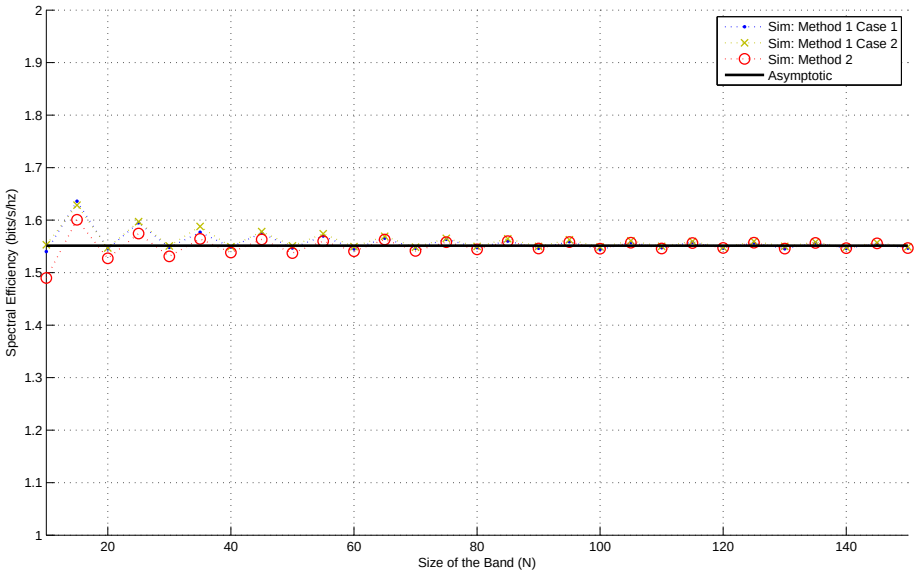

Figure 6.9: Impact of the number of frequency samples N.

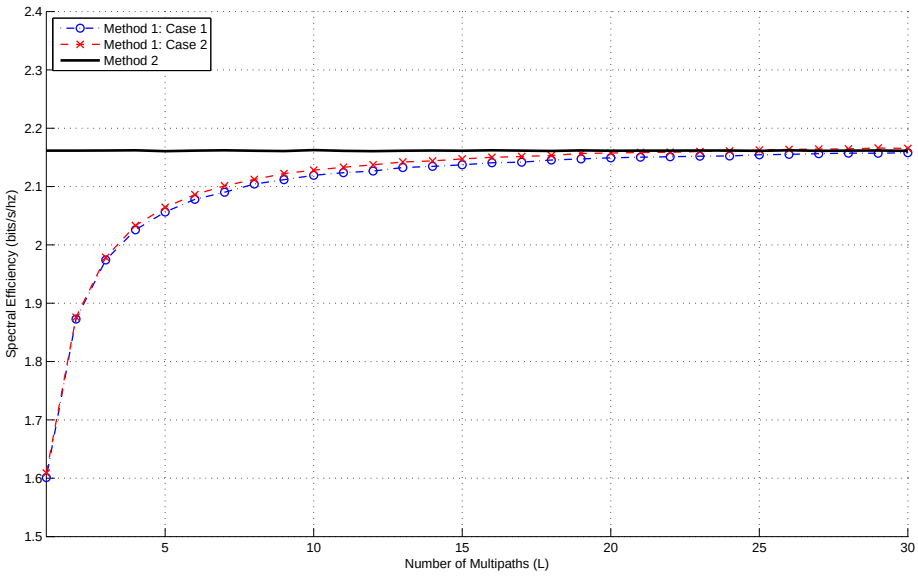

Figure 6.10: Impact of the number of paths L.

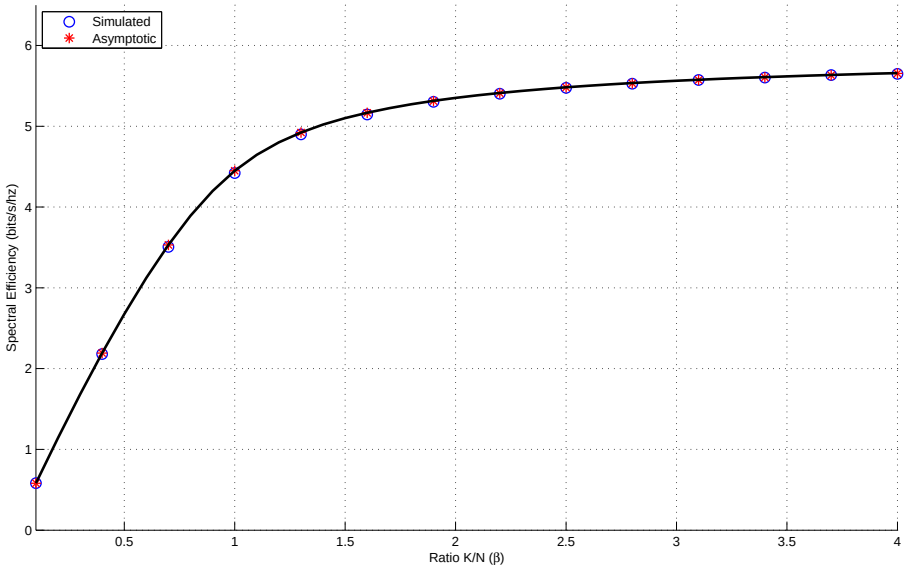

Figure 6.11: Validation of ChDMA with the CDMA result ($E_b/N_0 = 10dB$).

the information transmitted by different users. On the other hand, for smaller values of α, the system performance tends to the performance of a system with uniform PDP, as we would expect.

6.3 Summary

In this chapter we provided an analysis of ChDMA systems in terms of spectral efficiency. We observed that ChDMA performs quite well under various system configurations and we can conclude that it really is an interesting option to be adopted in IR-UWB systems.

In Section 6.1, we presented some numerical analysis of the performance of the ChDMA for different system parameters. We observe that the number of users per spreading factor is an important parameter for the ChDMA (as it is for the CDMA case [81]). Furthermore, the performance of the scheme is directly related to the kind of receiver that is employed at the base station, and the performance under the same conditions is very close to the one achieved by CDMA systems transmitting over flat-fading channels. Nevertheless, in some cases ChDMA performs better performance than CDMA, even when orthogonal codes were employed. We also observed that asynchronism is beneficial for ChDMA and provide some gain when the delay spread is low relative

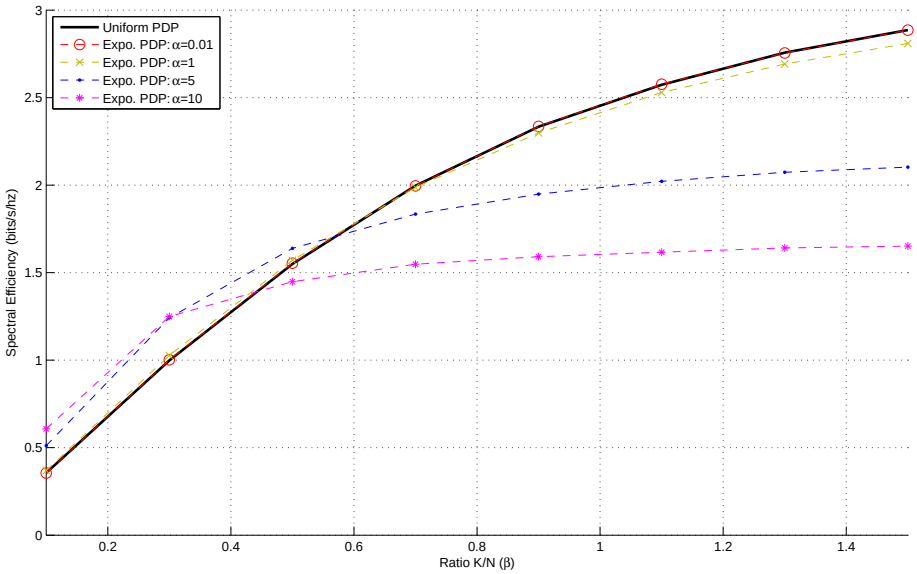

Figure 6.12: Impact of the Power Delay Profile.

to the interval between consecutive transmissions.

In Section 6.2, the performance of ChDMA is evaluated assuming that the system size is large. Under this asymptotic condition, the spectral efficiency is independent of the channel realization and becomes deterministic. Two channel models were considered and analytic expressions of the spectral efficiency were derived based on results of random matrix theory. We validated the asymptotic equations via simulation results and verified the impact of the power delay profile on ChDMA systems.

Part III

Conclusions and Perspectives

Chapter 7

Conclusions and Perspectives

"Believe those who are seeking the truth. Doubt those who find it."

(André Gide)

7.1 Part I: MaxEnt Modeling

The first part of this thesis aims at providing a unified framework to perform statistical inferences on channel models based on the Bayesian probability theory, particularly, the maximum entropy principle. This principle affirms that the distribution that maximizes the entropy is the most consistent distribution to represent the randomness of what is being modeled.

In Chapter 3, we have studied the wideband channel case. We have shown that, although in modeling one should take into account all the information at hand, there is a compromise to be made in terms of model complexity. In the wideband channel case, we have concluded that it is possible to reproduce the channel frequency behavior with a limited number of coefficients. However, each information added will not have the same effect on the channel model and might as well add more complexity to the model for nothing rather than bring useful insight on the behavior of the propagation environment. In this respect, entropy has been show to be a useful measure, and we have employed it to identify the optimum number of parameters to represent the bandwidth. Moreover, the entropy allowed us to analyze how the channel scales with the bandwidth. For the two models that have been derived, when the knowledge available is the correlation vector or

the channel power, we have shown that the necessary number of parameters to describe the channel scales linearly with the channel bandwidth.

In Chapter 4, we have studied the MIMO channel case. The models aim at representing the pdf of the channel matrix entries based on some knowledge available of the wireless environment. Three different models have been devised to represent different states of knowledge: average channel energy, full covariance matrix and rank of the covariance matrix. Remarkably, the first two models have resulted in a Gaussian pdf of the channel matrix entries. The third model, which has been devised through the marginalization property of the MaxEnt framework, resulted in a very different pdf. Nevertheless, full covariance matrix rank has been introduced as a new metric to characterize the environment based only in one single parameter. To evaluate this new metric, we carried out some MIMO measurements to verify if different environments would be represented by different full covariance matrix rank. For such an approach, we have considered the distribution of the singular values of the channel matrix. We have verified that different scenarios are represented by different singular value distributions. To identify the best representation of the environment, we have employed the relative entropy and have concluded that different environments can be characterized by different values of the covariance matrix rank.

7.2 Part II: ChDMA

In this part, we aim at introducing a new multiple access scheme to IR-UWB systems that could cope with the distortions of the wireless environment while providing high spectral efficiencies. The result is a very simple scheme that exploits the channel diversity as codes to perform the multiple access.

In Chapter 5, we have studied the impact of multiple access in IR-UWB systems. We have concluded that none of the conventional multiple access schemes were designed to cope with the low duty cycle characteristic of IR-UWB systems combined with the high temporal dispersion of UWB channels. Although some of the multiple access schemes could be employed, they would present very low spectral efficiencies. While studying CDMA, we have had the idea to use the natural channel dispersion as code signatures. This approach, that we have called ChDMA, simplifies the transmitter while allowing simultaneous access.

In Chapter 6, we have analyzed the spectral efficiency of ChDMA. First, we have evaluated the impact of different system parameters on the performance of ChDMA. We have considered three different receivers: optimal receiver, MF and Linear MMSE.

For some system configurations, we have compared the ChDMA with the CDMA. We have verified that even if CDMA operates in ideal conditions (no channel dispersion and perfect synchronism), ChDMA could provide very similar results. Sometimes, ChDMA could even outperform CDMA. After that, we have presented an asymptotic analysis when the system is large, *i.e.*, the number of users and the system bandwidth grows to infinity with the same rate. Under the asymptotic regime assumption, we have shown that the spectral efficiency becomes deterministic, which means that it is independent of the channel realizations. Finally, we validate the analytical expressions via simulation results, where we have also shown the impact of the power delay profile.

7.3 Perspectives and Future Works

The work carried during this three years could answer some questions, but others have emerged. In the following, we present some interesting extensions of this thesis:

Generalize the MaxEnt framework: The MaxEnt framework has been applied in this thesis to model the wideband and the MIMO channel under very specific priors. A direct extension is to consider other kinds of priors. Furthermore, the same approach can be also employed to model other characteristics of wireless systems.

Exploit the MaxEnt models: MaxEnt models enabled us to introduce new metrics to characterize the environment. As an example, we obtained for the MIMO channel that the environment could be represented by the rank of the full covariance matrix. Consequently, the performance evaluation of MIMO systems when this knowledge is available in one or both transceiver sides is to be conducted. Moreover, the same methodology can be employed to introduce new metrics.

ChDMA performance: We have introduced ChDMA in this thesis, but all the results presented have been performed under the assumption of ideal channel knowledge. The effect of channel estimation on the ChDMA performed is to be conducted. Problems related to errors on channel estimations, the impact of training on the spectral efficiency of the system and refine the UWB channel models to include typical behaviors such as the non-linear frequency attenuation need to be investigated.

ChDMA feasibility: The feasibility of ChDMA is also a research topic to be investigated. Although the idea seems interesting, some aspects on the deployment of such a system require further analysis.

Part IV

Appendix and References

Appendix A

Eurecom MIMO Openair Sounder (EMOS)

In order to analyze the MIMO channel, Eurecom has developed a MIMO platform called Eurecom MIMO Openair Sounder (EMOS) which employs 4 transmit antennas and 2 receive antennas. The main idea behind EMOS is to carry out real MIMO channel measurements on a real-time basis, unlike [47]. EMOS is capable of providing real time measurements with polarization and adjustable antenna spacing. This appendix presents some initial results concerning the MIMO channel capacity of real wireless channels in the UMTS-TDD band using Eurecom MIMO Openair Sounder (EMOS). We describe the necessary steps to estimate in real-time the wireless MIMO environment, offering the possibility to identify reliable MIMO channels as well as the instantaneous channel capacity. Finally, based on the measurements, we present some results for the analysis of the polarization impact on the capacity performance.

A.1 The EMOS

EMOS is a real-time platform able to carry out real transmissions using the UMTS-TDD band. Based on the OpenAir system developed at Eurecom [53, 83], EMOS is able to operate in real-time dealing with real RF signals. It is developed with the purpose to create an ideal architecture for experimenting with real wireless environments as well as analytical results validation.

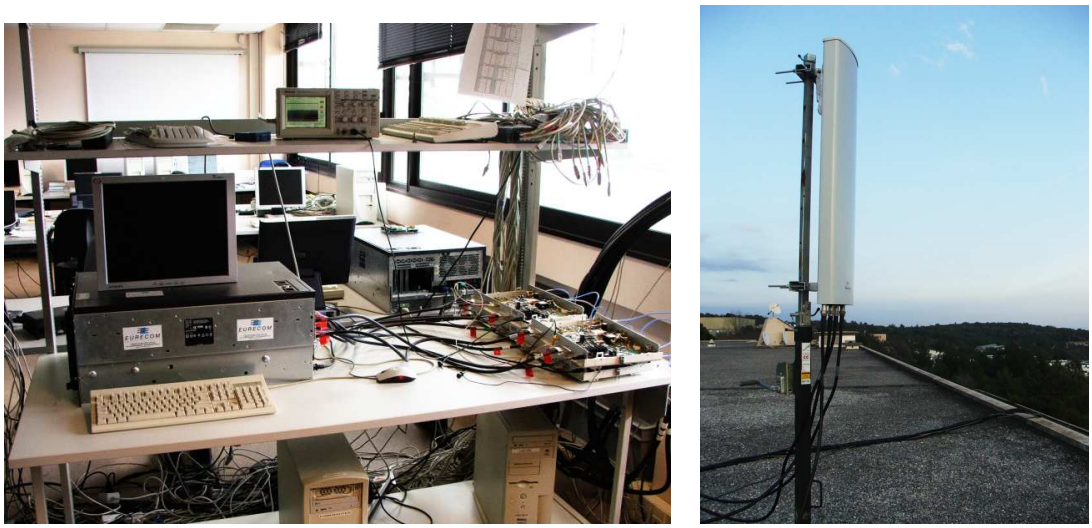

(a) Base Station server. (b) Powerwave Antenna.

Figure A.1: Base-station antenna configuration.

The platform consists of a base-station that sends a signaling frame continuously, and some (one or more) terminals that receive the frames to estimate the channel. For the base-station (see Fig. A.1(a)), an ordinary server PC is employed with four PLATON Cards[1] [9], where each card is connected to a power amplifier which feeds an antenna. As far as the terminals are concerned, an ordinary laptop computer is used along with Eurecom's dual-RF CardBus/PCMCIA card [53], which allows to employ two antennas for two-way real-time experimentation.

[1]The PLATON cards were originally built as an UMTS-TDD testbed and include much more functionalities than required for EMOS.

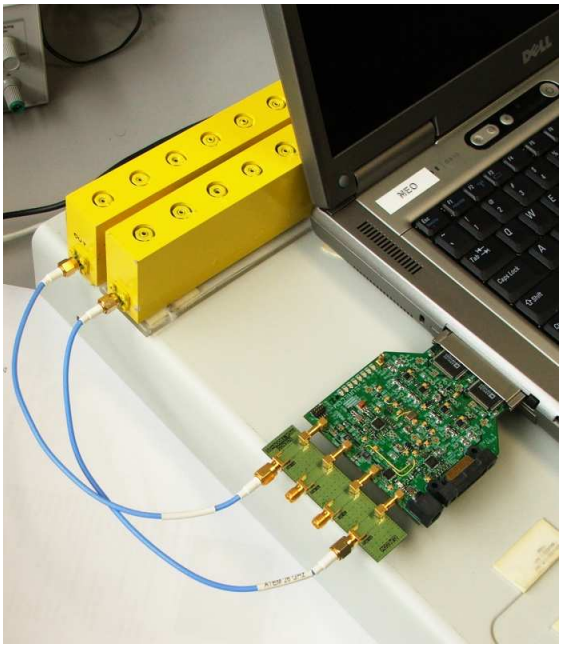

(a) Dual-RF CardBus/PCMCIA Card.

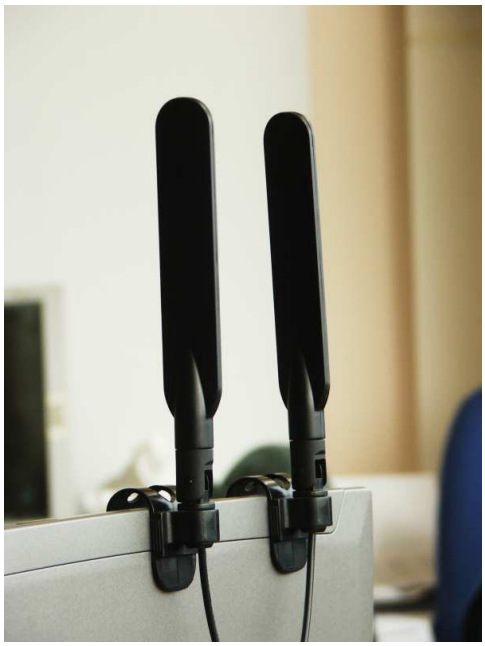

(b) Panorama Antennas.

Figure A.2: Terminal antenna configuration.

Table A.1: Powerwave antenna (part no. 7760.00)

Parameter	Value
Frequency range (MHz)	1710-2170
Frequency band (MHz)	(1710-1800) (1850-1900) (1900-2025) (2110-2170)
Electrical downtilt	0^o to 8^o
Number of elements	4

A.1.1 Antenna Settings

The antenna employed at the base-station is the Powerwave part no. 7760.00 (see Fig. A.1(b)). It is a 3G broadband antenna composed of four elements which are arranged in two cross-polarized pairs. The main parameters concerning the base-station antenna are listed in Table A.1.

The antennas employed at the terminal are the Panorama Antennas, part no. TCLIP-DE3G (see Fig. A.2(b)). It is basically a 3G antenna with a clip mount for laptop computers. The main parameters concerning the terminal antenna are listed in Table A.2.

Table A.2: Panorama antenna (part no. TCLIP-DE3G)

Paramater	Value
Frequency range (MHz) Frequency band	(824-960) (1710-2170) (GSM850) (GSM900) (GSM1800) (GSM1900) (3G UMTS)

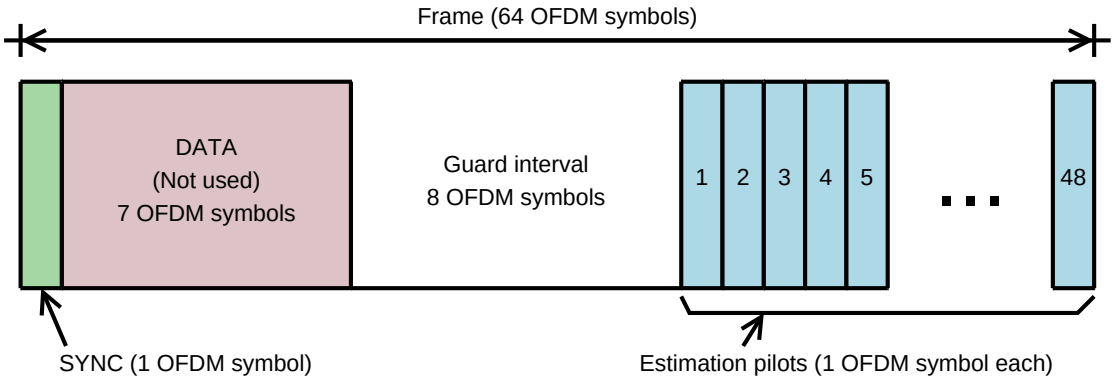

Figure A.3: Frame structure.

A.1.2 Transmit Frame

Although originally based on the UMTS-TDD standard, recent developments have pushed the Eurecom's team to use an OFDMA based signaling. Hence, at the base-station, four data sequences are transmitted in parallel, i.e., each TX chain has its own sequence. To simplify the processing complexity at the receiver, four frequency-orthogonal sequences were employed.

The transmit frame is illustrated in Fig. A.3. Because of the constant variation of the wireless channel and in order to take into account the coherence time of the channel, we considered a small frame (the frame duration is approximately of $2.5ms$). For a reliable estimation, we divided the frame in 64 packets, where each packet represents an OFDM symbol composed only by 320 symbols (256 useful symbols and 64 symbols of cyclic prefix, which give 64 symbols for each TX chain). For processing purposes, the frame is constituted by 4 different kinds of data:

- The first part of the frame is composed of one single OFDM symbol. This symbol has a special structure that permits the terminal to easily synchronize with the base-station.

- The second part of the frame is composed of useful data. For the moment, it is not used.

- The third part is composed of zeros. This part is used to estimate the noise characteristics.
- The fourth and last part of the frame, is composed of a sequence of OFDM pilot symbols.

A.1.3 Receiver Processing

At the receiver, the terminal does the frame synchronization procedure and suppresses the phase-shift noise generated by the dual-RF CardBus/PCMCIA card. After that, it estimates the MIMO channel for channel capacity analysis.

A.1.3.1 Frame Synchronization

The first step of the receiver processing is the frame synchronization. At this step, the receiver stores the received data in a memory with twice the size of a frame. After that, the receiver does a correlation analysis between the received data and the OFDM symbol dedicated to the synchronization purpose. Then, the synchronization is decided based on the position of the maximum value resulting from that correlation.

It is important to notice that for the moment, this synchronization procedure is employed for each frame, with the objective to guarantee that no error due to synchronization will occur during the channel estimation and/or capacity analysis.

A.1.3.2 Phase-Shift Noise Suppression

The second step of the receiver processing is the phase-shift noise suppression. Generated by the RF circuit, the phase-shift noise was observed to have a slow variation characteristic. For this reason, to guarantee a good phase-shift suppression for the received signal at each receive antenna, we mitigate the phase shift for each OFDM pilot symbol of each frame.

Assuming that $\mathbf{y}^{(k)}$ is the received OFDM pilot symbol vector (1×320) of the kth OFDM pilot symbol of the received frame, where $17 \leq k \leq 64$. We model the phase-shift noise as being constant for each OFDM symbol and different for different OFDM symbols, which turns out to be a good model for the Eurecom's dual-RF CardBus/PCMCIA. For the noise-shift suppression, first the ratio between the phase-shift of the first OFDM pilot symbol ($k = 17$) and all the other pilots are estimated by the following equation:

$$\upsilon^{(k)} = \frac{1}{320} \sum_{a=1}^{320} \frac{\mathbf{y}^{(17)}[a]}{\mathbf{y}^{(k)}[a]}. \tag{A.1}$$

After that, we multiply each vector $\mathbf{y}^{(k)}$ by the respective normalized and estimated phase-offset $\upsilon^{(k)}$, which give us a constant phase-shift for each frame

$$\mathbf{y}_{new}^{(k)} = \upsilon^{(k)} \cdot \mathbf{y}_{old}^{(k)}. \tag{A.2}$$

A.1.3.3 Channel Estimation

The next step is the most important one and it concerns the estimation of the MIMO channel. To diminish the effects of the white noise, each OFDM pilot is used to estimate the MIMO channel and all estimations of one frame are averaged. As a consequence, a reliable MIMO channel estimation is obtained per frame.

Consider $\mathbf{x}$ as being the transmitted signal, $\mathbf{H}$ the MIMO channel matrix, $\mathbf{n}$ the additive white gaussian noise and $\mathbf{y}$ the received signal, the system model can be represented in frequency by the following equation

$$\mathbf{y}_i^{(k)}[f] = \mathbf{H}_i^{(k)}[f]\mathbf{x}^{(k)}[f] + \mathbf{n}_i^{(k)}[f] \tag{A.3}$$

where i represents the frame index, k represents the index of an OFDM symbol of a frame, f represents the discrete and normalized frequency generated by the OFDM signaling, $\mathbf{y}_i^{(k)}[f]$, $\mathbf{x}^{(k)}[f]$ and $\mathbf{n}_i^{(k)}[f]$ are respectively the received vector $(N_r \times 1)$, the transmitted symbol vector $(N_t \times 1)$ and the AWGN vector $(N_t \times 1)$, and $\mathbf{H}_i^{(k)}[f]$ is the channel matrix $(N_r \times N_t)$.

By using the OFDM signaling properties, the MIMO channel matrix estimated by each transmitted OFDM pilot is given by

$$\begin{aligned}
\bar{\mathbf{H}}_i^{(k)}[f]_{(rx,tx)} &= \frac{\mathbf{y}_i^{(k)}[f]_{(tx)}}{\mathbf{x}_{PILOT}^{(k)}[f]_{(tx)}} && \text{(A.4)}\\
&= \frac{\mathbf{H}_i^{(k)}[f]_{(rx,tx)}\mathbf{x}^{(k)}[f]_{(tx)} + \mathbf{n}_i^{(k)}[f]_{(rx)}}{\mathbf{x}_{PILOT}^{(k)}[f]_{(tx)}} && \text{(A.5)}\\
&= \mathbf{H}_i^{(k)}[f]_{(rx,tx)} + \frac{\mathbf{n}_i^{(k)}[f]_{(rx)}}{\mathbf{x}_{PILOT}^{(k)}[f]_{(tx)}} && \text{(A.6)}
\end{aligned}$$

where rx and tx represents respectively the receive and the transmit antennas.

To mitigate the noise of the channel estimation procedure, we average all the 48 channel estimations of one frame. Assuming that the channel is constant during the transmission of one frame (the expected coherence time of our measurements is around

$10ms$), we have that

$$\mathtt{E}(\bar{\mathbf{H}}_i^{(k)}[f]_{(rx,tx)}) = \mathtt{E}\left[\mathbf{H}_i^{(k)}[f]_{rx,tx} + \frac{\mathbf{n}_i^{(k)}[f]_{rx}}{\mathbf{x}_{PILOT}^{(k)}[f]_{tx}}\right] \tag{A.7}$$

$$\begin{aligned}\bar{\mathbf{H}}_i[f]_{(rx,tx)} &= \mathtt{E}\left[\mathbf{H}_i^{(k)}[f]_{(rx,tx)}\right] + \mathtt{E}\left[\frac{\mathbf{n}_i^{(k)}[f]_{(rx)}}{\mathbf{x}_{PILOT}^{(k)}[f]_{(tx)}}\right] &\text{(A.8)}\\ &= \mathbf{H}_i^{(k)}[f]_{(rx,tx)} + \frac{1}{48}\sum_{i=1}^{48}\frac{\mathbf{n}_i^{(k)}[f]_{(rx)}}{\mathbf{x}_{PILOT}^{(k)}[f]_{(tx)}} &\text{(A.9)}\end{aligned}$$

and for high SNR, we have

$$\bar{\mathbf{H}}_i[f] \cong \mathbf{H}_i^{(k)}[f] \tag{A.10}$$

A.1.3.4 MIMO Capacity Analysis

The last step of the receiver processing is the MIMO capacity estimation. Based on the classical results available in the literature [72, 22, 23, 74], we calculate the capacity by analyzing the estimated MIMO channel matrix. The result gives us an estimated capacity per frequency

$$C_i[f] = \log_2\left[\det\left(\mathbf{I}_2 + \frac{\rho}{4}\bar{\mathbf{H}}_i[f]\bar{\mathbf{H}}_i^{\dagger}[f]\right)\right] \tag{A.11}$$

where ρ is the signal-to-noise ratio (SNR) for each receiver chain. As one can see, for the capacity analysis, the constant phase-shift of each frame ($\upsilon^{(k)}$) does not affect the capacity because it disappears during the calculation of the capacity. For the analysis presented in this paper, two different capacity results are considered: 1) Assuming a given SNR, which means that the columns of the channel are normalized; 2) Assuming the real SNR, which means that after the channel normalization we analyze the capacity for the estimated SNR.

A.2 Measurement

As described before, the analysis conducted in this paper are based on the transmission from the base-station with four transmit antennas to the terminal with two receive antennas. On the analysis, along with 4x2 MIMO architecture, we also show the capacity

Table A.3: Measurement Characteristics

Parameter	Value
Center frequency	1907.6 MHz
Bandwidth	5 MHz
Base-Station Tx Power	34 dBm
Number of Tx Antennas	4
Number of Rx Antennas	2

performance obtained when 2x2 and 1x1 antenna combination is considered. The main radio characteristics adopted by EMOS for this measurement are listed in the Table A.3

A.2.1 Environment

For the measurement, an outdoor scenario very close to Eurecom Institute is considered, which is characterized by a semi-urban hilly environment, composed by short buildings and vegetation (see Fig. A.4). The base-station antenna is situated in one of the highest buildings of the region and has a direct view of the environment. The outdoor measurements were conducted in a parking very close to the buildings that we see in the figure.

A.2.2 Polarization

For the capacity evaluation, two different kinds of polarizations are considered. The goal is to analyze the impact of the use of co-polarized antennas with space diversity and cross-polarized co-located antennas at the transmitter. The considered transmit structures are shown in Fig. A.5. For the case where we have 4 transmit antennas, it is considered the two pairs of co-polarized/cross-polarized antennas.

A.3 Some Results

In this section we present some measurements performed in an outdoor environment. The purpose of these results is to show the impact of the transmit architecture (number of antennas and/or polarization). Furthermore, we can evaluate the gains offered by the use of MIMO structures in a usual realistic environment. For this reason, we analyze the achievable capacity when we employ not only a 4×2 MIMO, but also assuming other antenna combinations: 1×1 MIMO, 2×2 MIMO with co-polarized antennas at the transmitter, 2×2 MIMO with cross-polarized antennas at the transmitter. The results shown here represent only an illustrative measurement campaign made with the EMOS

Figure A.4: View from the BS.

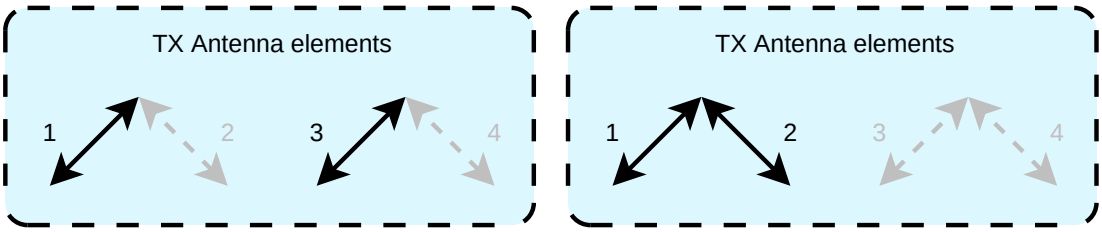

(a) Co-polarized configuration.

(b) Cross-polarized configuration.

Figure A.5: Transmit antenna polarizations.

platform and performed at the route shown in Fig. A.6.

At the receiver, the MIMO channel is estimated and the instantaneous capacity is derived as described before. In Fig. A.7, an estimated channel between the transmit antenna 1 and the receiver antenna 1 is shown (for each pair of transmit-receive antennas an estimated matrix like the one presented in the figure is obtained). As it can be noted, a route with constant channel characteristics and with a good SNR ($\simeq 30dB$) was chosen. The measurement was performed at a storage rate of a frame at each 0.1s and with a

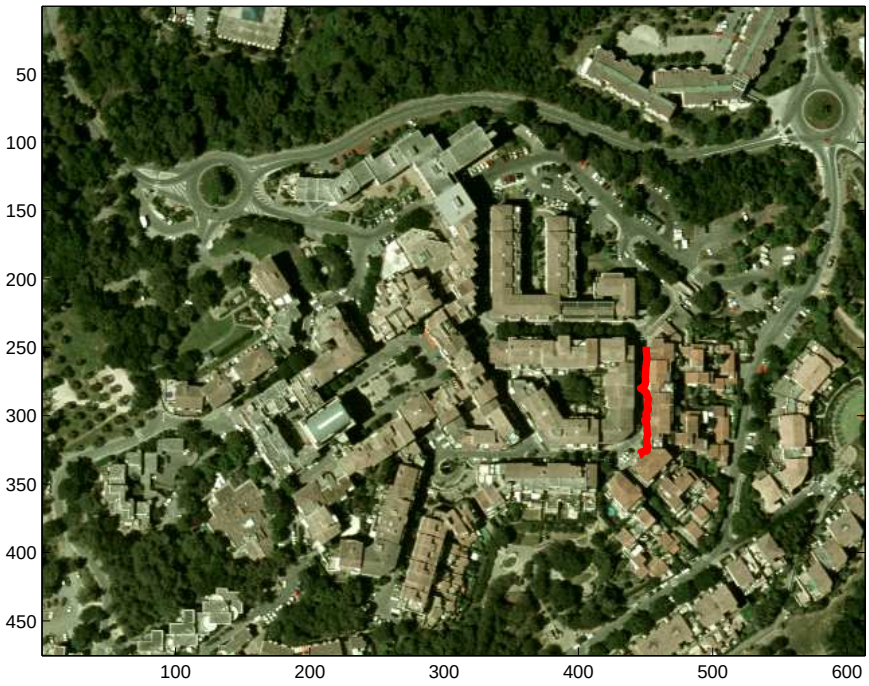

Figure A.6: Route where the measurements where performed.

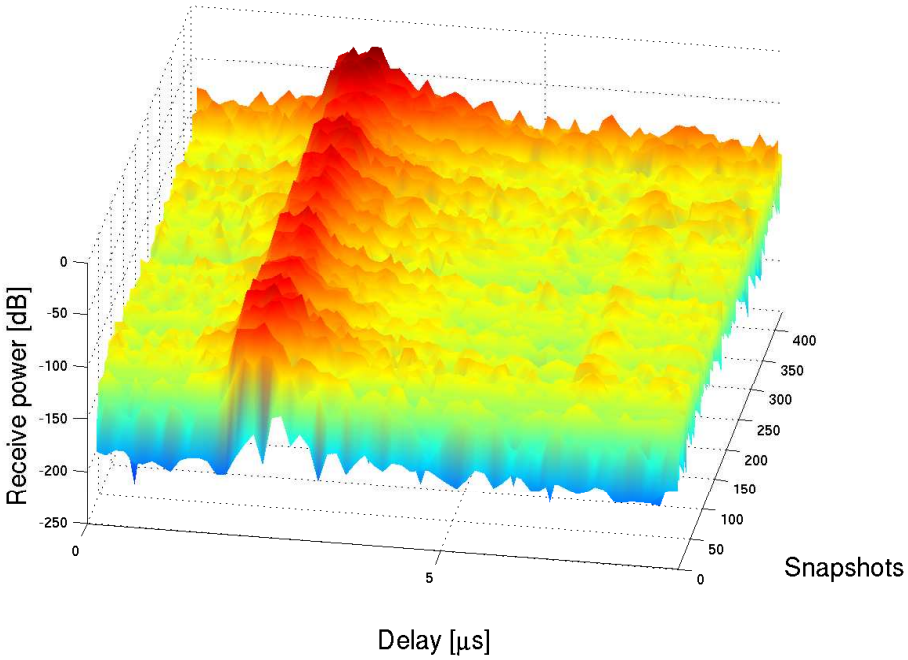

Figure A.7: Estimated channel over measurement (TX1 - RX1).

receive antenna space equal to $\lambda/2$.

The plot shown in Fig. A.8 shows the instantaneous capacity achieved by each frame over the measurement run. This result is obtained by the capacity average among all considered frequencies. As it can be noted, the average behavior of the capacity for all antenna combinations follows the signal fluctuation due to the path loss and fast fading.

The capacity CDF shown in Fig. A.9 assumes a constant receive SNR of 10dB and an average of the obtained capacity among different frequencies. Furthermore, we also plotted the achievable capacities when i.i.d. MIMO channels randomly generated are considered.

As it can be seen, the real environment performs worse than the i.i.d. MIMO channels. It can also be seen that the use of MIMO increases the capacity when we compare it with the SISO case. It is important to note that the gain offered by the use of 2×2 MIMO is really important, almost doubling the SISO capacity. On the other hand, increasing the number of antennas in this environment for more than 2 antennas at the transmitter does not yield in a further increase. Another important conclusion of the presented result is that we see an important gain when a cross-polarization antenna is used as compared with the obtained capacity when co-polarized antennas are used at the transmitter.

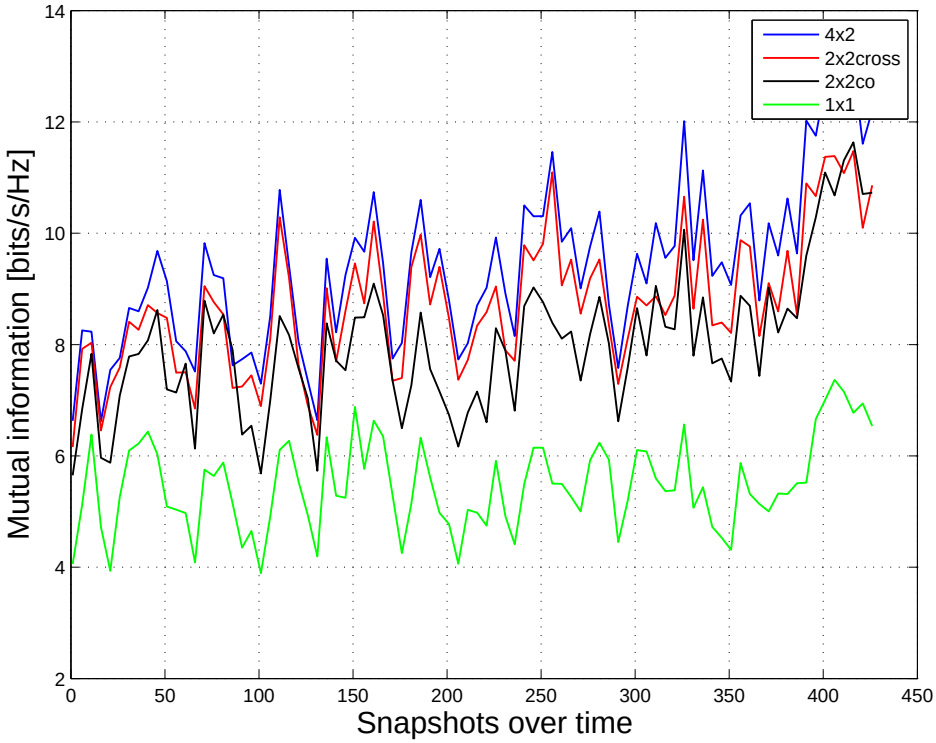

Figure A.8: Capacity over measurement (actual frame SNR).

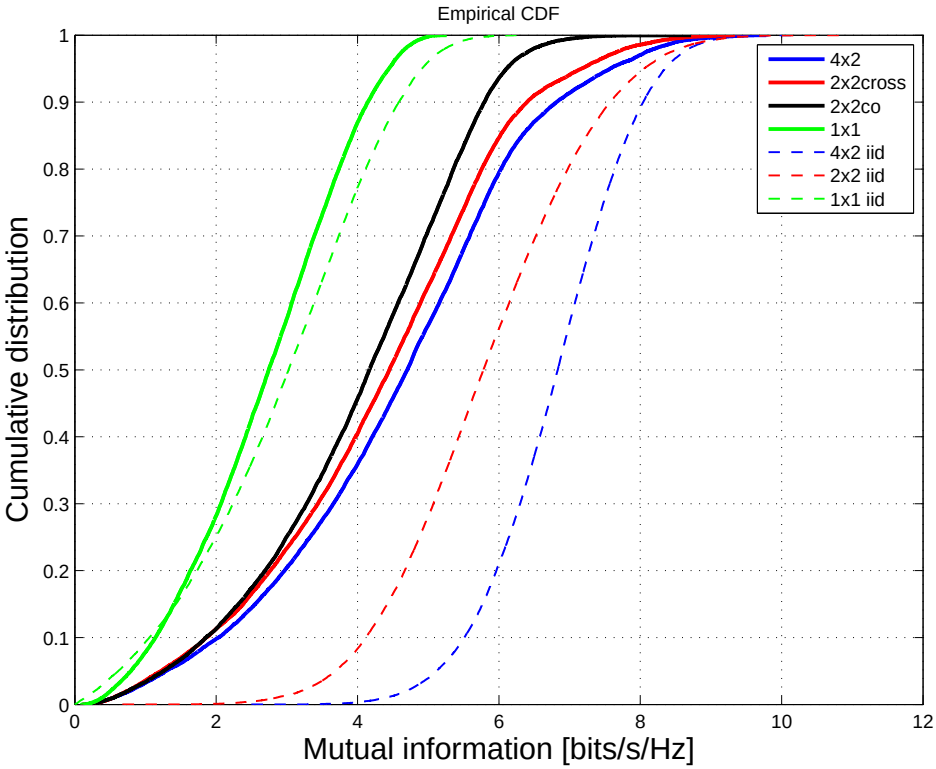

Figure A.9: Capacity for a given SNR (10dB).

Appendix B

Mutual Information for BPSK and QPSK Signaling

In the following pages we present the proof of the mutual information equations when BPSK and QPSK signaling is employed.

Based on the mutual information equation presented in Section 2.2, Eq. (2.4), the average mutual information for a specific signal space S can be represented as being:

$$I(x;y) = \sum_{x \in S} \int_{-\infty}^{+\infty} P(x)P(y|x) \log_2 \left[\frac{P(y|x)}{\sum_x' P(x')P(y|x')} \right] dy. \tag{B.1}$$

Substituting within the expression the probabilities of the BPSK and QPSK signaling schemes, we can derive the spectral efficiency for these schemes.

B.1 BPSK Case

In a BPSK modulation the points of the constellation belong to $S = \{+A, -A\}$, which means that they lie on the real axis as shown in the Figure B.1. The conditional probabilities of y given x are represented by the formulas:

$$P(y|x = -A) = \frac{1}{\sqrt{2\pi N_0}} e^{-\frac{(y+A)^2}{2N_0}} \tag{B.2}$$

$$P(y|x = +A) = \frac{1}{\sqrt{2\pi N_0}} e^{-\frac{(y-A)^2}{2N_0}} \tag{B.3}$$

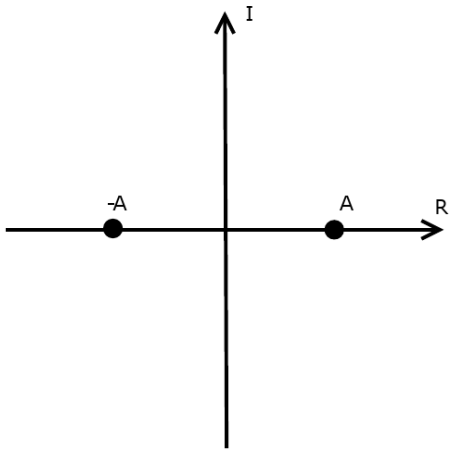

Figure B.1: BPSK constellation.

Substituting (B.3) in the formula of the average mutual information (B.1) we obtain:

$$
\begin{aligned}
I(x;y) &= \int_{-\infty}^{+\infty} \frac{e^{-\frac{(y+A)^2}{2N_0}}}{(2\sqrt{2\pi N_0})} \log_2 \left[\frac{\frac{1}{(\sqrt{2\pi N_0})} e^{-\frac{(y+A)^2}{2N_0}}}{\frac{1}{(2\sqrt{2\pi N_0})}(e^{-\frac{(y+A)^2}{2N_0}} + e^{-\frac{(y-A)^2}{2N_0}})} \right] dy \\
&\quad + \int_{-\infty}^{+\infty} \frac{e^{-\frac{(y-A)^2}{2N_0}}}{(2\sqrt{2\pi N_0})} \log_2 \left[\frac{\frac{1}{(\sqrt{2\pi N_0})} e^{-\frac{(y-A)^2}{2N_0}}}{\frac{1}{(2\sqrt{2\pi N_0})}(e^{-\frac{(y+A)^2}{2N_0}} + e^{-\frac{(y-A)^2}{2N_0}})} \right] dy \\
&= \int_{-\infty}^{+\infty} \frac{e^{-\frac{(y+A)^2}{2N_0}}}{(2\sqrt{2\pi N_0})} \log_2 \left[2(1 + e^{-\frac{(y-A)^2-(y+A)^2}{2N_0}})^{-1} \right] dy \\
&\quad + \int_{-\infty}^{+\infty} \frac{e^{-\frac{(y-A)^2}{2N_0}}}{(2\sqrt{2\pi N_0})} \log_2 \left[2(1 + e^{-\frac{(y+A)^2-(y-A)^2}{2N_0}})^{-1} \right] dy \\
&= \int_{-\infty}^{+\infty} \frac{e^{-\frac{(y+A)^2}{2N_0}}}{(2\sqrt{2\pi N_0})} \left[1 - \log_2(1 + e^{\frac{2yA}{N_0}}) \right] dy \\
&\quad + \int_{-\infty}^{+\infty} \frac{e^{-\frac{(y-A)^2}{2N_0}}}{(2\sqrt{2\pi N_0})} \left[1 - \log_2(1 + e^{-\frac{2yA}{N_0}}) \right] dy
\end{aligned}
\tag{B.4}
$$

which results in

$$\begin{aligned} I(x;y) &= \int_{-\infty}^{+\infty} \frac{e^{-\frac{(y+A)^2}{2N_0}}}{(\sqrt{2\pi N_0})} dy - \int_{-\infty}^{+\infty} \frac{e^{-\frac{(y+A)^2}{2N_0}}}{(2\sqrt{2\pi N_0})} \log_2\left(1+e^{\frac{2Ay}{N_0}}\right) dy \\ &\quad - \int_{-\infty}^{+\infty} \frac{e^{-\frac{(y-A)^2}{2N_0}}}{(2\sqrt{2\pi N_0})} \log_2\left(1+e^{\frac{-2Ay}{N_0}}\right) dy \end{aligned} \tag{B.5}$$

Let us now perform some variable changes to simplify (B.5). Assuming

$$\frac{(y+A)}{\sqrt{2N_0}} = t, \tag{B.6}$$

$$dy = \sqrt{2N_0}dt, \tag{B.7}$$

the first integral of the right hand part of (B.5) is reduced to

$$\int_{-\infty}^{+\infty} \frac{e^{-\frac{(y+A)^2}{2N_0}}}{(\sqrt{2\pi N_0})} dy = \frac{1}{\sqrt{\pi}} \int_{-\infty}^{+\infty} e^{-t^2} dt = \mathrm{erf}(\infty) = 1. \tag{B.8}$$

$\mathrm{erf}(x)$ is the Gauss error function.

For the second integral of (B.5), assuming that

$$\frac{(y+A)}{\sqrt{N_0}} = t, \tag{B.9}$$

$$dy = \sqrt{N_0}dt, \tag{B.10}$$

the integral is reduced to

$$\begin{aligned} \int_{-\infty}^{+\infty} \frac{e^{-\frac{(y+A)^2}{2N_0}}}{(2\sqrt{2\pi N_0})} \log_2\left(1+e^{\frac{2Ay}{N_0}}\right) dy &= \int_{-\infty}^{+\infty} \frac{e^{-\frac{t^2}{2}}}{(2\sqrt{2\pi N_0})} \log_2\left(1+e^{\frac{2A(\sqrt{N_0}t-A)}{N_0}}\right) \sqrt{N_0}dt \\ &= \int_{-\infty}^{+\infty} \frac{1}{(2\sqrt{2\pi})} e^{-\frac{t^2}{2}} \log_2\left(1+e^{-\frac{2A^2}{N_0}+\frac{2A\sqrt{N_0}}{N_0}t}\right) dt \end{aligned} \tag{B.11}$$

which is similar to the third one

$$\begin{aligned} \int_{-\infty}^{+\infty} \frac{e^{-\frac{(y-A)^2}{2N_0}}}{(2\sqrt{2\pi N_0})} \log_2\left(1+e^{\frac{-2Ay}{N_0}}\right) dy &= \int_{-\infty}^{+\infty} \frac{1}{(2\sqrt{2\pi})} e^{-\frac{t^2}{2}} \log_2\left(1+e^{-\frac{2A^2}{N_0}-\frac{2A\sqrt{(N_0)}}{N_0}t}\right) dt. \\ &= \int_{-\infty}^{+\infty} \frac{1}{(2\sqrt{2\pi})} e^{-\frac{t^2}{2}} \log_2\left(1+e^{-\frac{2A^2}{N_0}+\frac{2A\sqrt{N_0}}{N_0}t}\right) dt \end{aligned} \tag{B.12}$$

Since (B.11) and (B.12) are equal, knowing that $SNR = \frac{A^2}{N_0}$, the spectral efficiency when BPSK signaling is employed is :

$$\gamma_{\text{BPSK}} = 1 - \int_{-\infty}^{+\infty} \frac{e^{-\frac{t^2}{2}}}{\sqrt{2\pi}} \log_2 \left(1 + e^{-2\ \text{SINR} - 2\sqrt{\text{SINR}}t}\right) dt \tag{B.13}$$

B.2 QPSK Case

For a QPSK modulation, represented in the Figure B.2, the conditional probabilities of y given x become the following formulas:

$$\begin{aligned} P(y|x = -\frac{A}{\sqrt{2}} - i\frac{A}{\sqrt{2}}) &= \frac{1}{\sqrt{2\pi N_0}} e^{-\frac{(y_R + \frac{A}{\sqrt{2}})^2}{2N_0}} \frac{1}{\sqrt{2\pi N_0}} e^{-\frac{(y_I + \frac{A}{\sqrt{2}})^2}{2N_0}} \\ &= \frac{1}{2\pi N_0} e^{-\frac{(y_R + \frac{A}{\sqrt{2}})^2 + (y_I + \frac{A}{\sqrt{2}})^2}{2N_0}} \end{aligned} \tag{B.14}$$

$$\begin{aligned} P(y|x = +\frac{A}{\sqrt{2}} + i\frac{A}{\sqrt{2}}) &= \frac{1}{\sqrt{2\pi N_0}} e^{-\frac{(y_R - \frac{A}{\sqrt{2}})^2}{2N_0}} \frac{1}{\sqrt{2\pi N_0}} e^{-\frac{(y_I - \frac{A}{\sqrt{2}})^2}{2N_0}} \\ &= \frac{1}{2\pi N_0} e^{-\frac{(y_R - \frac{A}{\sqrt{2}})^2 + (y_I - \frac{A}{\sqrt{2}})^2}{2N_0}} \end{aligned} \tag{B.15}$$

$$\begin{aligned} P(y|x = -\frac{A}{\sqrt{2}} + i\frac{A}{\sqrt{2}}) &= \frac{1}{\sqrt{2\pi N_0}} e^{-\frac{(y_R + \frac{A}{\sqrt{2}})^2}{2N_0}} \frac{1}{\sqrt{2\pi N_0}} e^{-\frac{(y_I - \frac{A}{\sqrt{2}})^2}{2N_0}} \\ &= \frac{1}{2\pi N_0} e^{-\frac{(y_R + \frac{A}{\sqrt{2}})^2 + (y_I - \frac{A}{\sqrt{2}})^2}{2N_0}} \end{aligned} \tag{B.16}$$

$$\begin{aligned} P(y|x = +\frac{A}{\sqrt{2}} - i\frac{A}{\sqrt{2}}) &= \frac{1}{\sqrt{2\pi N_0}} e^{-\frac{(y_R - \frac{A}{\sqrt{2}})^2}{2N_0}} \frac{1}{\sqrt{2\pi N_0}} e^{-\frac{(y_I + \frac{A}{\sqrt{2}})^2}{2N_0}} \\ &= \frac{1}{2\pi N_0} e^{-\frac{(y_R - \frac{A}{\sqrt{2}})^2 + (y_I + \frac{A}{\sqrt{2}})^2}{2N_0}} \end{aligned} \tag{B.17}$$

Treating (B.1) as for the BPSK case, we can develop the integrals and make analogous

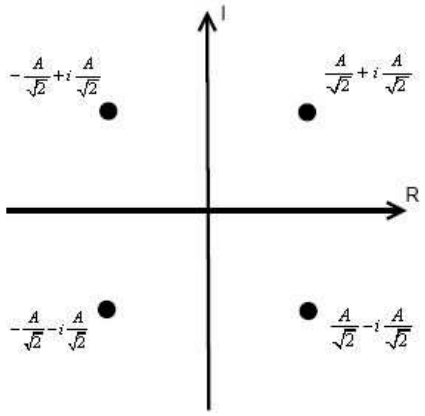

Figure B.2: QPSK constellation.

substitutions to reach the final expression for the capacity, and we get:

$$
\begin{aligned}
I(x;y) \quad = \quad & \int_{-\infty}^{+\infty}\int_{-\infty}^{+\infty}\frac{1}{4}\frac{1}{2\pi N_0}e^{-\frac{(y_R+\frac{A}{\sqrt{2}})^2+(y_I+\frac{A}{\sqrt{2}})^2}{2N_0}}\cdot \\
& \cdot\log_2\left[\frac{\frac{1}{2\pi N_0}e^{-\frac{(y_R+\frac{A}{\sqrt{2}})^2+(y_I+\frac{A}{\sqrt{2}})^2}{2N_0}}}{\frac{1}{4}\frac{1}{2\pi N_0}(e^{-\frac{(y_R+\frac{A}{\sqrt{2}})^2+(y_I+\frac{A}{\sqrt{2}})^2}{2N_0}}+e^{-\frac{(y_R-\frac{A}{\sqrt{2}})^2+(y_I-\frac{A}{\sqrt{2}})^2}{2N_0}}+e^{-\frac{(y_R+\frac{A}{\sqrt{2}})^2+(y_I-\frac{A}{\sqrt{2}})^2}{2N_0}}+e^{-\frac{(y_R-\frac{A}{\sqrt{2}})^2+(y_I+\frac{A}{\sqrt{2}})^2}{2N_0}})}\right]dy_R dy_I + \\
& +\int_{-\infty}^{+\infty}\int_{-\infty}^{+\infty}\frac{1}{4}\frac{1}{2\pi N_0}e^{-\frac{(y_R-\frac{A}{\sqrt{2}})^2+(y_I-\frac{A}{\sqrt{2}})^2}{2N_0}}\cdot \\
& \cdot\log_2\left[\frac{\frac{1}{2\pi N_0}e^{-\frac{(y_R-\frac{A}{\sqrt{2}})^2+(y_I-\frac{A}{\sqrt{2}})^2}{2N_0}}}{\frac{1}{4}\frac{1}{2\pi N_0}(e^{-\frac{(y_R+\frac{A}{\sqrt{2}})^2+(y_I+\frac{A}{\sqrt{2}})^2}{2N_0}}+e^{-\frac{(y_R-\frac{A}{\sqrt{2}})^2+(y_I-\frac{A}{\sqrt{2}})^2}{2N_0}}+e^{-\frac{(y_R+\frac{A}{\sqrt{2}})^2+(y_I-\frac{A}{\sqrt{2}})^2}{2N_0}}+e^{-\frac{(y_R-\frac{A}{\sqrt{2}})^2+(y_I+\frac{A}{\sqrt{2}})^2}{2N_0}})}\right]dy_R dy_I + \\
& +\int_{-\infty}^{+\infty}\int_{-\infty}^{+\infty}\frac{1}{4}\frac{1}{2\pi N_0}e^{-\frac{(y_R-\frac{A}{\sqrt{2}})^2+(y_I+\frac{A}{\sqrt{2}})^2}{2N_0}}\cdot \\
& \cdot\log_2\left[\frac{\frac{1}{2\pi N_0}e^{-\frac{(y_R-\frac{A}{\sqrt{2}})^2+(y_I+\frac{A}{\sqrt{2}})^2}{2N_0}}}{\frac{1}{4}\frac{1}{2\pi N_0}(e^{-\frac{(y_R+\frac{A}{\sqrt{2}})^2+(y_I+\frac{A}{\sqrt{2}})^2}{2N_0}}+e^{-\frac{(y_R-\frac{A}{\sqrt{2}})^2+(y_I-\frac{A}{\sqrt{2}})^2}{2N_0}}+e^{-\frac{(y_R+\frac{A}{\sqrt{2}})^2+(y_I-\frac{A}{\sqrt{2}})^2}{2N_0}}+e^{-\frac{(y_R-\frac{A}{\sqrt{2}})^2+(y_I+\frac{A}{\sqrt{2}})^2}{2N_0}})}\right]dy_R dy_I + \\
& +\int_{-\infty}^{+\infty}\int_{-\infty}^{+\infty}\frac{1}{4}\frac{1}{2\pi N_0}e^{-\frac{(y_R+\frac{A}{\sqrt{2}})^2+(y_I-\frac{A}{\sqrt{2}})^2}{2N_0}}\cdot \\
& \cdot\log_2\left[\frac{\frac{1}{2\pi N_0}e^{-\frac{(y_R+\frac{A}{\sqrt{2}})^2+(y_I-\frac{A}{\sqrt{2}})^2}{2N_0}}}{\frac{1}{4}\frac{1}{2\pi N_0}(e^{-\frac{(y_R+\frac{A}{\sqrt{2}})^2+(y_I+\frac{A}{\sqrt{2}})^2}{2N_0}}+e^{-\frac{(y_R-\frac{A}{\sqrt{2}})^2+(y_I-\frac{A}{\sqrt{2}})^2}{2N_0}}+e^{-\frac{(y_R+\frac{A}{\sqrt{2}})^2+(y_I-\frac{A}{\sqrt{2}})^2}{2N_0}}+e^{-\frac{(y_R-\frac{A}{\sqrt{2}})^2+(y_I+\frac{A}{\sqrt{2}})^2}{2N_0}})}\right]dy_R dy_I
\end{aligned}
\tag{B.18}
$$

We compute the logarithms separately as performed in the BPSK case:

$$-\log_2\left[\frac{1}{4}(1+e^{-\frac{(y_R-\frac{A}{\sqrt{2}})^2-(y_R+\frac{A}{\sqrt{2}})^2}{2N_0}}+e^{-\frac{(y_I-\frac{A}{\sqrt{2}})^2-(y_I+\frac{A}{\sqrt{2}})^2}{2N_0}}+e^{-\frac{(y_R-\frac{A}{\sqrt{2}})^2+(y_I-\frac{A}{\sqrt{2}})^2-(y_R+\frac{A}{\sqrt{2}})^2-(y_I+\frac{A}{\sqrt{2}})^2}{2N_0}})\right]$$
$$=-\log_2\frac{1}{4}-\log_2\left[1+e^{\frac{2y_RA}{\sqrt{2N_0}}}+e^{\frac{2y_IA}{\sqrt{2N_0}}}+e^{\frac{2y_RA+2y_IA}{\sqrt{2N_0}}}\right] \quad \text{(B.19)}$$

$$-\log_2\left[\frac{1}{4}(1+e^{-\frac{(y_R+\frac{A}{\sqrt{2}})^2-(y_R-\frac{A}{\sqrt{2}})^2}{2N_0}}+e^{-\frac{(y_I+\frac{A}{\sqrt{2}})^2-(y_I-\frac{A}{\sqrt{2}})^2}{2N_0}}+e^{-\frac{(y_R+\frac{A}{\sqrt{2}})^2+(y_I+\frac{A}{\sqrt{2}})^2-(y_R-\frac{A}{\sqrt{2}})^2-(y_I-\frac{A}{\sqrt{2}})^2}{2N_0}})\right]$$
$$=-\log_2\frac{1}{4}-\log_2\left[1+e^{-\frac{2y_RA}{\sqrt{2N_0}}}+e^{-\frac{2y_IA}{\sqrt{2N_0}}}+e^{-\frac{2y_RA+2y_IA}{\sqrt{2N_0}}}\right] \quad \text{(B.20)}$$

$$-\log_2\left[\frac{1}{4}(1+e^{-\frac{(y_R-\frac{A}{\sqrt{2}})^2-(y_R+\frac{A}{\sqrt{2}})^2}{2N_0}}+e^{-\frac{(y_I+\frac{A}{\sqrt{2}})^2-(y_I-\frac{A}{\sqrt{2}})^2}{2N_0}}+e^{-\frac{(y_R-\frac{A}{\sqrt{2}})^2+(y_I+\frac{A}{\sqrt{2}})^2-(y_R+\frac{A}{\sqrt{2}})^2-(y_I-\frac{A}{\sqrt{2}})^2}{2N_0}})\right]$$
$$=-\log_2\frac{1}{4}-\log_2\left[1+e^{\frac{2y_RA}{\sqrt{2N_0}}}+e^{-\frac{2y_IA}{\sqrt{2N_0}}}+e^{\frac{2y_RA-2y_IA}{\sqrt{2N_0}}}\right] \quad \text{(B.21)}$$

$$-\log_2\left[\frac{1}{4}(1+e^{-\frac{(y_R+\frac{A}{\sqrt{2}})^2-(y_R-\frac{A}{\sqrt{2}})^2}{2N_0}}+e^{-\frac{(y_I-\frac{A}{\sqrt{2}})^2-(y_I+\frac{A}{\sqrt{2}})^2}{2N_0}}+e^{-\frac{(y_R+\frac{A}{\sqrt{2}})^2+(y_I-\frac{A}{\sqrt{2}})^2-(y_R-\frac{A}{\sqrt{2}})^2-(y_I+\frac{A}{\sqrt{2}})^2}{2N_0}})\right]$$
$$=-\log_2\frac{1}{4}-\log_2\left[1+e^{-\frac{2y_RA}{\sqrt{2N_0}}}+e^{\frac{2y_IA}{\sqrt{2N_0}}}+e^{\frac{-2y_RA+2y_IA}{\sqrt{2N_0}}}\right] \quad \text{(B.22)}$$

We obtain four very similar terms which can be solved with a simple variable change like (B.23) and (B.24) with a minor difference in the signs, obtaining (B.25):

$$\frac{(y_R+\frac{A}{\sqrt{2}})}{\sqrt{2N_0}}=t \qquad \rightarrow \qquad dy_R=\sqrt{2N_0}dt \quad \text{(B.23)}$$

$$\frac{(y_I+\frac{A}{\sqrt{2}})}{\sqrt{2N_0}}=w \qquad \rightarrow \qquad dy_I=\sqrt{2N_0}dw \quad \text{(B.24)}$$

$$\begin{aligned}\int_{-\infty}^{+\infty}\int_{-\infty}^{+\infty} & \frac{2}{8\pi N_0}e^{-\frac{(y_R+\frac{A}{\sqrt{2}})^2+(y_I+\frac{A}{\sqrt{2}})^2}{2N_0}}dy_Rdy_I \\ &=\int_{-\infty}^{+\infty}\int_{-\infty}^{+\infty}\frac{2}{8\pi N_0}e^{-\frac{(y_R+\frac{A}{\sqrt{2}})^2}{2N_0}}e^{-\frac{(y_I+\frac{A}{\sqrt{2}})^2}{2N_0}}dy_Rdy_I \\ &=\frac{1}{4\pi N_0}\int_{-\infty}^{+\infty}e^{-\frac{(y_R+\frac{A}{\sqrt{2}})^2}{2N_0}}dy_R\int_{-\infty}^{+\infty}e^{-\frac{(y_I+\frac{A}{\sqrt{2}})^2}{2N_0}}dy_I \\ &=\frac{1}{4\pi N_0}\int_{-\infty}^{+\infty}e^{t^2}\sqrt{2N_0}dt\int_{-\infty}^{+\infty}e^{w^2}\sqrt{2N_0}dw=\frac{1}{2}\end{aligned} \quad \text{(B.25)}$$

Since we have four terms, by summing them we obtain a factor 2 and the substitutions

done lead to the following passages:

$$
\begin{aligned}
I(x;y) &= 2-\int_{-\infty}^{+\infty}\int_{-\infty}^{+\infty}\frac{1}{4}\frac{1}{2\pi N_0}e^{-\frac{(y_R+\frac{A}{\sqrt{2}})^2+(y_I+\frac{A}{\sqrt{2}})^2}{2N_0}}\log_2\left[1+e^{-\frac{2y_RA}{\sqrt{2}N_0}}+e^{-\frac{2y_IA}{\sqrt{2}N_0}}+e^{-\frac{2y_RA+2y_IA}{\sqrt{2}N_0}}\right]dy_Rdy_I+\\
&\quad-\int_{-\infty}^{+\infty}\int_{-\infty}^{+\infty}\frac{1}{4}\frac{1}{2\pi N_0}e^{-\frac{(y_R-\frac{A}{\sqrt{2}})^2+(y_I-\frac{A}{\sqrt{2}})^2}{2N_0}}\log_2\left[1+e^{-\frac{-2y_RA}{\sqrt{2}N_0}}+e^{-\frac{-2y_IA}{\sqrt{2}N_0}}+e^{-\frac{-2y_RA-2y_IA}{\sqrt{2}N_0}}\right]dy_Rdy_I+\\
&\quad-\int_{-\infty}^{+\infty}\int_{-\infty}^{+\infty}\frac{1}{4}\frac{1}{2\pi N_0}e^{-\frac{(y_R+\frac{A}{\sqrt{2}})^2+(y_I-\frac{A}{\sqrt{2}})^2}{2N_0}}\log_2\left[1+e^{-\frac{2y_RA}{\sqrt{2}N_0}}+e^{-\frac{-2y_IA}{\sqrt{2}N_0}}+e^{-\frac{2y_RA-2y_IA}{\sqrt{2}N_0}}\right]dy_Rdy_I+\\
&\quad-\int_{-\infty}^{+\infty}\int_{-\infty}^{+\infty}\frac{1}{4}\frac{1}{2\pi N_0}e^{-\frac{(y_R-\frac{A}{\sqrt{2}})^2+(y_I+\frac{A}{\sqrt{2}})^2}{2N_0}}\log_2\left[1+e^{-\frac{-2y_RA}{\sqrt{2}N_0}}+e^{-\frac{2y_IA}{\sqrt{2}N_0}}+e^{-\frac{-2y_RA+2y_IA}{\sqrt{2}N_0}}\right]dy_Rdy_I\\
&= 2-\int_{-\infty}^{+\infty}\int_{-\infty}^{+\infty}\frac{1}{4}\frac{1}{2\pi N_0}e^{-\frac{(y_R+\frac{A}{\sqrt{2}})^2+(y_I+\frac{A}{\sqrt{2}})^2}{2N_0}}\log_2\left[\left(1+e^{-\frac{2y_RA}{\sqrt{2}N_0}}\right)\left(1+e^{-\frac{2y_IA}{\sqrt{2}N_0}}\right)\right]dy_Rdy_I+\\
&\quad-\int_{-\infty}^{+\infty}\int_{-\infty}^{+\infty}\frac{1}{4}\frac{1}{2\pi N_0}e^{-\frac{(y_R-\frac{A}{\sqrt{2}})^2+(y_I-\frac{A}{\sqrt{2}})^2}{2N_0}}\log_2\left[\left(1+e^{-\frac{-2y_RA}{\sqrt{2}N_0}}\right)\left(1+e^{-\frac{-2y_IA}{\sqrt{2}N_0}}\right)\right]dy_Rdy_I+\\
&\quad-\int_{-\infty}^{+\infty}\int_{-\infty}^{+\infty}\frac{1}{4}\frac{1}{2\pi N_0}e^{-\frac{(y_R+\frac{A}{\sqrt{2}})^2+(y_I-\frac{A}{\sqrt{2}})^2}{2N_0}}\log_2\left[\left(1+e^{-\frac{2y_RA}{\sqrt{2}N_0}}\right)\left(1+e^{-\frac{-2y_IA}{\sqrt{2}N_0}}\right)\right]dy_Rdy_I+\\
&\quad-\int_{-\infty}^{+\infty}\int_{-\infty}^{+\infty}\frac{1}{4}\frac{1}{2\pi N_0}e^{-\frac{(y_R-\frac{A}{\sqrt{2}})^2+(y_I+\frac{A}{\sqrt{2}})^2}{2N_0}}\log_2\left[\left(1e^{-\frac{-2y_RA}{\sqrt{2}N_0}}\right)\left(1e^{-\frac{2y_IA}{\sqrt{2}N_0}}\right)\right]dy_Rdy_I\\
&= 2-\int_{-\infty}^{+\infty}\int_{-\infty}^{+\infty}\frac{1}{4}\frac{1}{2\pi N_0}e^{-\frac{(y_R+\frac{A}{\sqrt{2}})^2+(y_I+\frac{A}{\sqrt{2}})^2}{2N_0}}\left[\log_2\left(1+e^{-\frac{2y_RA}{\sqrt{2}N_0}}\right)+\log_2\left(1+e^{-\frac{2y_IA}{\sqrt{2}N_0}}\right)\right]dy_Rdy_I+\\
&\quad-\int_{-\infty}^{+\infty}\int_{-\infty}^{+\infty}\frac{1}{4}\frac{1}{2\pi N_0}e^{-\frac{(y_R-\frac{A}{\sqrt{2}})^2+(y_I-\frac{A}{\sqrt{2}})^2}{2N_0}}\left[\log_2\left(1+e^{-\frac{-2y_RA}{\sqrt{2}N_0}}\right)+\log_2\left(1+e^{-\frac{-2y_IA}{\sqrt{2}N_0}}\right)\right]dy_Rdy_I+\\
&\quad-\int_{-\infty}^{+\infty}\int_{-\infty}^{+\infty}\frac{1}{4}\frac{1}{2\pi N_0}e^{-\frac{(y_R+\frac{A}{\sqrt{2}})^2+(y_I-\frac{A}{\sqrt{2}})^2}{2N_0}}\left[\log_2\left(1+e^{-\frac{2y_RA}{\sqrt{2}N_0}}\right)+\log_2\left(1+e^{-\frac{-2y_IA}{\sqrt{2}N_0}}\right)\right]dy_Rdy_I+\\
&\quad-\int_{-\infty}^{+\infty}\int_{-\infty}^{+\infty}\frac{1}{4}\frac{1}{2\pi N_0}e^{-\frac{(y_R-\frac{A}{\sqrt{2}})^2+(y_I+\frac{A}{\sqrt{2}})^2}{2N_0}}\left[\log_2\left(1e^{-\frac{-2y_RA}{\sqrt{2}N_0}}\right)+\log_2\left(1e^{-\frac{2y_IA}{\sqrt{2}N_0}}\right)\right]dy_Rdy_I\\
&= 2-\int_{-\infty}^{+\infty}\int_{-\infty}^{+\infty}\frac{1}{4}\frac{1}{2\pi N_0}e^{-\frac{(y_R+\frac{A}{\sqrt{2}})^2+(y_I+\frac{A}{\sqrt{2}})^2}{2N_0}}\left[\log_2\left(1+e^{-\frac{2y_RA}{\sqrt{2}N_0}}\right)\right]dy_Rdy_I+\\
&\quad-\int_{-\infty}^{+\infty}\int_{-\infty}^{+\infty}\frac{1}{4}\frac{1}{2\pi N_0}e^{-\frac{(y_R+\frac{A}{\sqrt{2}})^2+(y_I+\frac{A}{\sqrt{2}})^2}{2N_0}}\left[+\log_2\left(1+e^{-\frac{2y_IA}{\sqrt{2}N_0}}\right)\right]dy_Rdy_I+\\
&\quad-\int_{-\infty}^{+\infty}\int_{-\infty}^{+\infty}\frac{1}{4}\frac{1}{2\pi N_0}e^{-\frac{(y_R-\frac{A}{\sqrt{2}})^2+(y_I-\frac{A}{\sqrt{2}})^2}{2N_0}}\left[\log_2\left(1+e^{-\frac{-2y_RA}{\sqrt{2}N_0}}\right)\right]dy_Rdy_I+\\
&\quad-\int_{-\infty}^{+\infty}\int_{-\infty}^{+\infty}\frac{1}{4}\frac{1}{2\pi N_0}e^{-\frac{(y_R-\frac{A}{\sqrt{2}})^2+(y_I-\frac{A}{\sqrt{2}})^2}{2N_0}}\left[+\log_2\left(1+e^{-\frac{-2y_IA}{\sqrt{2}N_0}}\right)\right]dy_Rdy_I+\\
&\quad-\int_{-\infty}^{+\infty}\int_{-\infty}^{+\infty}\frac{1}{4}\frac{1}{2\pi N_0}e^{-\frac{(y_R+\frac{A}{\sqrt{2}})^2+(y_I-\frac{A}{\sqrt{2}})^2}{2N_0}}\left[\log_2\left(1+e^{-\frac{2y_RA}{\sqrt{2}N_0}}\right)\right]dy_Rdy_I+\\
&\quad-\int_{-\infty}^{+\infty}\int_{-\infty}^{+\infty}\frac{1}{4}\frac{1}{2\pi N_0}e^{-\frac{(y_R+\frac{A}{\sqrt{2}})^2+(y_I-\frac{A}{\sqrt{2}})^2}{2N_0}}\left[+\log_2\left(1+e^{-\frac{-2y_IA}{\sqrt{2}N_0}}\right)\right]dy_Rdy_I+\\
&\quad-\int_{-\infty}^{+\infty}\int_{-\infty}^{+\infty}\frac{1}{4}\frac{1}{2\pi N_0}e^{-\frac{(y_R-\frac{A}{\sqrt{2}})^2+(y_I+\frac{A}{\sqrt{2}})^2}{2N_0}}\left[\log_2\left(1e^{-\frac{-2y_RA}{\sqrt{2}N_0}}\right)\right]dy_Rdy_I+\\
&\quad-\int_{-\infty}^{+\infty}\int_{-\infty}^{+\infty}\frac{1}{4}\frac{1}{2\pi N_0}e^{-\frac{(y_R-\frac{A}{\sqrt{2}})^2+(y_I+\frac{A}{\sqrt{2}})^2}{2N_0}}\left[+\log_2\left(1e^{-\frac{2y_IA}{N_0}}\right)\right]dy_Rdy_I
\end{aligned}
\tag{B.26}
$$

The first integral is solved by integrating in y_I using the substitution (B.23):

$$\begin{aligned}\int_{-\infty}^{+\infty}\int_{-\infty}^{+\infty} & \frac{1}{4}\frac{1}{2\pi N_0}e^{-\frac{(y_R+\frac{A}{\sqrt{2}})^2}{2N_0}}e^{-\frac{(y_I+\frac{A}{\sqrt{2}})^2}{2N_0}}\left[\log_2\left(1+e^{-\frac{2y_RA}{\sqrt{2}N_0}}\right)\right]dy_Rdy_I \\ &= \int_{-\infty}^{+\infty}\frac{1}{4}\frac{1}{\pi\sqrt{2N_0}}e^{-\frac{(y_R+\frac{A}{\sqrt{2}})^2}{2N_0}}\int_{-\infty}^{+\infty}e^{-t^2}\left[\log_2\left(1+e^{-\frac{2y_RA}{\sqrt{2}N_0}}\right)\right]dtdy_R \\ &= \int_{-\infty}^{+\infty}\frac{1}{4}\frac{1}{\sqrt{2\pi N_0}}e^{-\frac{(y_R+\frac{A}{\sqrt{2}})^2}{2N_0}}\left[\log_2\left(1+e^{-\frac{2y_RA}{\sqrt{2}N_0}}\right)\right]dy_R \qquad \text{(B.27)}\end{aligned}$$

The integral (B.27) is similar to (B.11). The other seven integrals can be solved in a similar manner and using the same reasoning as in the BPSK case, the spectral efficiency expression to the QPSK case is then:

$$\gamma_{\text{QPSK}} = 2\left[1-\int_{-\infty}^{+\infty}\frac{e^{-\frac{t^2}{2}}}{\sqrt{2\pi}}\log_2\left(1+e^{-2\ \text{SINR}-2\sqrt{\text{SINR}}t}\right)dt\right] \qquad \text{(B.28)}$$

Bibliography

[1] S. Adhikari. A non-parametric approach for uncertainty quantification in elastodynamics. In *47th AIAA/ASME/ASCE/AHS/ASC Structures, Structural Dynamics and Materials Conference*, Newport, RI, USA, May 2006.

[2] G. R. Aiello and G. D. Rogerson. Ultra-wideband wireless systems. *Microwave Magazine, IEEE*, 4(2):36–47, 2003.

[3] Hirotugu Akaike. Factor analysis and aic. *Psychometrika*, 52(3):317–332, 1987.

[4] P. Almers, E. Bonek, A. Burr, N. Czink, M. Debbah, V. Degli-Espoti, and et al. Survey of channel and radio propagation models for wireless MIMO systems. *EURASIP Journal on Wireless Communications and Networking*, accepted for publication, 2007.

[5] N. Askar. Overview of general atomics PHY proposal to the IEEE 802.15.3a. In *IEEE P802.15*, March 2003.

[6] S. Bagga, W. A. Serdijn, and J. R. Long. A PPM Gaussian monocycle transmitter for ultra-wideband communications. In *International Workshop on Ultra-Wideband Systems. Joint with Conference on Ultra-Wideband Systems and Technologies*, pages 130–134, Kyoto, Japan, May 2004.

[7] J. M. Bernardo and T. Z. Irony. A general multivariate Bayesian process capability index. *The Statistician, Blackwell Publishing for the Royal Statistical Society*, 45(4):487–502, 1996.

[8] H. Bolcskei and A. J. Paulraj. Space-frequency coded broadband OFDM systems. *Wireless Communications and Networking Conference*, 1:1–6, Sept. 2000.

[9] C. Bonnet, L. Gauthier, P. A Humblet, R. Knopp, A. Menouni Hayar, Y. Moret, A. Nordio, D. Nussbaum, and M. Wetterwald. An all-IP software radio architecture under RTLinux. *Annales des télécommunications Volume 57, n7-8, July-Aug. 2002*, 2002.

[10] G. L. Bretthorst. *Bayesian Spectrum Analysis and Parameter Estimation*. PhD thesis, Washington University, St. Louis, 1987.

[11] D. Cassioli, M. Z. Win, and A. F. Molisch. The ultra-wide bandwidth indoor channel from statistical model to simulations. *IEEE Journal on Selected Areas in Communications*, 20(6):1247–1257, August 2002.

[12] A. Caticha. Information and entropy. In *The 27th International Workshop on Bayesian Inference and Maximum Entropy Methods*, pages 8–13. Saratoga, Springs, New York, USA, July 2007.

[13] A. Caticha and A. Giffin. Updating probabilities. In *Bayesian Inference and Maximum Entropy Methods in Science and Engineering, Ali Mohammad-Djafari ed., AIP Conf. Proc.*, 2006.

[14] T. Cover and J. Thomas. *Elements of Information Theory*. Wiley, 1991.

[15] R. de Lacerda, L. S. Cardoso, R. Knopp, D. Gesbert, and M. Debbah. Emos platform: Real-time capacity estimation of mimo channels in the umts-tdd band. In *Wireless Communication Systems, 2007. ISWCS 2007. 4th International Symposium on*, pages 782–786, 2007.

[16] R. L. de Lacerda Neto, M. Debbah, and A. Menouni Hayar. Channel division multiple access. In *1st IEEE International Conference on Wireless Broadband and Ultra-Wideband Communications*, New South Wales, Australia, March 2006.

[17] R. L. de Lacerda Neto, A. Menouni Hayar, and M. Debbah. Channel division multiple access based on high UWB channel temporal resolution. In *64th IEEE Vehicular Technology Conference 2006 Fall*, pages 1–5, Montreal, Canada, September 2006.

[18] R. L. de Lacerda Neto, A. Menouni Hayar, M. Debbah, and B. Fleury. A maximum entropy approach to ultra-wideband channel modelling. In *IEEE International Conference on Acoustics, Speech and Signal Processing*, pages III–III, Toulouse, France, May 2006.

[19] M. Debbah and R. Muller. MIMO channel modeling and the principle of maximum entropy. *IEEE Transactions on Information Theory*, 51(5):1667–1690, May 2005.

[20] G. D. Durgin. *Space-Time Wireless Channels*. Prentice Hall, Upper Saddle River, NJ, USA, 2003.

[21] S. V. Fomin and I. M. Gelfand. *Calculos of Variations*. Dover Publications, 2000.

[22] G. J. Foschini. Layered space-time architecture for wireless communication in a fading environment when using multi-element antennas. *Bell Labs Technical Journal*, 1(2):41–59, 1996.

[23] G. J. Foschini and M. Gans. On limits of wireless communications in fading environment when using multiple antennas. *Wireless Personal Communications*, 6(6):41–59, March 1998.

[24] L. Georgiadis, M. J. Neely, and L. Tassiulas. *Foundations and Trends in Resource Allocation and Cross-layer Control in Wireless Networks*. NOW, Hanover, MA, USA, 2006.

[25] Adom Giffin and Ariel Caticha. Updating probabilities with data and moments, Aug 2007.

[26] M. Golay. Notes on digital coding. In *Proceedings of the IRE*, June 1949.

[27] A. Goldsmith. *Wireless Communications*. Cambridge University Press, 2005.

[28] I.S. Gradshteyn and I.M. Ryzhik. *Table of Integrals, Series and Products*. Academic Press, 2000.

[29] R. M. Gray. *Toeplitz and Circulant Matrices: A Review*. Technical Report No. 6504-1, Informations Systems Laboratory, Stanford Univity, Stanford, CA, April 1977.

[30] M. Guillaud, M. Debbah, and A. L. Moustakas. Maximum entropy characterization of spatially correlated MIMO wireless channels. In *IEEE Wireless Communications and Networking Conference*, pages 1039–1044, Hong Kong, China, March 2007.

[31] A. Gupta and P. Mohapatra. A survey on ultra wide band medium access control schemes. *Computer Networks*, 51(11):2976–2993, August 2007.

[32] L. Hanzo, M. Munster, B. J. Choi, and T. Keller. *OFDM and MC-CDMA for Broadband Multi-User Communications, WLANs and Broadcasting*. Wiley-IEEEPress, September 2003.

[33] A. M. Hayar, R. Knopp, and R. Saadane. Subspace analysis of indoor UWB channels. *EURASIP Journal on Applied Signal Processing, Special Issue on UWB - State of the Art*, 3:287–295, 2005.

[34] S. Haykin. *Communication Systems*. John Wiley & Sons, Inc, 2000.

[35] S. Haykin. *Adaptive Filter Theory*. Prentice Hall, 2001.

[36] W. He and C. N. Georghiades. Computing the capacity of a MIMO fading channel under PSK signaling. *IEEE Transactions on Information Theory*, 51(5), February 2005.

[37] M. Honig, U. Madhow, and S. Verdu. Blind adaptive multiuser detection. *IEEE Transactions on Information Theory*, 41(4):944–960, July 1995.

[38] E. T. Jaynes. Information theory and statistical mechanics. *Physical Review*, 106(4):620–630, May 1957.

[39] E. T. Jaynes. On the rationale of maximum-entropy methods. *Proceedings of the IEEE*, 70(9):939–952, September 1982.

[40] E. T. Jaynes. *Probability Theory: The Logic of Science*. Cambridge University Press, Cambridge, United Kingdom, 2003.

[41] J. Joe. Cellonics UWB pulse generators. In *Proceedings of International Workshop on Ultra-Wideband System*, Oulu, Finland, June 2003.

[42] R. S. Kennedy. *Fading Dispersive Communication Channels*, volume 18. Wiley, New York, USA, 1969.

[43] U. Madhow and M. L. Honig. MMSE interference suppression for direct-sequence spread-spectrum CDMA. *IEEE Transactions on Communications*, 42(12):3178–3188, December 1994.

[44] V. A. Marchenko and L. A. Pastur. Distributions of eigenvalues for some sets of random matrices. *Mathematics of the USSR-Sbornik*, 1(4):457–483, 1967.

[45] J. W. Mark and W. Zhuang. *Wireless Communications and Networking*. Prectice Hall, Upper Saddle River, NJ, 2003.

[46] M. Médard and R. G. Gallager. Bandwidth scaling for fading multipath channels. *IEEE Transactions on Information Theory*, 48(4):840–852, Apr. 2002.

[47] A. Molisch, M. Steinbauer, M. Toeltsch, E. Bonek, and R. Thoma. Capacity of MIMO systems based on measured wireless channels. *IEEE Journal on Selected Areas in Communications*, 20(3):561–569, April 2002.

[48] A. F. Molisch. *Wireless Communications*. Wiley, The Atrium, Southern Gate, Chichester, England, 2005.

[49] D. Molony. Fixed-mobile integration. *Communications Week*, pages 23–27, December 1998.

[50] R. A. Monzingo and T. W. Miller. *Introduction of Adaptive Arrays*. Wiley, New York, 1980.

[51] R. R. Muller. Channel capacity and minimum probability of error in large dual antenna array systems with binary modulation. *IEEE Transactions on Signal Processing*, 51(11), November 2003.

[52] C. T. Mullis and R. A. Roberts. On the use of second-order information in the approximation of discrete-time linear systems. *IEEE Transactions on Accoustics, Speach and Signal Processing*, 24:226–238, June 1976.

[53] The openair interface. http://www.openairinterface.org/, 2006.

[54] D. Porcino and W. Hirt. Ultra-wideband radio technology: potential and challenges ahead. *Communications Magazine, IEEE*, 41(7):66–74, 2003.

[55] D. Porrat, D. N. C Tse, and S. Nacu. Channel uncertainty in ultra wideband communication systems. *IEEE Transactions on Information Theory*, 53(1):194–208, January 2005.

[56] J. Proakis. *Digital Communications*. McGraw Hill, 2000.

[57] P. Rapajic and B. Vucetic. Adaptive receiver structures for asynchronous CDMA systems. *IEEE Journal on Selected Areas in Communications*, 12:685–697, May 1994.

[58] P. A. Regalia, M. Mboup, and M. Ashari. A class of first- and second-order interpolation problems in model reduction. *Archiv fr Elektronik und Ubertragungstechnik*, 49:332–343, September 1995.

[59] M. Rupf, F. Tarkoy, and J. Massey. User-separating demodulation for code-division multiple access systems. *IEEE Journal on Selected Areas in Communications*, 12:786–795, June 1994.

[60] R. Saadane, D. Aboutajdine, A. M. Hayar, and R. Knopp. On the estimation of the degrees of freedom of indoor uwb channel. In *Vehicular Technology Conference, 2005. VTC 2005-Spring. 2005 IEEE 61st*, volume 5, pages 3147–3151 Vol. 5, 2005.

[61] A. Saleh and R. Valenzuela. A statistical model for indoor multipath propagation. *Selected Areas in Communications, IEEE Journal on*, 5(2):128–137, February 1987.

[62] G. Shafer and V. Vovk. The sources of kolmogorov's grundbegriffe. *Statistical Science*, 21(1):70–98, 2006.

[63] C. E. Shannon. A mathematical theory of communications. *The Bell System Technical Journal*, 27:379–423, October 1948.

[64] D. S. Shiu, G. J. Foschini, M. J. Gans, and J. M Kahn. Fading correlation and its effect on the capacity of multielement antenna systems. *IEEE Transactions on Communications*, 48(3):502–513, March 2000.

[65] J. E. Shore and R. W. Johnson. Axiomatic derivation of the principle of maximum entropy and the principle of minimum cross-entropy. *IEEE Transactions on Information Theory*, 26(1):26–37, January 1980.

[66] J. W. Silverstein and Z. D. Bai. On the empirical distribution of eigenvalues of a class of large dimensional random matrices. *Journal of Multivariate Analysis*, 54(2):175–192, 1995.

[67] J. Skilling. *The Axioms of Maximum Entropy. in Maximum-Entropy and Bayesian Methods in Science and Engineering*, G. J. Erickson and C. R. Smith (eds.), Kluwer Academic, Dordrecht, 1983.

[68] Xiaoyi Tang, M. S. Alouini, and A. J. Goldsmith. Effect of channel estimation error on m-qam ber performance in rayleigh fading. *Communications, IEEE Transactions on*, 47(12):1856–1864, 1999.

[69] V. Tarokh, A. Naguib, N. Seshadri, and A. R. Calderbank. Space-time codes for high data rate wireless communication: performance criteria in the presence of channel estimation errors, mobility, and multiple paths. *Communications, IEEE Transactions on*, 47(2):199–207, 1999.

[70] J. D. Taylor. *Introduction to Ultra-Wideband Radar Systems*. CRC Press, Boca Raton, 1995.

[71] J. D. Taylor. *Ultra-Wideband Radar Technology*. CRC Press, Boca Raton, 2001.

[72] I. E. Telatar. Capacity of multi-antenna gaussian channels. *AT&T Technical Memorandum*, October 1995.

[73] I. E. Telatar and D. N. C. Tse. Capacity and mutual information of wideband multipath fading channels. *IEEE Transactions on Information Theory*, 46(4):1384–1400, July 2000.

[74] I.E. Telatar. Capacity of multi-antenna gaussian channels. *European Transactions on Telecommunications*, 10(6):585–595, Nov.-Dec. 1999.

[75] D. Tse and S. Hanly. Linear multiuser receivers: Effective interference, effective bandwidth and user capacity. *IEEE Transactions on Information Theory*, 45(2):641–657, March 1999.

[76] A. M. Tulino and S. Verdú. *Random Matrix Theory and Wireless Communications*. NOW, Hanover, MA, USA, 2004.

[77] W. Turin, R. Jana, S. S. Ghassemzadeh, C. W. Rice, and T. Tarokh. Autoregressive modelling of an indoor UWB radio channel. In *IEEE Conference on Ultra Wideband Systems and Technologies*, pages 71–74, May 2002.

[78] J. Uffink. The constraint rule of the maximum entropy principle. *Studies In History and Philosophy of Science Part B: Studies In History and Philosophy of Modern Physics*, 27(1):47–79, March 1996.

[79] S. Verdú. Fifty years of Shannon theory. *IEEE Transactions on Information Theory*, 44(6):2057–2078, October 1998.

[80] S. Verdú. *Multiuser Detection*. Cambridge, United States of America, 1999.

[81] S. Verdú and S. Shamai. Spectral efficiency of CDMA with random spreading. *IEEE Transactions on Information Theory*, 45(2):622–640, March 1999.

[82] M. Vrdoljak, S. I. Vrdoljak, and G. Skugor. Fixed-mobile convergence strategy: technologies and market opportunities. *IEEE Communications Magazine*, pages 116–121, February 2000.

[83] M. Wetterwald, C. Bonnet, H. Callewaert, L. Gauthier, R. Knopp, P. Mayani, A. M. Hayar, and D. Nussbaum. *A UMTS-TDD software radio platform*. Chapter of "Reconfigurable Mobile Radio Systems :A Snapshot of Key Aspects Related to Reconfigurability in Wireless Systems" by Vivier, Guillaume (Ed), April 2007.

[84] M. Z. Win and R.A. Scholtz. Impulse radio: How it works. *IEEE Communication Letters*, 2(2):36–38, February 1998.

[85] Z. Xie, R. Short, and C. Rushforth. A family of suboptimum detectors for coherent multiuser communications. *IEEE Journal on Selected Areas in Communications*, 8:683–690, May 1990.

[86] J. Zander. Radio resource management in future wireless networks: Requirements and limitations. *IEEE Communications Magazine*, 35(8):30–36, August 1997.